METHODS FOR RAPID ESTIMATION OF MOTOR INPUT POWER IN HVAC ASSESSMENTS

A Thesis

by

KEVIN DAVID CHRISTMAN

Submitted to the Office of Graduate Studies of
Texas A&M University
in partial fulfillment of the requirements for the degree of

MASTER OF SCIENCE

May 2010

Major Subject: Mechanical Engineering

METHODS FOR RAPID ESTIMATION OF MOTOR INPUT POWER IN HVAC ASSESSMENTS

A Thesis

by

KEVIN DAVID CHRISTMAN

Submitted to the Office of Graduate Studies of
Texas A&M University
in partial fulfillment of the requirements for the degree of

MASTER OF SCIENCE

Approved by:

Chair of Committee, David E. Claridge
Committee Members, Charles Culp
Michael Pate
Head of Department, Dennis O'Neal

May 2010

Major Subject: Mechanical Engineering

ABSTRACT

Methods for Rapid Estimation of Motor Input Power in HVAC Assessments.

(May 2010)

Kevin David Christman, B.S.E., Walla Walla University

Chair of Advisory Committee: Dr. David E. Claridge

In preliminary building energy assessments, it is often desired to estimate a motor's input power. Motor power estimates in this context should be rapid, safe, and noninvasive. Existing methods for motor input power estimation, such as direct measurement (wattmeter), Current Method, and Slip Method were evaluated. If installed equipment displays input power or average current, then using such readings are preferred. If installed equipment does not display input power or current, the application of wattmeters or current clamps is too time-consuming and invasive for the preliminary energy audit. In that case, if a shaft speed measurement is readily available, then the Slip Method is a satisfactory method for estimating motor input power.

An analysis of performance data for 459 motors suggests comparable performance for predicting normalized (to the nominal motor input power) motor input power with the Current and Slip Methods: 10.0% and 9.9% RMSE, respectively. Both of these methods may be improved by applying regression on the predicted variable and/or nameplate parameters. For example, the Slip Method could be improved by applying a second-order regression, thereby reducing the predicted load factor residual RMSE of the data set from 9.0% to 8.2%. The Current and Slip Methods were also evaluated on two real motors. The normalized (to the nominal motor input power) predicted input power RMSE for the Current Method was on average 15% for the two motors; for the Slip Method the corresponding average was 17.5%.

In some cases, shaft speed measurements may not be available. A temperature-based approach for estimating motor input power was investigated. Other required parameters include ambient temperature, motor efficiency, and a motor thermal constant. The temperature approach offers quick, safe, and non-invasive motor power estimation. However, thermal coefficients may vary significantly across motors and a model to predict the thermal coefficients has yet to be developed. Furthermore, the temperature approach has a very strong dependence on motor

efficiency uncertainty. Experiments were performed on two motors to determine their motor thermal constants. If a motor's thermal constants and running efficiency are known, then this method gave motor input power estimates with a RMSE (normalized to the nominal input power) on the order of 4% for the studied motors.

DEDICATION

To my parents

ACKNOWLEDGEMENTS

This research would not have been possible without my adviser, Dr. David Claridge; I thank him for his insight, encouragement, and patience. Much of the time I felt like I was stumbling in the woods, but every meeting with Dr. Claridge brought clarity. I would also like to thank Dr. Charles Culp and Dr. Michael Pate for their constructive advice.

I am indebted to Kelly Milligan, Manager of the Energy Systems Laboratory's Riverside Testing Facility on the Riverside Campus of Texas A&M University, for his resources, time, and encouragement when I tested motors. I thank Kathryn Wadle for taking care of administrative paper work for the experiment construction and James Sweeney for the use of his tools. I also thank Don Gilman for his data-processing advice and Tim Brundidge for his extensive knowledge of motors in the field.

TABLE OF CONTENTS

Page

Page

LIST OF TABLES

Page

LIST OF FIGURES

Page

Page

Page

Page

1. INTRODUCTION

1.1. MOTIVATION

Commercial buildings use 18% of the total energy consumption in the United States (U.S. Dept. of Energy. Energy Information Administration 2008a, 36). While much of this energy provides comfortable and safe environments for people, an excessive amount of this energy is often wasted. In order to improve the energy performance of buildings, the Energy Systems Laboratory at the Texas Engineering Experiment Station has developed a method—Continuous Commissioning®[1]—that optimizes a building's HVAC system and control for improved comfort and financial savings. Buildings that have undergone the Continuous Commissioning® method yield average energy cost savings of about 20%; simple payback is often less than 2 years (Liu, Claridge, and W. Dan Turner 2002, ch.1 p.1).

The U.S. Dept. of Energy reports that electricity accounts for 55% of the energy consumed by commercial buildings (2008b, 1). Motors account for much of the electrical usage in buildings; Little estimates that motors account for somewhat less than 40% of commercial building electrical energy use, whereas Krarti puts the figure at more than 50% (Little 1999, 4-2; Krarti 2001, 4.4.2). Motor usage in commercial buildings is composed of refrigeration, HVAC compressors, and HVAC thermal distribution (Little 1999, 4-3). Supply fans, return fans, and exhaust fans comprise over 80% of the energy usage in commercial building HVAC thermal distribution systems (Westphalen and Koszalinski 1999, 1-2).

During the Continuous Commissioning® process it is often desired to know how much electrical input power a pump or fan motor is using in order to develop baselines. Such power consumption baselines can be used to quickly identify cost-effective measures and retrofits that reduce energy costs (Liu, Claridge, and W. Dan Turner 2002, 1-6 & 2-4; Haasl and Heinemeier 2006, 36). The well-known fan and pump affinity laws state that fan/pump input power varies as the cube[2] of the speed of the fan/pump (ASHRAE 2000a, 39.7). It follows that small changes in

---

This thesis follows the style of *International Journal of HVAC&R Research*.

[1] Continuous Commissioning® and CC® are registered trademarks of the Texas Engineering Experiment Station, Texas A&M University System.

[2] The literature reports that the relationship between flowrate and input power may be less than cubic in practice because fan/pump efficiency, motor efficiency, and VFD efficiency vary with speed (Chan

HVAC and pump system parameters can have large effects on the required shaft power, and therefore also the motor power. However, if the shaft power is already relatively low, a further reduction in flowrate may yield a minimal reduction in shaft power. Therefore establishing power baselines for motors may help in identifying candidates for energy-saving measures. For example, the cost evaluation for applying a VFD to a motor requires adequate knowledge of the motor's power consumption, since VFDs are most cost-effective when driving equipment between 1/3 and 2/3 of full-speed most of the time (Stebbins 1994, 1-2; Kao Chen and Nailen 2004, 188). Fans that usually run at full-load are not good candidates for applying a VFD (Little 1999, 4-15).

It is recognized that motor loads may fluctuate significantly throughout the day or season; thus data logging may be required to obtain a thorough understanding of a motor's load (Hsu et al. 1998, 123). However, installing power meters with logging functionality may not be appropriate or cost-effective at the beginning stages of a building energy assessment. "There are various levels of an energy audit. A walk-through analysis or energy survey can identify high-cost measures that need more in-depth consideration. Even at preliminary stages of the energy audit, an initial estimate of the potential costs and savings for a capital-intensive measure is often required" (ASHRAE 2004, 5). Thus there is an opportunity for rapid measurement of motor input power.

Existing methods of measuring motor power input—such as using a power meter or measuring current with a clamp ammeter—may not be rapid and safe, especially for non-electricians (Gopalakrishnan et al. 2006, 37). However, if installed equipment already displays input power or average current, such values are useful for predicting motor input power in the preliminary energy audit context. Another existing method of estimating motor power input relies on comparing the slip with the rated full load slip; this method, while promising, is limited to motors where measurement of shaft speed is possible and driven across-the-line (ATL). Finally, in the absence of instrumentation, the nameplate power or a certain fraction thereof (e.g., 75%) has been used as an extremely rough estimate of motor power (Barney L. Capehart and Lynne C. Capehart 2007, 73).

2004, 37; Bernier and Bourret 1999, 38-40; Stebbins 1994, 6).

While relying exclusively on nameplate data to estimate motor consumption input power may seem reckless, the additional costs associated with metering motor input power often limit proper measurements (Liu, Claridge, and W. Dan Turner 2002, 2-4; Pawlik, Lynne C. Capehart, and Barney L. Capehart 2001, 10). Motor power estimates that are higher than actual may lead to an overestimation of savings potential and unhappy customers that don't experience the stated cost savings (Barney L. Capehart and Lynne C. Capehart 2007, 69). On the other hand, underestimating the motor power may result in less-than-optimal measures and neglecting cost-saving retrofits. Measurements must be rapid because in-house technicians may have little time to offer to the Continuous Commissioning® team (Liu, Claridge, and W. Dan Turner 2002, 1-5). In addition, measurements should be safe and non-invasive[3] because even for properly-trained electricians, the risk of injury from electrical accidents cannot be ignored (Gilbert A. McCoy and Douglass 2000, 4-2; Nailen 1998, 21).

Motors driven by variable frequency drives (VFDs) are also considered. Some VFDs may not display input power or may require a complicated combination of buttons to be pressed in order for input power to be displayed. As described by the affinity laws, slowing a pump/fan shaft speed often results in considerable power reduction. While the affinity law may be useful to predict the reduction in input power from a decrease in shaft speed, an initial working point must be known in order to fix the affinity curve (ASHRAE 2000b, 18.5). Due to unknowns in system sizing, it may not be prudent to assume that the nameplate motor horsepower corresponds to the nominal speed condition (e.g., 60 Hz).

1.2. OBJECTIVE

The objective of this research is to explore and refine methods for rapid, safe, and non-invasive estimation of input power for motors used in commercial HVAC and pumping applications. Table 1 defines and elaborates the terms used in this objective statement.

[3] Others have also considered the “invasiveness” of methods for estimating motor performance, especially in the estimation of motor efficiency (Douglass 1997, 8; Kueck et al. 1996, 3-4).

Table 1: Definition of terms used in the objective statement.

Term	Definition or Performance Requirement
Rapid	means that measurement time is less than two minutes.
Safe	means that risk of injury from electrical and mechanical dangers (e.g., rotating shaft or belt) is negligible. Methods that require access to bare electrical wires are excluded because the technician may not have electrical training.
Non-invasive	means that measurements must be performed without removing covers, accessing difficult-to-reach locations, and without changing the operation of the system (e.g. manipulating the system to full-load or no-load conditions).
Estimation	estimation within ±20% of the motor's rated power is desired. Based on ESL experience, preliminary energy assessments would benefit with motor power estimates with such an uncertainty.
Input power	refers to the real—not apparent—input power to the motor (including its Variable Frequency Drive if present).
Motors used in commercial HVAC and pumping applications	refers to induction motors that drive fans or pumps and are driven across-the-line (ATL) or by Variable Frequency Drives (VFDs). This effort requires that motors of interest are in good condition and nameplate information is available. In addition, it is assumed that motors are connected to standard electrical service conditions[*].

[*] NEMA describes standard electrical service conditions (NEMA 2007, 2). Voltage variation (e.g., unbalanced lines, under/over-voltage effects, and etc.) can have a large effect on motor efficiency and performance (Nailen 1989, 395).

2. LITERATURE REVIEW

2.1. BACKGROUND FOR MOTOR LOAD ESTIMATION

2.1.1. Introduction to Motors

Electric motors convert electrical energy into mechanical energy in order to provide torque (Guru and Hiziroğlu 2001, 511). Torque in HVAC applications is used to drive compressors in vapor-compression refrigeration systems, pumps that circulate water, and fans that deliver conditioned air throughout buildings.

The reliability and low cost of induction motors make them the most widespread type of motor in residential, commercial, and industrial applications (E Source 1999, 111; Hoffmeyer, Martiny, and Johnson 2004, 35). They are also the most widespread type of motor in commercial HVAC (Krarti 2001, 4.4.2).

As the name illustrates, induction motors use the principle of induction to transfer power from the stator (stationary part) to the rotor (rotating part) (Hoffmeyer, Martiny, and Johnson 2004, 35). When energized, the stator windings produce a rotating magnetic field (Guru and Hiziroğlu 2001, 511). The rotational speed of the stator's magnetic field—known as the synchronous speed —is dependent on the frequency of the electrical supply and the number of poles in the stator:

$$N_{sync} = \frac{60 \cdot f}{p/2} = \frac{120 \cdot f}{p} \tag{1}$$

for synchronous speed N_{sync}, electrical supply frequency f, and number of poles in the stator p (Guru and Hiziroğlu 2001, 511; Hoffmeyer, Martiny, and Johnson 2004, 36). In the United States, the electrical supply frequency from the electrical grid is generally 60 Hz.

In this paper, rotational speed N is in RPM units; rotational speed ω is in rad/sec units; speed f is in Hz units. They are related by

$$\omega = 2\pi f = \left(\frac{2\pi}{60}\right) N \tag{2}$$

The revolving magnetic field created by the stator winding causes a voltage to be induced in the rotor, which ultimately leads to a current flow in the rotor. The rotor experiences a torque because of the interaction between the current flowing through its conductors and the magnetic field produced by the stator (Guru and Hiziroğlu 2001, 139; Hoffmeyer, Martiny, and Johnson 2004, 35). If the rotor's torque is greater than the torque provided by the load (e.g. fan), then rotor will rotate. The rotor will attempt to rotate at the synchronous speed. However, it will never reach synchronous speed because if it did then there would be no relative motion between the stator's magnetic field and the rotor, and therefore no current flow due to an induced voltage. Therefore induction motors rotate at speeds less than the synchronous speed. The normalized difference between the synchronous speed and the shaft speed is the slip:

$$s = \frac{N_{sync} - N_{shaft}}{N_{sync}} \tag{3}$$

for slip s and shaft speed N_{shaft} (Guru and Hiziroğlu 2001, 512; Hoffmeyer, Martiny, and Johnson 2004, 36). For most induction motors, the slip at full load is less than 5% (Hoffmeyer, Martiny, and Johnson 2004, 36).

If various assumptions are made, the torque developed T_{dev} by an induction motor can be approximated as

$$T_{dev} \approx \frac{3 V^2 \cdot s}{\omega_{sync} \cdot R_{rotor}} \tag{4}$$

for supply voltage V, slip s, synchronous speed ω_{sync} (rad/s), and rotor resistance R_{rotor} (Guru and Hiziroğlu 2001, 534).

From Equation 4, it is evident that if the supply voltage, synchronous speed, and rotor resistance are held constant, then the slip is proportional to the developed torque. Motors that are unloaded run near the synchronous speed. As an induction motor's load increases, the slip increases so

that current flow in the rotor will increase and therefore the rotor will experience a greater torque due to its interaction with the stator's magnetic field (Guru and Hiziroğlu 2001, 511).

The shaft power P_{shaft} is dependent on the torque and speed of the shaft:

$$P_{shaft} = T_{shaft} \cdot \omega_{shaft} = T_{shaft} \cdot N_{shaft} \cdot \frac{2\pi}{60} \tag{5}$$

(Hoffmeyer, Martiny, and Johnson 2004, 39).

It is often advantageous to control a motor's rotational speed. In commercial HVAC applications, motors often run fans and pumps, which behave as variable-torque loads. More specifically, fans and centrifugal pumps are categorized as cube-law loads and obey the fan/pump affinity laws. Cube-law loads are named such because the required power varies with the cube of the speed

$$P \propto N_{shaft}^3 \tag{6}$$

and the torque varies with the square of the speed:

$$T \propto N_{shaft}^2 \tag{7}$$

(Barnes 2003, 185; Nadel et al. 2002, 127).

Such behavior is also reflected in one of the fan laws:

$$\frac{P_{shaft,1}}{P_{shaft,2}} = \left(\frac{N_{shaft,1}}{N_{shaft,2}} \right)^3 \tag{8}$$

Assumptions in Equation 8 include constant fluid density, constant fan size, constant impeller efficiency, and similar flow conditions (ASHRAE 2000b, 18.4). This relationship also holds for pumps, where it is a member of the affinity laws (ASHRAE 2000a, 39.7).

It should be recognized that Equation 8 does not account for VFD efficiency, motor efficiency, a geodetic head, varying impeller efficiency, or system interaction. Various authors have

attempted to account for these parameters. For example, instead of power varying with the cube of the shaft speed, some authors use a slightly smaller exponent (E Source 1999, 62; Chan 2004, 37; Bernier and Bourret 1999, 38-40; Stebbins 1994, 6).

In any case, it is apparent from Equation 8 that cube-law loads may experience large drops in power with small changes in speed. While fans/pumps can be slowed down by adjusting pulley size, it is often advantageous for motors to have a form of speed control that is easily varied to account for changing demands (Nadel et al. 2002, 170).

For a given supply frequency and number of motor poles, an induction motor's synchronous speed is constant (see Equation 1). As shown earlier, the shaft speed—and therefore the motor's slip—may vary due to the amount of load the motor experiences (see Equation 4). Combining Equations 1 and 3 and solving for shaft speed N_{shaft} gives

$$N_{shaft} = \frac{120 \cdot f}{p} \cdot (1 - s) \tag{9}$$

From Equation 9, it is evident that an induction motor's shaft speed can be changed by varying the number of poles in the stator p, varying the motor's slip s, or the supply frequency f.

Varying the number of poles in the stator p is done in multi-speed motors that have additional windings in the stator; unfortunately, these have limited speed control (e.g., either 1800 or 900 RPM synchronous speeds). Controlling the motor's slip s can be done by varying the rotor's resistance (e.g., wound-rotor induction motors), varying the stator's voltage, among other methods (Guru and Hiziroğlu 2001, 551-553; Boldea and Nasar 2002, 8.3).

Another method for controlling motor speed is by varying the supply frequency f. This method allows a wide range of speed control and is often applicable to many existing motors. There are many types of VFDs, with Pulse-Width Modulated (PWM) drives being the most common; such inverters vary the voltage and the supply frequency (Ontario Hydro 1997, 13; Lindeborg 1998, 34). There are various methods of speed control for PWM drives. The scalar approach (also known as volts-per-hertz) controls the motor speed by varying the supply voltage and frequency such that the volts to hertz ratio is kept somewhat constant (NEMA 2001, 12). For applications

where speed control must be precise (e.g. textile factories), a more complicated control scheme such as vector control is applied. Compared to scalar control, vector control offers much finer speed control, larger speed range, and higher starting torque (Bartos 2001, 64). However, scalar control (i.e., V/Hz) is cheaper than vector control and pumps/fans generally don't need precise speed control. That explains why V/Hz control is the predominant motor control scheme in HVAC applications (Bartos 2001, 64).

2.2. DETERMINING MOTOR POWER

The purpose of this investigation is to consider, refine, and develop methods that easily predict a motor's electrical input power (or VFD, if present). It is useful to consider a motor's load factor (*LF*), which is defined as

$$LF \equiv \frac{P_{shaft}}{P_{shaft,rated}} \tag{10}$$

where the shaft power is P_{shaft} and the rated shaft power is $P_{shaft,rated}$ (Gopalakrishnan et al. 2006, 39; Barney L. Capehart 2000, 1).

A motor's load factor relates to the motor's input power as

$$P_{in} = \frac{P_{shaft}}{\eta_{motor}} = \frac{LF \cdot P_{shaft,rated}}{\eta_{motor}} \tag{11}$$

for motor input power (real, not apparent) P_{in} and motor efficiency η_{motor}. It should be noted that a motor's efficiency is not constant but dependent on the motor's load factor (Gilbert A. McCoy and Douglass 2000, Appendix B; Agamloh 2007, 1463).

There are various methods of determining a motor's load factor including directly measuring the input power, measuring the current (amperage) to the motor, and measuring the motor's slip. Each of these methods is reviewed next.

2.2.1. Electrical Input Power Measurements

Direct-read input power measurements provide the most accurate method of measuring motor electrical consumption; an accuracy of 1% is achievable (Lobodovsky 2007, 282; Gopalakrishnan et al. 2006, 40; Nadel et al. 2002, 83; U.S. Dept. of Energy. Industrial Technologies Program 2005, 1). If installed equipment does not display input power, then this method entails applying a 3-phase wattmeter to the motor input leads (Nadel et al. 2002, 83).

If direct-read power instrumentation is not available, the input power for a three-phase motor can be determined by various multimeter measurements:

$$P_{input} = V \cdot I \cdot PF \cdot \sqrt{3} \tag{12}$$

where P_{input} is the input power (Watts), V is the mean of the 3 line-to-line RMS voltages, I is the mean RMS current of the 3 phases, PF is the power factor as a decimal (Krarti 2001, 4.4.2; Gilbert A. McCoy and Douglass 2000, 5-1).

Motors connected to Variable Frequency Drives (VFDs) may make electrical measurements more difficult. While it is preferable to take electrical measurements on the line side of the VFD (Lobodovsky 2007, 282), various authors note that VFDs not only shape the current and voltage waveforms on the load side of the VFD but also on the line side (Domijan and Czarkowski 1997, 32; NEMA 2001, 66).

In the preliminary energy audit context, directly measuring input power is only feasible if installed equipment displays input power. Manually applying a wattmeter would require taking voltage measurements[4], which in this research is considered invasive and unsafe due to the handling of live electrical circuits (Gopalakrishnan et al. 2006, 37).

2.2.2. Current Method

Avoiding exposure to live electrical circuits entails no voltage measurement. Current measurement can be done without access to exposed electrical conductors. If the supply voltage

[4] Current measurements are also required, which may or may not be invasive depending on available instrumentation and access to the various wire phases.

and power factor is assumed, then Equation 12 can be used to estimate a motor's input power by only taking current measurements. However it is recognized that on-site voltage may vary and that power factor drops significantly at low loads, thus the literature warns of the accuracy of this method for motor load factor estimation (Nadel et al. 2002, 100).

Another method—which is referred to in this investigation as the Current Method—compares the measured drawn current to the motor's rated full-load current, which is a nameplate value. Figure 1 shows that current draw increases as the motor is loaded. However, below 50% load, the power factor degrades considerably due to magnetizing currents and so the amperage curve becomes increasingly non-linear (Gopalakrishnan et al. 2006, 40). This is one reason why current measurements may give inaccurate load estimates at low loads (Gilbert A. McCoy and Douglass 2000, 5-2).

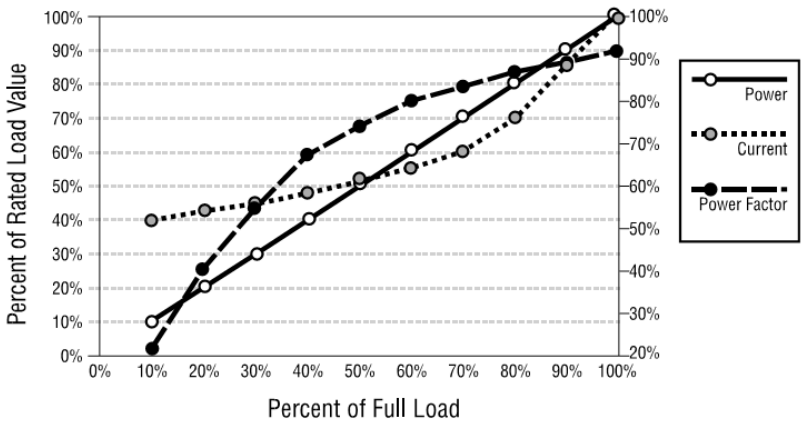

Figure 1: Relationship between various electrical properties and motor load factor (McCoy and Douglass 2000, 5-2).

Fitting a line onto Figure 1 yields a motor's load factor as a function of current:

$$LF = \frac{I - I_{No\ Load}}{I_{Full\ Load} - I_{No\ Load}} \tag{13}$$

where current I is the RMS current (mean of 3 phases), $I_{Full\ Load}$ is the nameplate full-load

current, and $I_{No\ Load}$ is the no-load RMS current (mean of 3 phases) (Hsu et al. 1998, 119).

Unlike the full-load current which is typically a nameplate value, a motor's no-load current is more difficult to determine because it often requires uncoupling the load from the motor's shaft (Lobodovsky 2007, 284). To get around this, the no-load current is often assumed to be zero or a certain fraction of the full-load current (Nailen 1994, 36). Various authors give rough estimates for the no-load fraction, ranging from 25% to 40% (Holmquist, Rooks, and Richter 2004, 245; Gopalakrishnan et al. 2006, 40; Penrose 2004). The lower the horsepower and higher the number of poles, the higher the no-load current if harmonics and differing voltage is not present (Electrical Apparatus 2007, 6). If it is assumed that the motor draws a negligible amount of current at no load (i.e., $I_{No\ Load} = 0$), then

$$LF = \frac{I}{I_{Full\ Load}} \tag{14}$$

which is the form of the Current Method given by other authors (Gilbert A. McCoy and Douglass 2000, 4-2; Nailen 1998, 21).

Some authors slightly modify Equation 13 to account for the non-linear relationship between motor load and current (Lobodovsky 2007, 284; Nailen 1994, 36; Holmquist, Rooks, and Richter 2004, 245):

$$LF = \frac{2 \cdot I - I_{No\ Load}}{2 \cdot I_{Full\ Load} - I_{No\ Load}} \tag{15}$$

Hsu et al. recommend taking the average of Equations 13 and 14 (1998, 119).

In addition, various authors give a voltage correction factor of V / V_{rated} to the Current Method to help account for under/over-voltage conditions (Gilbert A. McCoy and Douglass 2000, 5-3; Gopalakrishnan et al. 2006, 40). Applying this factor to Equation 15 yields

$$LF = \frac{2 \cdot I - I_{No\ Load}}{2 \cdot I_{Full\ Load} - I_{No\ Load}} \cdot \left(\frac{V}{V_{rated}} \right) \tag{16}$$

where voltage V is the RMS voltage (mean line-to-line of 3 phases), and V_{rated} is the

nameplate rated voltage.

A disadvantage of the Current Method is the nonlinearity and limited accuracy at motor load factors below 40 or 50% (Barney L. Capehart and Lynne C. Capehart 2007, 70; Gopalakrishnan et al. 2006, 40; Lobodovsky 2007, 284). In addition, Lobodovsky notes that the Current Method should not be applied to motors less than 7.5 HP and motors should be connected to voltages that are within 5% of the nameplate rating (Lobodovsky 2007, 284).

Applying current clamps to all three phases of the wiring may require opening or unscrewing electrical enclosures could increase the setup time and may expose personnel to live electrical circuits. It should be noted that even if exposure to bare wires is not required, taking current measurements with a current transformer (CT) can be very dangerous if not done with proper equipment and training (Gilbert A. McCoy and Douglass 2000, 4-9; Elkor Technologies 2006, 2-3). In addition, current measurements using a current transformer (CT) have many failure modes, such as applying a CT with reversed polarity to a phase (O'Neal, Bryant, and Carlson 1998, 343-344; Elkor Technologies 2006, 3). Thus safety concerns and setup time limit applying current clamps to wire phases. In the preliminary energy audit context, the Current Method is only viable if installed equipment displays the current.

2.2.3. Slip Method

It is well-known that an induction motor's slip is an indication of actual motor power output (Nailen 1994, 31; Kueck et al. 1996, 3-50). The Slip Method for estimating a motor's load factor relies on assuming that the motor's load factor is proportional to the ratio of the slip at the working load to the slip at the rated load:

$$LF = \frac{N_{sync} - N_{shaft}}{N_{sync} - N_{shaft,\,Full\,Load}} \tag{17}$$

where N_{shaft} represents shaft speed and $N_{shaft,\,Full\,Load}$ represents the nameplate full-load shaft speed (Nadel et al. 1992, 76; Gilbert A. McCoy and Douglass 2000, 5-4). The synchronous speed N_{sync} that the motors strives for is

$$N_{sync} = \frac{120 \cdot f}{p} \tag{18}$$

where f is the electrical supply frequency and p is the number of poles in the motor (Holmquist, Rooks, and Richter 2004, 243).

In order to account for under/over-voltage conditions, various authors include a voltage correction factor of $(V / V_{rated})^2$ to Equation 17:

$$LF = \frac{N_{sync} - N_{shaft}}{N_{sync} - N_{shaft,\,Full\,Load}} \cdot \left(\frac{V}{V_{rated}} \right)^2 \tag{19}$$

where V is the supply voltage and V_{rated} is the motor's rated voltage (Gilbert A. McCoy and Douglass 2000, 5-5; Gopalakrishnan et al. 2006, 41). In Section 3.1. and Appendix A, the rationale for the voltage correction factor is explained.

Note that the voltage correction factor for the Slip Method is slightly different from the one used for the Current Method (compare Equations 16 and 19). That difference is due to the fact that varying voltage conditions have a greater effect on a motor's slip than on the amount of current drawn (Nailen 1994, 36).

2.2.3.1. Gopalakrishnan's Improved Slip Method

Gopalakrishnan et al. studied several methods of estimating motor load factors in the field: wattmeter measurements, Slip Method, and Current Method.

Gopalakrishnan et al. complained that wattmeter readings—while accurate—are too time-consuming and have safety hazards that need to be mitigated (2006, 37 & 47). Using a wattmeter, the Load Factor can be determined by measuring the input power—a somewhat invasive measurement:

$$LF = \frac{P_{input} \cdot \eta_{motor}}{P_{shaft,\,rated} \cdot 0.746} \tag{20}$$

where input power P_{input} is in kW and rated shaft power $P_{shaft,\,rated}$ is in HP.

Gopalakrishnan et al. studied 52 constant-speed motors (ranging from 20 to 250 hp) under constant loads in industrial applications (2006, 44). After taking wattmeter, shaft speed, and nameplate measurements of the motors, a linear regression was created to correlate input power with shaft speed. The linear regression yielded the motor's load factor as

$$LF = 0.18374 + 0.9695 \cdot \frac{N_{sync} - N_{meas}}{N_{sync} - N_{rated}} \tag{21}$$

This regression model had a R^2 of 0.749 and a RMSE (Root Mean Square Error) of 0.16. The effect of nameplate variables on the slip model was also investigated. Gopalakrishnan et al. further improved the slip model by accounting for the motor's nameplate rated voltage (2006, 55 & 57).

Gopalakrishnan et al. used ANOVA and multiple regression to determine if other variables—especially easily acquired variables such as nameplate values—could help refine the model. Of the various variables investigated, it was found that the (nameplate) rated voltage improved the model somewhat:

$$LF = 0.14511 + 0.77860 \cdot \frac{N_{sync} - N_{meas}}{N_{sync} - N_{rated}} + 0.0000207 \cdot (N_{sync} - N_{meas}) \cdot Volt_{rated} \tag{22}$$

Compared to the linear model above, this model gave a higher R^2 of 0.784 and a reduced RMSE (Gopalakrishnan et al. 2006, 58).

2.2.3.2. Summary of Slip Method

The Slip Method has several disadvantages to the Current Method. For example, NEMA requires tighter tolerances with the nameplate full-load current parameter than the nameplate full-load slip parameter (Nailen 1994, 36). Thus the Slip Method may suffer from a larger uncertainty in the nameplate value than the Current Method does. In addition, motor terminal voltage affects current to the first power, whereas slip varies with voltage squared (Nailen 1994, 36; Gilbert A. McCoy and Douglass 2000, 5-5). Thus the Slip Method may be more vulnerable to under/over-voltage conditions than the Current Method. Lobodovsky stipulates that the Slip Method should only be applied to motors subjected to voltages within 5% of the nameplate

rating; in addition the motors should not be rewound (2007, 282 & 284).

The Slip Method requires some form of shaft speed measurement. Anecdotal evidence suggests that shaft speed measurements may be difficult or unsafe for motors where the shaft is not accessible or where rotating belts pose a safety hazard. Contact tachometers are discouraged due to safety concerns and inaccuracy (Hoshide 1994, 13). Stroboscopes and digital tachometers are recommended for taking shaft measurements; the error from these shaft readings should not be greater than ±1 rev/min (da Costa Bortoni 2007, 1387; Gopalakrishnan et al. 2006, 41; EASA 1999, 16). Santos and da Costa Bortoni claim that the error from digital tachometers varies from 0.1% to 0.3% of the measured shaft speed (1995, 1703). Stroboscopes tend to be favored over digital tachometers due to ease-of-use (since they don't require the marker to be reflective) and greater accuracy (Hoshide 1994, 13; Johnson 2004, 404; Energy Ideas Clearinghouse 2007). Measuring shaft speed has varied results: Gopalakrishnan et al. notes that shafts are sometimes inaccessible (2006, 43), whereas others claim that a powerful stroboscope and a trained user can measure shaft speeds by using existing shaft features (e.g., shaft keyway) without stopping the motor to apply a marker on the shaft (Ramsay 1996, 71; Energy Ideas Clearinghouse 2007).

The Slip Method of estimating power is noninvasive and quick. However, it is not a low-cost method of comparing true power consumption between an existing motor and its replacement (Revelt 1997, 3). Kueck is even more downcast: the Slip Method may vary from dynamometer power measurement by 40% (1996, 3-51). In order to improve the Slip Method, Hsu notes that a modified version of the Slip method in conjunction with other nameplate values and built-in statistical data can improve the accuracy for a targeted group of motors (1998, 120).

In addition, several sources warn about the accuracy of the Slip Method and recommend the Current Method (Jowett and Biesemeyer 1994, 249; Gilbert A. McCoy and Douglass 2000, 5-5). Another source gives the opposite recommendation: Nadel et al. warns against the inaccuracies of the Current Method and recommends the Slip Method (1992, 76). Revelt points out that the Slip Method should only be used as a preliminary screening tool and not the sole justification for expensive retrofits (1997). Finally, the Slip Method, as is, cannot be applied to motors driven by VFDs.

2.2.4. ORMEL96

The "Oak Ridge Motor Efficiency and Load" (ORMEL96) algorithm was developed to be a nonintrusive method of estimating motor efficiency and was granted U.S. Patent #5661386 in 1997 (Kueck and Otaduy 1997). The load estimation portion of ORMEL96 is implemented in the *MotorMaster+* software which is developed by the Washington State University Cooperative Extension Energy Program (Washington State University Cooperative Extension Energy Program 2003, i & 58).

The ORMEL96 algorithm derives an equivalent circuit model of the motor from nameplate information. Once this is done, the running efficiency of the motor at any loading can be determined by measuring the motor's shaft speed (Kueck 1998, 69). Based on the given information, the algorithm estimates the frictional/windage losses and locked rotor current assumptions to create an equivalent circuit of the motor (Kueck and Otaduy 1997, col. 2). Entering additional information (such as stator resistance) can substantially improve its accuracy (Wallace et al. 2001, 523-524).

When estimating motor load factors, ORMEL96 requires nameplate data (including the kVA locked rotor code[5]), measured shaft speed, and measured supply voltage (Washington State University Cooperative Extension Energy Program 2003, 58). Like the Slip Method, the ORMEL96 algorithm's accuracy is highly dependent upon the accuracy of the nameplate data (Kueck 1998, 69). Unfortunately, very little literature elaborates on ORMEL96; when it does it's often in the context of determining motor efficiency, not motor load factor or input power. As far as measurements are concerned, this method suffers from any measurement problems that the Slip Method has because it also requires a shaft speed measurement.

2.3. MOTOR EFFICIENCY

While estimating motor efficiency is not the goal of this research, understanding methods for estimating motor efficiency is helpful because some of the motor power estimation methods require a value for efficiency. Motor efficiency is defined as

[5] The kVA locked rotor code represents the ratio of a motor's locked rotor current to its horsepower and is often listed on the nameplate (NEMA 2002, 6,7,28).

$$\eta_{motor} \equiv \frac{P_{shaft}}{P_{in}} \tag{23}$$

for motor efficiency η_{motor}, shaft power P_{shaft}, and electrical input power P_{in} (NEMA 2007, 3; Nadel et al. 2002, 41). While Equation 23 is useful and is used in IEEE Standard 112 Method A, it is generally not used in the field to determine motor efficiency due to difficulties in accurately measuring shaft power (Nailen 2002, 33; IEEE 2004, 34).

Motor efficiency peaks somewhere between 60% and 100% load; the literature often reports the peak at around 75% load (Nailen 1996, 2-2; Auinger 2001, 165; E Source 1999, 165 & 171; Bonnett 1994, 1366). Below 50% load, the motor efficiency drops precipitously (E Source 1999, 166). Therefore, motor efficiency estimates of motors loaded less than 50% of its rated load becomes difficult (Nadel et al. 2002, 83 & 204).

2.3.1. Motor Loss Components

A motor's efficiency is a metric used to determine how well a motor converts electrical energy to mechanical shaft energy (Barnes 2003, 51). An induction motor's losses can be categorized as

- Electrical losses. Also known as Joule losses, I^2R losses, or copper losses, these losses are found in the stator windings and rotor bars due to the resistance to current flow. The Stator loss is $P_{loss,stator} = 3 I^2_{stator} R_{stator}$ and is inversely proportional to the square of the motor efficiency and power factor (Emadi 2005, 36). The Rotor Loss is $P_{loss,rotor} = 3 I^2_{rotor} R_{rotor}$ and approximately proportional to the motor's slip s under typically running conditions (Guru and Hiziroğlu 2001, 518; Emadi 2005, 37).
- Magnetic losses. More commonly known as the Core Loss, this loss is magnetic in nature and depends on the magnetic induction, as well as the frequency of the source voltage and quality of the motor materials (Mello and Pires 2008, 46). This loss is essentially independent of load (Barnes 2003, 51).
- Friction and Windage (F&W) losses. This loss is found in the motor bearings, motor cooling fan, and essentially any rotating part of the motor[6] (Emadi 2005, 38). This loss is constant and essentially independent of load (Barnes 2003, 51).

[6] For wound-rotor induction motors, brush contact resistance becomes relevant (IEEE 2004, 32).

- Stray losses. Predicting the above loss components to a high precision is difficult. Therefore stray losses are considered the residual losses unaccounted for in the above loss categories (Emadi 2005, 40; D.R. Turner et al. 1991, 233). They are load related and often assumed to vary with the square of the torque (Emadi 2005, 40).

The sum of the motor losses is

$$P_{losses} = P_{loss,stator} + P_{loss,rotor} + P_{loss,core} + P_{loss,FW} + P_{loss,stray} \quad (24)$$

(Emadi 2005, 49). Table 2 shows the distribution of the motor component losses for a typical NEMA design B motor.

Table 2: Distribution of motor component losses for a typical NEMA Design B motor (Emadi 2005, 41).

Motor Component Loss	% of Total Loss
Stator I^2R Loss	37%
Rotor I^2R Loss	18%
Magnetic Core Loss	20%
Friction and Windage Loss	9%
Stray Loss	16%

Since the magnetic and F&W losses are essentially independent of load, the overall efficiency of an AC induction motor drop significantly at low load fractions (Barnes 2003, 51).

2.3.2. Determining Motor Efficiency

An upper-bound estimate for an induction motor's efficiency can be determined from the motor's slip. If it is assumed that the stator has negligible copper loss and the frictional/windage losses are negligible as well, then it can be shown that

$$\eta = 1 - s \quad (25)$$

for η efficiency and s slip (Guru and Hiziroğlu 2001, 534; Barnes 2003, 47). That is an upper-

bound limit because real motors have stator copper loss and frictional/windage losses. In practice, that upper-bound limit may not be useful for many motors because maximum rated slip is typically 5% and efficiency—even for premium efficiency motors—approaches 95% only for motors sized above 50 HP (Hoffmeyer, Martiny, and Johnson 2004, 36; NEMA 2006, sec. 12.61).

2.3.2.1. Laboratory Measurements

Directly measuring motor efficiency using Equation 23 is the approach specified in IEEE Standard 112 Method A. Due to the impracticality of accurately measuring shaft power, this method is only recommended for very small motors of less than 1 kW (IEEE 2004, 34; Renier, Hameyer, and Belmans 1999, 514). The shaft power measurement makes this method highly intrusive (Hsu et al. 1998, 122; U.S. Dept. of Energy. Industrial Technologies Program 2005, 1).

A more common approach for measuring motor efficiency is to indirectly measure shaft power by comparing the measured input power with the motor's losses:

$$\eta_{motor} = \frac{P_{shaft}}{P_{in}} = \frac{P_{in} - P_{losses}}{P_{in}} = 1 - \frac{P_{losses}}{P_{in}} \tag{26}$$

where P_{losses} represents the lost power (IEEE 2004, 33; Emadi 2005, 52; Hoffmeyer, Martiny, and Johnson 2004, 37). Recall the losses are composed of stator Joule losses, rotor Joule losses, core losses, FW losses, and stray losses (Emadi 2005, 49).

IEEE Standard 112 Method B determines a motor's stray loss at various load factors by subtracting measured shaft power and calculated losses (stator I^2R, rotor I^2R, core loss, F&W) from the measured input power. After applying curve-smoothing to the motor stray loss—it's a function of load factor—the motor efficiency is determined using Equation 26 (IEEE 2004, 35-38). This method is used widely and is recommended by NEMA for use in motor nameplate efficiency tests (Nadel et al. 2002, 44; NEMA 2002, 16). Although this method uses Equation 26 to determine efficiency, it still requires a dynamometer to develop the stray load loss curve (IEEE 2004, 36).

IEEE Standard 112 Method E also uses the segregated loss approach (Equation 26) but doesn't require the shaft power measurement to determine the stray load loss. The stray load loss is calculated using a reverse rotation test. In IEEE Standard 112 Method E1, the stray load loss is assumed instead of calculated (IEEE 2004, 15-18,46).

IEEE Standard 112 Method F further simplifies testing by not requiring the motor to be loaded at various part loads; values for the impedance of the equivalent circuit are calculated and from these the motor efficiency is estimated. Unfortunately, a no-load test is still required (IEEE 2004, 48; Emadi 2005, 53-54).

While Method E and F (and their variants) don't require shaft power measurements, they are still invasive for rapid field use, since they require no-load tests and electrical measurements (IEEE 2004, 46 & 48).

2.3.2.2. Field Measurements

The running efficiency of most motors is usually unknown and using the defined efficiency standards in the field is often not possible (Munoz and Maldonado 2003, 41). The literature is consistent in the lack of convenient and inexpensive methods for measuring motor efficiency in the field. The available efficiency estimation methods for the field are time-consuming, expensive, or have questionable accuracy (Nadel et al. 2002, 83; E Source 1999, 163 & 170). This leads to efficiency estimates in the field based on nameplate information or performance curves (E Source 1999, 170).

2.3.2.2.1. Estimating Motor Efficiency by Nameplate Value

The least intrusive method for estimating motor efficiency is taking nameplate full-load efficiency. Obviously, this method works best if the motor's efficiency does not vary considerably with motor load (Hsu et al. 1998, 118).

Using nameplate full-load efficiency to approximate a motor's running efficiency is reasonable for many motors. For example, 10 hp motors and larger tend to have the efficiency peak at 75%

load; the efficiency at 100% load and 50% load are both usually less than 1% point below the efficiency peak. Therefore, assuming nameplate efficiency for a motor may be reasonable for a large band of motor load fractions, from 50% to 100% load (E Source 1999, 171). Unfortunately, the nameplate full-load efficiency can grossly differ from the actual motor's efficiency for loads below 50% (Gopalakrishnan et al. 2006, 40).

Besides the fact that a motor is not necessarily driven at full-load, using the nameplate efficiency has several other problems. First of all, it is not uncommon for nameplate efficiency to be missing or inaccessible (Gilbert A. McCoy and Douglass 2000, 4-3; Thumann and Franz 2009, 367).

Secondly, motor efficiency tends to drop after a motor rewind (Nadel et al. 2002, 63). In order to account for the efficiency drop, E Source recommends a 1% point drop in motor efficiency for each motor rewind; Hsu et al. goes further and recommends a 2% point drop per rewind (E Source 1999, 170; Hsu et al. 1998, 118); McCoy recommends a 0.5% to 2% drop per rewind (Gilbert A. McCoy and Douglass 2000, 7-4).

Thirdly, motors operating under non-ideal conditions—such as voltage unbalance or under/over-voltage—may deviate from the nameplate efficiency (Hsu et al. 1998, 118; Gopalakrishnan et al. 2006, 40; Auinger 2001, 166). The effect from under/over-voltage varies and is graphically demonstrated in Auinger (2001, 166). At full-load, a 110% over-voltage results in a 0.5% to 1% increase in motor efficiency. At 50% load, that same 110% over-voltage results in a 1 to 2% decrease in motor efficiency (ASHRAE 2000c, 40.2). However, Emadi gives very different under/over-voltage effects on efficiency of standard efficiency design B motors (Emadi 2005, 140). Ambient temperature, motor age, winding connection (Y vs. delta), voltage unbalance, and harmonic distortion also have an effect on motor efficiency (Auinger 2001, 166-167; Kao Chen and Nailen 2004, 186).

NEMA allows a motor to have losses within ±20% of the nominal losses: therefore a motor labeled with a nameplate efficiency of 93% may actually have an efficiency of 91.7% at full-load (E Source 1999, 145). Even at full-load, a motor with a nameplate efficiency of 85.5% is allowed by NEMA to have a running full-load efficiency of 82.5% (NEMA 2006, sec. 12.58.2).

Angers tested 182 motors and found that their losses were generally within the ±20% boundary established by NEMA (Angers 2003, 59).

Even if a motor is running exactly at rated load, it's efficiency may deviate ±2% from the nameplate full-load efficiency (via visual inspection of a graph in Angers 2003, 57). In practice, however, for load factors between 50% and 100%, Hsu estimates that using the nameplate efficiency value gives an accuracy of ±10% (Hsu et al. 1998, 122). Below 50% load factor, motor efficiency falls dramatically from the nameplate value (Thumann and Franz 2009, 367).

2.3.2.2.2. Estimating Motor Efficiency by Load Curve

While a motor's nameplate may only list the full-load efficiency, manufacturers often provide motor load versus efficiency curves. If the motor's load fraction is known, then the efficiency at that load can be determined (Nailen 1994, 32).

In the field, however, a motor manufacturer's load factor vs. efficiency curve may not be readily available (Nailen 1994, 32). To remedy this, average motor efficiency tables are available as a function of motor rated speed, motor rated power, enclosure type (TEFC vs. ODP), and motor load fraction (Gilbert A. McCoy and Douglass 2000, Appendix B; Mecker 1994, 33; NEMA 2006, 12.60). The MotorMaster+ software provides generic motor efficiency curves based on various motor parameters, such as load factor, rated horsepower, rated speed, and efficiency category[7] (Gilbert A. McCoy and Douglass 2000, 5-7; U.S. Dept. of Energy Motor Challenge Program, 3). Caution should be exercised, since the uncertainty of these average values is not given. Emadi gives tables with large nominal efficiency ranges for various motor sizes (2005, 33 & 50).

2.3.2.2.3. Estimating Motor Efficiency using the Slip Method

The Slip Method for estimating motor load (Equation 17) can be used to estimate a motor's efficiency. Once the motor's load factor is determined, the motor's running efficiency can be determined from the manufacturer's efficiency vs. motor-load curve (Nailen 1994, 32). If the

[7] The motor efficiency curves in MotorMaster+ are readily accessible by opening the MMCatlog.mdb database file in the MotorMaster+ folder.

manufacturer's curve is not available, general curves for high, medium, and low efficiency motors are used (Hsu et al. 1998, 119).

Another approach uses the basic Slip Method (Equation 17) to directly calculate the motor efficiency using Equation 23:

$$\eta = \frac{P_{shaft}}{P_{input}} = \frac{P_{rated} \cdot (0.746) \cdot LF}{P_{input}} = \frac{P_{rated} \cdot (0.746) \cdot \left(\frac{N_{sync} - N_{shaft}}{N_{sync} - N_{shaft,\,Full\,Load}} \right)}{P_{input}} \tag{27}$$

where P_{rated} is rated motor power (hp) and P_{input} is the electrical power into the motor (kW) (Nailen 1994, 35; Hsu et al. 1998, 119). Therefore this method of estimating motor efficiency requires a shaft speed measurement, power input measurement, and nameplate information.

The literature is often highly critical of the Slip Method when it is used to directly calculate motor efficiency[8] (Gilbert A. McCoy and Douglass 2000, 4-2; U.S. Dept. of Energy. Industrial Technologies Program 2005; Nailen 1994, 32-33). Even if the Slip Method's model is perfect and all parameter uncertainties are neglected accept for the nameplate full-load shaft speed $N_{shaft,\,Full\,Load}$, the uncertainty[9] in efficiency for Equation 27 is

$$\Delta \eta = \frac{\Delta N_{shaft\,Full\,Load}}{N_{sync} - N_{rated}} \cdot \eta \tag{28}$$

For an example motor with a full-load speed of 1760 RPM, full-load efficiency of 90%, and an uncertainty in full-load shaft speed of 5 RPM, this leads to a motor efficiency uncertainty of

$$\Delta \eta = \frac{5}{(1800 - 1760)} \cdot 90\,\% = 11\,\% \tag{29}$$

which is on par with the uncertainty in efficiency for assuming that motor efficiency is constant

[8] However, it is acceptable to use the Slip Method to estimate motor load, from which the efficiency can be estimated at the applied load using the motor manufacturer's efficiency vs. load curves (Nailen 1994, 32).

[9] Using the error propagation method demonstrated by Holman (Holman 2001, 52).

at various loads and equal to the nameplate efficiency (Hsu et al. 1998, 122). However, Kueck et al. notes that motor efficiency uncertainty should be within ±3% if it is to be useful for making motor replacement decisions[10] (Kueck et al. 1996, 1-2). As shown in this example, criticism on the use of the Slip Method to directly calculate motor efficiency is warranted.

2.3.2.2.4. Estimating Motor Efficiency using the Current Method

Like the Slip Method, the Current Method can be used to estimate a motor's efficiency indirectly —using an efficiency vs. motor load curve—or directly using Equation 23 (Hsu et al. 1998, 119). For motor efficiency estimation, Nailen tends to prefer the Current Method over the Slip Method because of tighter tolerances on nameplate values and decreased dependence on voltage and temperature variation (Nailen 1994, 36).

[10] The uncertainty in motor efficiency for making motor replacement decisions (±3%) given by Kueck et al. should not be confused with the the uncertainty in motor power estimation (±20%) specified in the objective.

3. MODEL DEVELOPMENT

3.1. EXTENDING THE SLIP METHOD TO VFD-DRIVEN MOTORS

A literature search regarding the application of the Slip Method of motor load estimation to motors driven by VFDs was unproductive. As mentioned earlier, VFDs may not not provide easy display of input power. Therefore it may be of use to extend the Slip Method to VFD-driven motors.

When a motor is operating at or near its rated slip (less than a slip of 10%), the torque developed by an induction motor can be approximated as:

$$T_{dev} \approx \frac{3 V_{stator}^2 \cdot s}{\omega_{sync} \cdot R_{rotor}} \tag{30}$$

(Guru and Hiziroğlu 2001, 534).

If the output shaft power is assumed to be the developed power (i.e., no friction/windage losses), then

$$P_{shaft} = T_{shaft} \cdot N_{shaft} \cdot \left(\frac{2\pi}{60} \right) = T_{dev} \cdot N_{shaft} \cdot \left(\frac{2\pi}{60} \right) \tag{31}$$

Inserting Equations 2, 3, and 30 into 31 results in

$$P_{shaft} = \frac{3 V_{stator}^2 (N_{sync} - N_{shaft})}{N_{sync}^2 \cdot R_{rotor}} \cdot N_{shaft} \cdot \left(\frac{2\pi}{60} \right)^2 \tag{32}$$

Similarly, the rated shaft power is

$$P_{shaft,\,rated} = T_{dev,\,rated} \cdot N_{shaft,\,rated} \cdot \left(\frac{2\pi}{60}\right) = \frac{3\,V^2_{stator,\,rated}\,(N_{sync,\,rated} - N_{shaft,\,rated})}{N^2_{sync,\,rated} \cdot R_{rotor,\,rated}} \cdot N_{shaft,\,rated} \cdot \left(\frac{2\pi}{60}\right)^2 \tag{33}$$

If it is assumed that the rotor resistance remains unchanged across the typical motor usage region, then $R_{rotor} = R_{rotor,\,rated}$. Solving Equation 33 for $R_{rotor,\,rated}$ and substituting it into Equation 32 as rotor resistance R_{rotor} gives:

$$P_{shaft} = \frac{V^2_{stator}}{V^2_{stator,\,rated}} \cdot \frac{N_{sync} - N_{shaft}}{N_{sync,\,rated} - N_{shaft,\,rated}} \cdot \frac{N_{shaft}}{N_{shaft,\,rated}} \cdot \frac{N^2_{sync,\,rated}}{N^2_{sync}} \cdot P_{shaft,\,rated} \tag{34}$$

From the definition of motor efficiency (Equation 23), Equation 34 can be written as motor input power:

$$P_{input} = \frac{V^2_{stator}}{V^2_{stator,\,rated}} \cdot \frac{N_{sync} - N_{shaft}}{N_{sync,\,rated} - N_{shaft,\,rated}} \cdot \frac{N_{shaft}}{N_{shaft,\,rated}} \cdot \frac{N^2_{sync,\,rated}}{N^2_{sync}} \cdot \frac{P_{shaft,\,rated}}{\eta_{motor}} \tag{35}$$

For a motor driven across-the-line (ATL), then the synchronous speed is assumed to be the rated synchronous speed $N_{sync} = N_{sync,\,rated}$, giving

$$P_{input} = \frac{N_{sync,\,rated} - N_{shaft}}{N_{sync,\,rated} - N_{shaft,\,rated}} \cdot \frac{N_{shaft}}{N_{shaft,\,rated}} \cdot \frac{P_{shaft,\,rated}}{\eta_{motor}} \cdot \left(\frac{V_{stator}}{V_{stator,\,rated}}\right)^2 \tag{36}$$

The Slip Method expressions shown earlier in Equations 17 and 19 are slightly different from the form used in Equation 36: the $N_{shaft}/N_{shaft,\,rated}$ factor in Equation 36 is very close to 1 and is usually neglected in the literature (Hsu et al. 1998, 119). Astrom does include it (2004, 12). The voltage factor $(V_{stator}/V_{stator,\,rated})^2$ is often neglected in the field due to the difficulty in voltage measurements.

For motors driven by VFDs, the supply voltage given to the motor is not necessarily the line voltage in the building. Most drives used in HVAC applications are open-loop drives that operate under Volts per Hertz control (Bartos 2001, 64). This type of control keeps a drive's Voltage to Frequency (V/F) ratio somewhat constant (Ontario Hydro 1997, 11). "[O]nce established this ratio of voltage to frequency does not change with load unless trimmed using voltage boost or IR compensation" (NEMA 2001, 12). The V/Hz ratio is held constant, except at low speeds where the voltage is increased to account for current losses from resistance (Chang 2006, 210).

If it is assumed that the drive maintains a constant voltage-to-frequency ratio over all frequencies, then

$$\frac{V_{rated}}{f_{rated}} = \frac{V_{supply}}{f_{supply}} \tag{37}$$

which is equivalent to

$$\frac{V_{supply}}{V_{rated}} = \frac{f_{supply}}{f_{rated}} = \frac{N_{sync}}{N_{sync,rated}} \tag{38}$$

If it is further assumed that voltage drops between the VFD and motor are negligible $V_{stator} = V_{supply}$, then substituting Equation 38 into Equation 35 yields

$$\begin{aligned} P_{input} &= \frac{N_{sync}^2}{N_{sync,rated}^2} \cdot \frac{N_{sync} - N_{shaft}}{N_{sync,rated} - N_{shaft,rated}} \cdot \frac{N_{shaft}}{N_{shaft,rated}} \cdot \frac{N_{sync,rated}^2}{N_{sync}^2} \cdot \frac{P_{shaft,rated}}{\eta_{motor}} \\ &= \frac{N_{sync} - N_{shaft}}{N_{sync,rated} - N_{shaft,rated}} \cdot \frac{N_{shaft}}{N_{shaft,rated}} \cdot \frac{P_{shaft,rated}}{\eta_{motor}} \end{aligned} \tag{39}$$

Since VFDs give the synchronous supply speed in Hertz (rather than shaft speed RPM), then Equation 39 can be manipulated to

$$P_{input} = \frac{\left(\frac{f_{supply}}{f_{rated}}\right) \cdot N_{sync,rated} - N_{shaft}}{N_{sync,rated} - N_{shaft,rated}} \cdot \left(\frac{N_{shaft}}{N_{shaft,rated}}\right) \cdot \left(\frac{P_{shaft,rated}}{\eta_{motor}}\right) \quad (40)$$

where f_{rated} (60 Hz in US) and f_{supply} (e.g. 45 Hz) need to be known instead of N_{sync}. Notice that Equation 40 is composed entirely of

- nameplate values: nameplate synchronous speed $N_{sync,rated}$, nameplate full-load shaft speed $N_{shaft,rated}$, nameplate motor power $P_{shaft,rated}$, and motor efficiency[11] η_{motor}
- measurable variables: supply synchronous speed f_{supply} and measured shaft speed N_{shaft}.

It should be recognized that this extension of the Slip Method to VFD-driven motors assumes the validity of Equation 30 and constant V/Hz control. Furthermore, the effect of the harmonic content in the supply signal on the motor's slip has not been evaluated (Romo and Adrian 1998, 96).

A graphical development for the VFD-Extended Slip Method (Equation 40) is given in Appendix A.

3.2. TEMPERATURE-BASED APPROACH TO MOTOR POWER ESTIMATION

The motivation for this research is rapid motor power estimation in the context of building energy assessments. The shortcomings of direct power measurement have already been discussed. Other motor power estimation methods, such as the Slip Method and Current Method may be impractical in certain situations. For example, a motor's shaft may not be easily accessible and current measurements may require opening of electrical boxes in order to individually access all three phases. Furthermore, both the Slip Method and Current Method require nameplate information (e.g., full-load shaft speed and full-load current) which may not be available or readable.

[11] While motor efficiency is often listed on motor nameplates, it should be noted that actual motor efficiency may vary from the nameplate value due to varying motor loads, motor repair, and other conditions.

A thermal approach to measuring motor input power has been proposed. This approach does not require electrical measurements, close proximity to rotating parts, or reflectors/markers on the shaft. The primary variable in this approach is temperature; Nailen notes that temperature measurements for motors are straightforward and easy (1994, 31).

3.2.1. Thermal Aspects of Motors

3.2.1.1. Heat Generation and Rejection in Motors

Electric motors have several primary sources of waste energy: I^2R (Joule) heating from electric current flow in the stator and rotor, hysteresis losses in the magnetic material, and frictional loss from the shaft bearing (Liao, C.L. Chen, and Katcher 1998, 424; Albers and Bonnett 2002, 1701-1702). This heat is transferred from the generation site to other motor locations via three heat transfer modes: conduction, convection, and radiation (Bousbaine 1999, 312; Albers and Bonnett 2002, 1702). The waste energy is eventually rejected to a liquid or gas coolant; in this investigation we restrict the coolant to be air (NEMA 2006, sec. 6.2.3).

The type of motor enclosure affects the motor's cooling scheme. NEMA categorizes motor enclosures as either open or closed. Open enclosures—such as the Open Drip-Proof (ODP) enclosure—allows ambient air to circulate inside the motor in order to cool the hot internal components (Robert M. McCoy and Owen 2004, 628). Closed enclosures—such as the Totally-Enclosed Fan-Cooled (TEFC) or Totally-Enclosed Non-Ventilated (TENV) enclosures—restrict ambient air from directly cooling the motor's internal components. Rather, the excess energy within the motor is transferred to the external surface. In order to increase heat rejection, closed motors—such as TEFC enclosures—use a cooling fan to blow across the enclosure, which may in addition have fins (E Source 1999, 115-116).

The most common types of motors used in HVAC applications are Open Drip-Proof (ODP), Totally-Enclosed Fan-Cooled (TEFC), Totally-Enclosed Air-Over (TEAO). ODP motors are located in dry locations (Stanford 2003, 142). They tend to run cooler, have smaller sizes, and have less capital costs than closed motors (Robert M. McCoy and Owen 2004, 628). TEFC motors are often used where moisture is present, such as cooling tower applications. TEAO

motors are located in the airflow stream (Stanford 2003, 142-143).

3.2.1.2. Relationship between Motor Temperature and Motor Load Factor

The stator windings and rotor surface are subject to high temperatures (Yoon and Kauh 2005, 83). In order to prolong motor life,[12] the mitigation of high motor temperatures are of major concern in motor design and operation (Albers and Bonnett 2002, 1702; Mukhopadhyay, Chowdhury, and Pal 1994, 139). In the field, high frame temperature is sometimes used as an indicator of motor problems (Nailen 2003, 33). However, that approach is criticized for its unreliability (Medinger 1996, 15).

Various authors have explored the relationship between winding temperature and motor load factor (Nailen 2003, 36). Albers and Bonnet give a plot of average winding temperature versus motor load factor for various nominal motor sizes, see Figure 2 (2002, 1708). Notice that approximately a 30-40 ºC increase in average winding temperature occurs between the no load condition (0% load factor) and the full-load condition (100% load factor) for motors large and small.

[12] A rule-of-thumb is that for every 8 to 10ºC rise in internal motor temperature, the insulation life is halved (McCoy and Owen, 619).

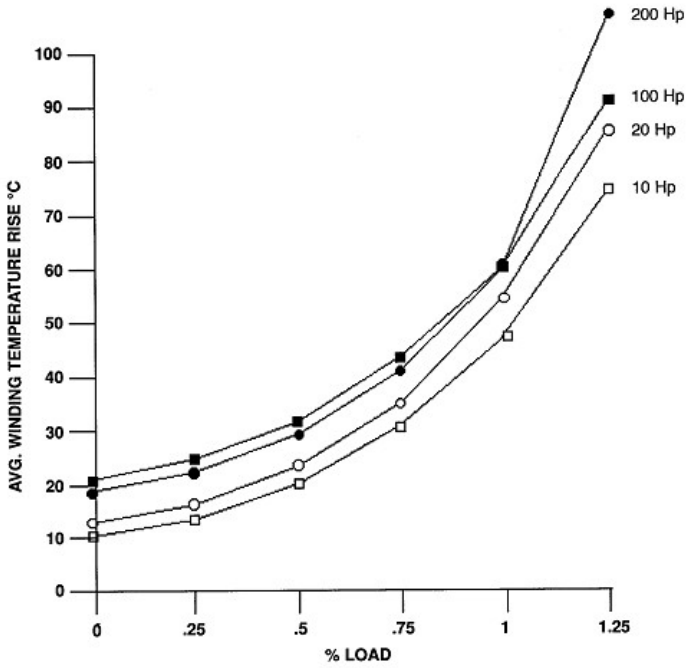

Figure 2: Relationship between winding temperature rise and motor load factor (Albers and Bonnett 2002, 1708). © 2002 IEEE.

Albers and Bonnett also give a correlation between frame temperature and winding temperature: depending on the nominal motor horsepower and motor load factor, the winding temperature rise is between 1.4 to 2.2 times the frame temperature rise[13] (2002, 1712). Valenzuela and Tapia state that "the temperature rise from the enclosure to the ambient is in the range of 30 – 40% of the total temperature rise of the hottest spot of the winding" (2006, 4840). That results in slightly higher values than given by Albers and Bonnett. In any case, it can be conjectured that there is a relationship between motor load factor and frame temperature; this is visually confirmed in Figure 3 (Maru and Zotos 1989, 885). However, Stone et al. state that the stator frame temperature "is only loosely correlated" with winding temperature (2004, 287).

[13] However, this relationship will also vary for motors with different enclosures and motor speeds. Due to the wide variation of enclosure types, it is not recommended to estimate winding temperature from frame temperature in the field (Albers and Bonnett 2002, 1711).

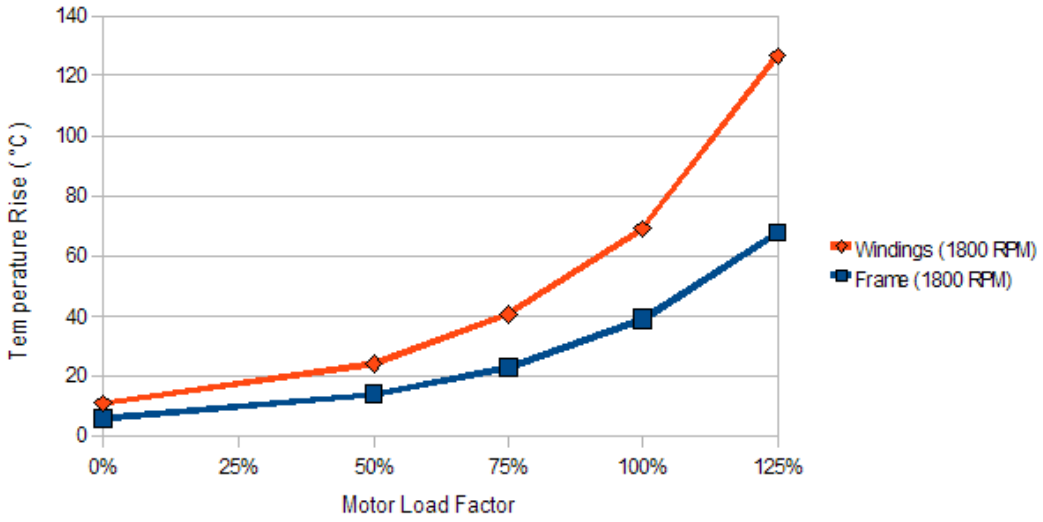

Figure 3: Winding and frame temperature rise (from the ambient) vs. motor load factor for a 50 HP, 1800 RPM, three-phase TEFC motor (figure created by author from data in Maru and Zotos 1989, 885).

The literature on the relationship between winding temperature and motor load factor is usually in the context of determining winding temperature, not the vice versa (Nailen 1996, 6-43; Albers and Bonnett 2002, 1709). Albers notes that the mathematics is somewhat complicated and does not perform well for large changes in load or at load extremum (Albers and Bonnett 2002, 1709).

3.2.2. Development of Temperature-based Method of Predicting Input Power

The previous section shows that some sort of temperature measurement may be useful for estimating motor load. This next section develops a model. A Temperature-based Method has been investigated so that a motor's input power can be estimated from temperature measurements. This is achieved by using heat transfer principles and studies regarding heat transfer behavior with motors. In addition, limited[14] experiments on real motors have been done to refine the model.

This temperature-based approach estimates a motor's electrical consumption by relating the

[14] Unlike motor experiments that only measure shaft speed and drawn current, motor experiments that involve temperature measurements require long time constants for motors to reach steady-state thermal conditions. Thus this limits the number of experiments allowed in this preliminary investigation.

motor's losses P_{waste} to the motor's input power P_{input}. Given a control-volume that surrounds a motor and assuming that the motor is at thermal steady-state conditions, an energy balance gives:

$$P_{input} = P_{shaft} + P_{waste} = \eta_{motor} P_{input} + P_{waste} \tag{41}$$

It should be noted that P_{shaft} refers exclusively to the mechanical power transferred via the shaft, and does not include heat transfer conducted by the shaft, which is considered in the losses P_{waste}.

Solving for P_{input} in Equation 41 gives

$$P_{input} = \frac{P_{waste}}{1 - \eta_{motor}} \tag{42}$$

Equation 42 expresses the motor input power as a function of the wasted power and motor efficiency.

If it assumed that the motor's wasted power P_{waste} is removed from a control volume that surrounds a motor entirely via heat transfer methods[15], then Equation 42 can be written as:

$$P_{input} = \frac{P_{waste}}{1 - \eta_{motor}} = \frac{P_{ext.cond.} + P_{ext.conv.} + P_{ext.rad.} + P_{int.reject.}}{1 - \eta_{motor}} \tag{43}$$

where $P_{ext.cond.}$, $P_{ext.conv.}$, and $P_{ext.rad.}$ refer to heat transfer modes occurring at the external surface of the motor: external conduction, external convection, and external radiation, respectively. Through-ventilated motors not only reject waste energy at the motor's external surface, but also draw air into the motor's interior where heat is rejected to the passing air. In Equation 43, the internal rejection term $P_{int.reject.}$ represents the heat transfer from the motor's interior to the passing air inside the motor. Figure 4 graphically details the energy transfer across a control volume that surrounds a motor.

[15] Latent heat transfer methods such as evaporation/condensation are not considered.

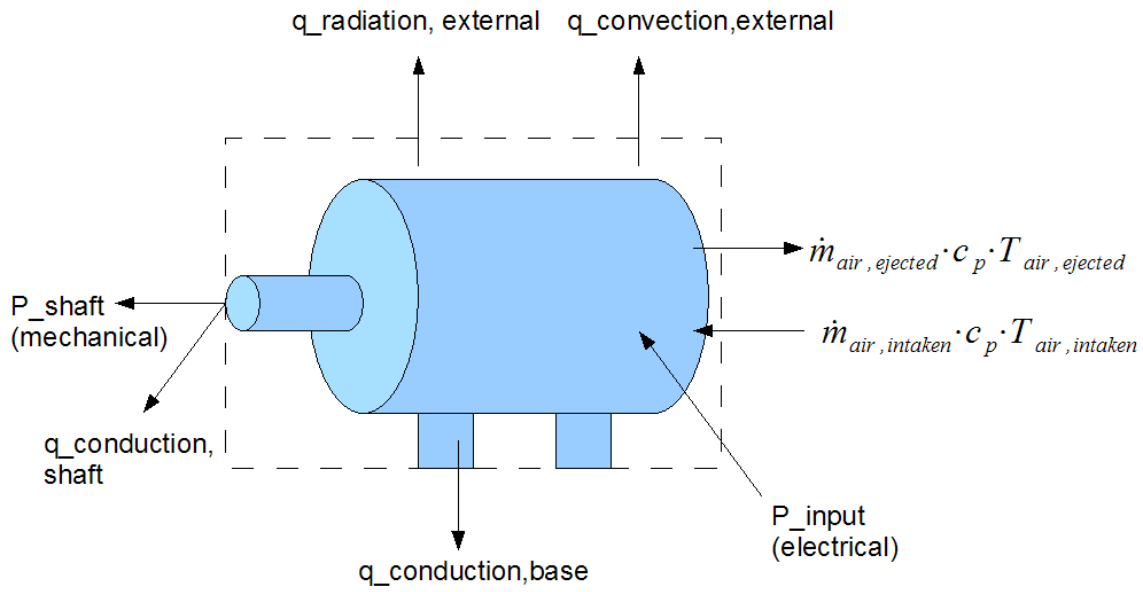

Figure 4: Energy transfer across a control volume that surrounds a motor.

3.2.3. Component External Loss Modes

Earlier in Section 2.3.1. the component loss modes (stator copper loss, rotor copper loss, core loss, stray load loss, and F&W loss) were described. No matter the source of the losses, they exit the motor's control volume generally as heat (Preecha et al. 2004, 608). The modes of heat transfer across the motor's control volume are summarized next.

3.2.3.1. Loss by External Conduction

One-dimensional steady-state heat transfer by conduction is generally given as

$$q_{cond} = \frac{k\,A}{l}\Delta T = \frac{\Delta T}{R} \tag{44}$$

for q_{cond} conduction heat transfer rate, k thermal conductivity, A area of flow path, l length of flow path, ΔT temperature difference between beginning and end of heat flow path, and $R = l/(k\,A)$ thermal resistance (Robert M. McCoy and Owen 2004, 620).

Conduction heat transfer plays an important role within the motor by transferring the excess power from the generation site to other locations (Bousbaine 1999, 312; Robert M. McCoy and Owen 2004, 621). However, this study is concerned with the heat transfer across a control volume that envelopes the motor, as shown in Figure 4. Thus the only likely avenues for conduction heat transfer across the control volume are via the shaft[16] and motor mount.

It should be recognized that the motor shaft—at least the portion of it that is within the motor—is a major avenue of heat transfer: it conducts thermal energy from within the motor to the external housing of the motor (Liao, C.L. Chen, and Katcher 1998, 425; Boldea and Nasar 2002, 12.3; Albers and Bonnett 2002, 1701). However, at the exterior of the motor, Turner et al. describe the heat transfer via the shaft as minimal due to the relatively small cross-sectional area, but it should be recognized that in their case steps were taken to reduce heat transfer via the shaft (1991, 242).

The conductive heat transfer via the motor base to the ground has a measurable effect: Liao, Chen, and Katcher show that changing the material that a TEFC motor is grounded to from wood to concrete resulted in a decrease in temperature of the motor frame near the base of the motor (1998, 427). Boglietti mounted motors on wood baseplates or hung the motors on thin wires while studying motor thermal behavior in order to reduce conduction heat transfer from the motor's base to the ground (Boglietti, Cavagnino, and D. Staton 2008, 1152 & 1156). However, "the high conductivity of ground may have strong enough effects on the temperature of the whole motor only when the motor is made of material with very high thermal conductivity or the motor is very small or both" (Liao, C.L. Chen, and Katcher 1998, 427).

3.2.3.2. Loss by External Convection

Convection heat transfer over motors is a complicated process and is affected by geometry, flow parameters, and other thermal properties (Robert M. McCoy and Owen 2004, 622; Bousbaine 1999, 318). Convection heat transfer is often modeled as

[16] The exposed portion of the rotating shaft may employ forced convection heat transfer, which Saari quantifies (1995, 37-38). In the present investigation, such heat transfer is not considered.

$$q_{conv} = h A (T_{surf} - T_{fluid}) \tag{45}$$

for q_{conv} convection heat transfer rate, h surface heat transfer coefficient, A effective surface area, T_{surf} surface temperature of the solid, and T_{fluid} fluid temperature (Robert M. McCoy and Owen 2004, 622; Boldea and Nasar 2002, 12.4).

Of primary concern is the convection coefficient from the external frame to the main environment. Heat transfer coefficients vary widely for a given motor; they vary by spatial position and airflow characteristics (Hay et al. 1995, 324).

3.2.3.3. Loss by External Radiation

Radiation heat transfer from motors is not as well understood as the other heat transfer modes (Boglietti, Cavagnino, and D. Staton 2008, 1155). Radiation heat transfer occurs between the surfaces of two bodies at differing temperatures. If the surroundings are assumed to be a blackbody (absorb all incident radiation), then the radiation heat transfer rate can be expressed as

$$q_{rad} = \sigma \varepsilon A (T^4_{motor\ surface} - T^4_{surr}) \tag{46}$$

for radiation heat transfer rate q_{rad}, Stefan-Boltzmann constant σ, motor surface emissivity ε, motor surface area A, absolute motor surface temperatures $T_{motor\ surface}$, and absolute surrounding blackbody surface temperature T_{surr} (Boglietti et al. 2006, 689; Robert M. McCoy and Owen 2004, 621). The assumptions in Equation 46 should be recognized: it assumes uniform motor surface temperature, uniform surrounding surface temperature, blackbody surrounding surfaces, and a view factor of unity. Boglietti et al. note that it is reasonable to approximate the room surrounding a motor as a blackbody if the room's surface walls have a much greater area than the motor enclosure (2006, 689). The literature gives various values for the motor surface emissivity values (Markovic, Saunders, and Perriard 2006, 59; Robert M. McCoy and Owen 2004, 622; Huai, Melnik, and Thogersen 2003, 794).

Equation 46 is nonlinear in terms of temperature. A simpler form for radiation heat transfer may be appropriate for many motors:

$$q_{rad} = h_{rad} A (T_{motor\ surface} - T_{surr}) \quad (47)$$

where radiative heat transfer coefficient h_{rad}. This linearized form may be appropriate for many motors because the radiative heat transfer coefficient does not vary significantly with temperature for typical operating conditions (Saari 1995, 32-33; Huai, Melnik, and Thogersen 2003, 785). Bousbaine notes that the "...nonlinearity associated with radiation is rarely of importance in electrical machines" (1999, 318). However, the linearized form of radiation transfer—Equation 47—should not be applied where radiation is a major component of heat transfer (Bousbaine 1999, 318).

Radiation transfer occurs in parallel to convection, so it is experimentally difficult to measure separately (Markovic, Saunders, and Perriard 2006, 59; Boglietti, Cavagnino, and D. Staton 2008, 1155). However, motor thermal models often assume that the motor frame temperature is not great enough for significant radiation heat transfer (Boglietti, Cavagnino, and D. Staton 2008, 1155). The magnitude of radiation heat transfer is similar to that of natural convection, therefore radiation heat transfer should not be ignored for motors without forced convection (Boglietti et al. 2006, 688; Saari 1995, 35). For example, radiation heat transfer should not be ignored with TENV (Totally Enclosed Non-Ventilated) motors, since radiation and natural convection are the dominant heat transfer modes for such motors (Robert M. McCoy and Owen 2004, 621; D.A. Staton and Cavagnino 2008, 3510). McCoy and Owen report that the surface heat transfer coefficient—even for the smallest of motors—at least 4.5 times the combined coefficient for natural convection and radiation (2004, 623).

Motors operating with reduced forced convection—such as a motor driven by a VFD at half-speed—will experience a greater reliance on radiation heat transfer than if operating at full-speed[17] (Boglietti et al. 2006, 688). Table 3 shows how radiation may become more of a factor for VFD-driven motors at low speeds (D.A. Staton and Cavagnino 2008, 3510).

[17] While motors that rely on forced convection (e.g., TEFC enclosures) may get hotter when driven at reduced speeds, motors that rely on natural convection (e.g. TENV enclosures) get cooler when driven at reduced speeds (Hodowanec 2000, 44).

Table 3: Comparison of convection heat transfer and radiation heat transfer for a 7.5 HP motor with a TEFC enclosure.

Motor Speed	q_{conv}/q_{rad} **ratio**
@ 1800 RPM	15
@ 900 RPM	8
@ 300 RPM	5

Table 3 assumes the ambient fluid temperature is 25C, surrounding surface temperature is also 25C, emissivity is 1, and respective surface areas are equal. In addition, the convection coefficient values used in the table represent a 7.5 HP TEFC motor (Valenzuela and Tapia 2006, 4837).

3.2.3.4. Loss by Internal Rejection

Some motors are considered "open" because they draw in ventilation air in order to cool the interior (e.g. Open Drip-Proof enclosures). Recall Equation 43, where the internal rejection term $P_{int.reject.}$ represents the heat transfer from the motor's interior to the passing air inside the motor. Although conduction and radiation mechanisms are utilized to transfer excess energy in the interior of the motor, the internal heat transfer to the air $P_{int.reject.}$ is effected by convection. Pickering et al. gives sample convection heat transfer coefficients for the interior of a through-ventilated motor (1998, 431). Knowledge of the interior convection heat transfer coefficient for through-ventilated motors is not directly useful for the present objective because the Newton equation for modeling convection (see Equation 45) requires temperature measurements of the surface involved. Unfortunately, access to the motor interior—such as for temperature measurement—is limited in field applications. Furthermore, interior surface temperatures vary widely within the motor (Pickering et al. 1998, 430).

An alternate method of modeling the internal heat rejection is by comparing the thermal energy gained by the air drawn into the motor interior.

$$P_{int.reject.} = \dot{m}_{air,intaken} c_p (T_{air,out} - T_{air,in}) = \rho \dot{V}_{air,intaken} c_p (T_{air,out} - T_{air,in}) \quad (48)$$

for thermal energy transferred to the intaken air $P_{int.reject.}$, mass flowrate of intaken air $\dot{m}_{air,intaken}$, volumetric flowrate of intaken air $\dot{V}_{air,intaken}$, air specific heat capacity c_p, air density ρ, and air temperature before intake and after ejection from motor interior $T_{air,in}$ and $T_{air,out}$, respectively (ASHRAE 2005, 3.28). Notice that Equation 48 consists entirely of air properties; it does not require knowledge of the motor interior, such as internal surface temperature values or internal convection heat transfer coefficients.

3.2.4. Motor Temperature Considerations

3.2.4.1. Temperature Deviation by Spatial Location

Frame temperatures can vary significantly by location. The variation in motor surface temperature can be explained by nonuniform airflow over the motor surface, different heat flux densities emitted from the motor, and a lack of symmetry in the motor (Mukosiej 2000, 168). Mukosiej warns that average frame temperatures (not local) should be used when temperature rises of a motor are compared. Mukosiej also provides a method of determining the average frame temperature with multiple local temperature measurements (1986, 360).

There is much literature on the thermal behavior of TEFC motors. There is substantial literature regarding ODP motors as well, but they tend to focus on temperatures and heat transfer in the motor interior and little is mentioned regarding external surface temperatures of ODP frames.

The literature notes that a motor should not be assumed to be have symmetric heat transfer coefficients along the axis, especially one with a TEFC. Yoon and Kauh measured significant variations between the motor's endcaps. Yoon and Kauh show how various motor temperature parts (e.g., frame, stator, rotor surface, windings, and etc.) vary as a function of axial position (2005, 81 & 83). Takahashi et al. give values for the local heat transfer coefficients at various axial locations; he reported local heat transfer coefficient at the output of the channel is 50-60% of the initial value (2002, 14).

Temperatures also vary circumferentially. Mukosiej reported local temperature rise (from ambient) of a TEFC frame varies by location from 10.4 K to 36.4 K; that is 51% to 179% of the average frame temperature value (1986, 363). Hay et al. give a table showing the local convective heat transfer coefficient for a TEFC motor at various circumferential and axial locations (1995, 324). Boglietti et al. reported how air speed varies by channel location (2008, 1157).

3.2.4.2. Temperature Deviation with Time

Yoon and Kauh reported that a 3.7 kW motor reached thermal steady-state in an hour when loaded from 0% to various load factors (2005, 83). However, manual inspection of other motor surface temperature versus time plots in the literature suggest a longer stabilization time (Mukhopadhyay, Chowdhury, and Pal 1994, 144; Chillet et al. 1990, 37-38).

3.2.4.3. Motors Driven by Variable Speed Drives

Variable Speed Drives complicate the matter a bit more. First, the air flow changes—which has a strong effect on convective heat transfer coefficients. Secondly, if speed control is achieved by nonsinusoidal signals (e.g. a PWM VFD), the electromagnetic losses in the motor will increase and therefore decrease motor efficiency. Finally, slower shaft rotation results in reduced frictional losses.

3.2.4.3.1. Issues Regarding Airflow Changes

Valenzuela and Tapia show how TEFC frame temperatures change in response to different VFD speeds—which effects the airflow speed over the motor. Note that less airspeed results in greater temperature deviations. They also reported the heat transfer coefficient as a function of axial distance for a 7.5 HP motor at various VFD speeds. They claim that this information can be extended to other motors that have frames of geometric similarity: similar diameter to axial length ratio (2006, 4837).

3.2.4.3.2. Motor Losses and Efficiency when Driven by VFD

When driven with electrical power that has harmonic content or modified by a VFD, it is necessary to consider the additional motor heating and the resulting temperature rise (Bonnett 2001, 1125). The literature reports how magnetic losses and motor temperature vary by VFD frequency (Valenzuela, Tapia, and Rooks 2004, 695-697; Romo and Adrian 1998, 97-98).

3.2.4.3.3. Issues Regarding Mechanical Loss changes

Note that mechanical losses generally dissipate as heat. The literature gives simple expressions to estimate frictional losses (e.g., motor cooling fan, bearings, etc.) of motors (Valenzuela, Tapia, and Rooks 2004, 693; Mukhopadhyay, Chowdhury, and Pal 1994, 143).

3.2.4.4. Safety of Temperature Measurements

In this temperature approach to estimating motor power, the only measurements are temperature-based; thus exposure to rotating belts and shafts for a shaft speed measurement or exposure to electrical wires for current measurements is avoided. However, enclosure surface may be hot and the risk of skin burns from accidental skin contact with the enclosure surface should be evaluated. Medinger notes that there are no published standards for motor surface temperature (1996, 16). T-frame motor surfaces are known to run especially hot, up to 95°C in a room temperature of 25°C (Taber 1998, 368; Nailen 2003, 35; Medinger 1996, 15). Nailen reports an old study which states that skin contact with a 100°C smooth surface may be tolerated for about one second, leading to the conclusion that “normal motor surface temperature” may not be a burn hazard (2003, 36). Even if a motor surface is a skin burn hazard, that hazard would likely also apply to the other power estimation methods—the Slip or Current methods—since these require nameplate information and therefore also require close proximity to motor surface temperatures. It should also be noted that IR thermometers do not require surface contact for temperature measurement, thereby mitigating skin burn hazard.

3.2.5. Experiment Development

While the general concept behind the thermal loss approach was established in Section 3.2.2., in

the given form it is not suitable for field application. Recall the general equation for the thermal loss approach of estimating motor power consumption (shown earlier as Equation 43):

$$P_{input} = \frac{P_{waste}}{1-\eta_{motor}} = \frac{P_{ext.cond.} + P_{ext.conv.} + P_{ext.rad.} + P_{int.reject.}}{1-\eta_{motor}} \tag{49}$$

where $P_{ext.cond.}$, $P_{ext.conv.}$, and $P_{ext.rad.}$ refer to heat transfer modes occurring at the external surface of the motor: external conduction, external convection, and external radiation, respectively. Through-ventilated motors not only reject waste energy at the motor's external surface, but also draw air into the motor's interior where heat is rejected to the passing air. In Equation 49, the internal rejection term $P_{int.reject.}$ represents the heat transfer from the motor's interior to the passing air inside the motor.

The waste power leaving the motor's control volume via conduction $P_{ext.cond.}$ was discussed earlier in Section 3.2.3.1. Conduction heat transfer from the motor's control volume—such as via the shaft or motor base—is not as large as the other heat transfer modes. In order to simplify this preliminary investigation, the conduction heat transfer from the motor's control volume $P_{ext.cond.}$ is ignored. Subsequent research may desire to explore this mode and include it in the model.

The waste power leaving the motor's control volume via convection $P_{ext.conv.}$ was discussed earlier in Section 3.2.3.2 and can be modeled as

$$P_{ext.conv.} = q_{conv} = h\,A\,(T_{surf} - T_{\infty}) \tag{50}$$

for q_{conv} convection heat transfer rate, h representative heat transfer coefficient over the motor's enclosure, A external surface area of motor enclosure, T_{surf} representative surface temperature of motor enclosure, and T_{∞} ambient air temperature. Earlier, Section 3.2.4.1. showed the variation in local heat transfer coefficients and temperature on motor enclosures. Due to the complexity of local variations in convection heat transfer coefficient and surface temperature, representative values for these two variables are assumed.

The waste power leaving the motor's control volume via radiation $P_{ext.rad.}$ was discussed earlier

in Section 3.2.3.3 and can be modeled as

$$P_{ext.rad.} = q_{rad} = \sigma \varepsilon A (T_{surf}^4 - T_{surr}^4) \tag{51}$$

for radiation heat transfer rate q_{rad}, Stefan-Boltzmann constant σ, representative motor surface emissivity ε, motor surface area A, representative absolute motor surface temperature T_{surf}, and representative absolute surrounding blackbody surface temperature T_{surr}. The assumptions in Equation 51 should be recognized: it assumes uniform motor surface temperature, uniform surrounding surface temperature, blackbody surrounding surfaces, and a view factor of unity.

Through-ventilated motors have an additional waste rejection method. The waste power leaving the motor's control volume via internal rejection $P_{int.reject.}$ was discussed earlier in Section 3.2.3.4 and can be modeled as

$$\begin{aligned} P_{int.reject.} &= \dot{m}_{air,intaken} c_p (T_{air,out} - T_{air,in}) \\ &= \dot{V}_{air,intaken} \rho c_p (T_{air,out} - T_{air,in}) \end{aligned} \tag{52}$$

for thermal energy transferred to the intaken air $P_{int.reject.}$, mass flowrate of intaken air $\dot{m}_{air,intaken}$, volumetric flowrate of intaken air $\dot{V}_{air,intaken}$, air specific heat capacity c_p, air density ρ, and air temperature before intake and after ejection from motor interior $T_{air,in}$ and $T_{air,out}$, respectively.

3.2.5.1. Adapting the Heat-loss Model for Field Use

Combining Equations 49 through 52 and ignoring heat loss from the motor via conduction gives:

$$\begin{aligned} P_{input} &= \frac{P_{waste}}{1-\eta_{motor}} = \frac{P_{ext.conv.} + P_{ext.rad.} + P_{int.reject.}}{1-\eta_{motor}} \\ &= \frac{h A (T_{surf} - T_\infty) + \varepsilon \sigma A (T_{surf}^4 - T_{surr}^4) + \dot{V}_{air,intaken} \rho c_p (T_{air,out} - T_{air,in})}{1-\eta_{motor}} \end{aligned} \tag{53}$$

Equation 53 contains the various parameters of interest in this heat-loss model. Some of the parameters are intrinsic to the motor and do not vary, such as external surface area A or the average external emissivity. Others, such as the average heat transfer coefficient may be considered constant for each motor, but upon closer inspection, may vary if the motor is driven

by a VFD. As shown earlier in Section 3.2.1.2., motor temperature—whether motor surface temperature T_{surf} or the ejected air temperature from the motor $T_{air,out}$—is dependent on the motor's load and VFD speed. The environment temperatures are ambient air temperature T_{∞}, surrounding surface temperature T_{surr}, and motor intake air temperature $T_{air,in}$; they are somewhat independent[18] of the motor's operating condition and are not necessarily equal to each other. Other environmental parameters include air density and air specific heat capacity. The universal physical constant in Equation 53—the Stefan Boltzmann constant sigma—is known and not subject to change. These parameters are summarized in Table 4.

Table 4: Summary of parameter qualities used in temperature-based input power estimation approach.

Parameter	Parameter Symbol	Environment parameter	Constant per motor at ATL	Load-dependent	VFD speed dependent
Average Heat Transfer Coefficient of Motor Surface	h	maybe	X		X
External Motor Surface Area	A		X		
Representative Motor Surface Temperature	T_{surf}			X	
Ambient Temperature	T_{∞}	X			
Motor Surface Emissivity	ε		X		
Representative Surrounding Surface Temperature	T_{surr}	X			
Volumetric Air Flowrate Intaken by Motor	$\dot{V}_{air,intaken}$	maybe	X		X
Air Density	ρ	X			
Air Specific Heat	c_p	X			
Temperature of Intaken Air	$T_{air,in}$	X			
Temperature of Ejected Air	$T_{air,out}$			X	X
Motor Efficiency	η_{motor}			X	X

[18] Strictly speaking, the surrounding ambient air temperature is dependent on the motor load, since a heavily-loaded motor will run hotter and may increase the ambient air temperature. However, classifying ambient air temperature as an environment parameter is useful because it allows us to distinguish the variables that are strongly load-dependent, such as surface temperature.

While this parameter classification may be simplistic and imperfect, it is useful for adapting Equation 53 for experimental and field use. As elegant as Equation 53 is, the thermal performance of many motors must be done empirically: testing the motor at different speeds, computing losses, and measuring temperatures (Valenzuela, Tapia, and Rooks 2004, 693). Boglietti et al. note that a superficial knowledge of a motor's geometry and other properties is not sufficient to create thermal predictions of motor behavior, due to complex thermal phenomena. "In most cases, empirical data are used to calibrate analytical models..." (2008, 1158).

The average convection coefficient, emissivity, and various surface areas are specific to a particular motor type operating at a certain speed. In order to make the multiple regression simpler, Equation 53 can be simplified by combining terms into some fitting constants. A convection constant is used:

$$C_{conv} \propto h_{rated\ speed} A_{conv} \tag{54}$$

where $h_{rated\ speed}$ represents the convective heat transfer coefficient over the motor's exterior when driven at rated speed (e.g., 60 Hz). A radiation constant is used:

$$C_{rad} \propto \varepsilon A_{rad} \tag{55}$$

For a given motor, various authors compare how the convection heat transfer coefficient h varies with the motor's shaft speed N_{shaft} using the following form:

$$h \propto N_{shaft}^{m} \tag{56}$$

The literature gives varying values for the exponent m in Equation 56. For the external heat transfer of TEFC motors, values of 0.6 and 0.65 are reported (Hay et al. 1995, 324; Yoon and Kauh 2005, 80). Pickering et al. report a value of 0.75 for the interior of a through-ventilated motor (1998, 431).

For closed motors—such as of the TEFC type—the final term in Equation 53 does not apply

because air is not generally drawn in to cool the motor interior. Combining Equations 53 through 56 then gives

$$P_{input} = \frac{C_{conv} N_{shaft}^{C_{speed}} (T_{surf} - T_{\infty})}{1 - \eta_{motor}} + \frac{C_{rad} \sigma (T_{surf}^4 - T_{surr}^4)}{1 - \eta_{motor}} \tag{57}$$

where C_{conv} represents convection heat transfer coefficient at rated speed and external convection surface area, C_{rad} represents the motor's surface emissivity and external radiation surface area, and the exponent C_{speed} replaces the dummy variable m from Equation 56.

For open motors—such as one with an ODP enclosure—the final term in Equation 53 is not discarded because air is drawn into the motor for direct cooling of the motor's interior. However, measuring the air flowrate $\dot{V}_{air,intaken}$ in the field may be impractical. This can be remedied by using the fan law:

$$\begin{aligned} \dot{V} &= \frac{N_{shaft}}{N_{shaft,\,rated\ speed}} \cdot \dot{V}_{rated\ speed} \\ &= \frac{\dot{V}_{rated\ speed}}{N_{shaft,\,rated\ speed}} \cdot N_{shaft} \\ &= C_{through} \cdot N_{shaft} \end{aligned} \tag{58}$$

where $C_{through} = \dot{V}_{rated\ speed} / N_{shaft,rated\ speed}$ and is constant for a given motor.

Combining Equations 53 through 56 and Equation 58 yields

$$P_{input} = \frac{C_{conv} N_{shaft}^{C_{speed}} (T_{surf} - T_{\infty})}{1 - \eta_{motor}} + \frac{C_{rad} \sigma (T_{surf}^4 - T_{surr}^4)}{1 - \eta_{motor}} + \frac{C_{through} N_{shaft} (\rho c_p)(T_{air,out} - T_{\infty})}{1 - \eta_{motor}} \tag{59}$$

where $C_{through}$ was defined above and is constant for a given motor.

Equations 57 and 59 predict motor input power for both closed and open motors. They rely exclusively on motor constants (C_{conv}, C_{speed}, C_{rad}, and possibly $C_{through}$), environment parameters (T_{∞}, T_{surr}, and possibly ρ and c_p), a universal constant (σ), measurable variables (N_{shaft} and T_s), and the elusive motor efficiency.

The difficult-to-determine heat transfer parameters (e.g. convective heat transfer coefficient, motor surface dimensions, through-motor airflow rates) that are intrinsic to a motor are lumped into several fitting constants (C_{conv} , C_{speed} , C_{rad} , and possibly $C_{through}$). Until another model is developed to predict the motor constants, these constants may be determined via regression of experimental data. While it appears that a shaft speed measurement is required, the shaft speed N_{shaft} will be estimated with the synchronous speed (N_{sync}) , which is easy to determine.

3.3. CONSIDERING UNCERTAINTY OF THE MOTOR INPUT POWER APPROACHES

3.3.1. Effect of Motor Efficiency Uncertainty on Motor Input Power

The Slip Method attempts to determine motor power by estimating a motor's shaft power, whereas the Temperature Approach determines motor power via an estimation of the motor's losses. The difference in approach has a significant effect on the resilience of the method from uncertainties in motor efficiency. The following analysis uses the Kline-McClintock propagation-of-error method to demonstrate the effect on the performance of each method from motor efficiency uncertainty.

3.3.1.1. Estimating Input Power Indirectly

Recall Equation 42 which is the kernel of the temperature-based approach:

$$\left(P_{in}\right)_{loss approach} = P_{shaft} + P_{waste} = \frac{P_{waste}}{1-\eta} \tag{60}$$

The partial derivative of Equation 60 with respect to efficiency is

$$\left(\frac{\partial P_{in}}{\partial \eta}\right)_{loss\ approach} = \frac{P_{waste}}{(1-\eta)^2} \tag{61}$$

If it is assumed that the model is error-free and all model parameters except for motor efficiency

have zero uncertainty, the uncertainty in input power using a motor loss method is[19]

$$\left(\Delta P_{in}\right)_{loss\ approach} = \sqrt{\left(\frac{\partial P_{in}}{\partial \eta}\cdot \Delta \eta\right)^2} = \left|\frac{P_{waste}}{(1-\eta)^2}\cdot \Delta \eta\right| = \frac{P_{waste}}{(1-\eta)^2}\cdot \Delta \eta \tag{62}$$

where the Δ operator signifies absolute uncertainty. In order to convert this absolute uncertainty into relative uncertainty, the equation is divided by input power:

$$\left(\frac{\Delta P_{in}}{P_{in}}\right)_{loss\ approach} = \frac{\frac{P_{waste}}{(1-\eta)^2}\cdot \Delta \eta}{\frac{P_{waste}}{(1-\eta)}} \tag{63}$$

Therefore the relative uncertainty in input power using a motor loss method is

$$\left(\frac{\Delta P_{in}}{P_{in}}\right)_{loss\ approach} = \frac{\Delta \eta}{1-\eta} \tag{64}$$

where Δ operator signifies absolute uncertainty, P_{in} is input power, and η is motor efficiency.

However, in this investigation it may be more useful to normalize the uncertainty to the rated input power, rather than input power itself. Indeed, that is how the uncertainty criteria is framed in Table 1. The rated input power is at the full-load condition:

$$P_{in,rated} = \frac{P_{waste,rated}}{1-\eta_{rated}} \tag{65}$$

Dividing Equation 62 with Equation 65 results in

$$\left(\frac{\Delta P_{in}}{P_{in,rated}}\right)_{loss\ approach} = \frac{P_{waste}\cdot(1-\eta)^{-2}\cdot \Delta \eta}{P_{waste,rated}\cdot(1-\eta_{rated})^{-1}} \tag{66}$$

If the assumed motor efficiency is the rated full-load efficiency $(\eta = \eta_{rated})$, then Equation 66

[19] Using the Kline-McClintock error propagation method (Holman 2001, 51-53).

reduces to

$$\left(\frac{\Delta P_{in}}{P_{in,\,rated}}\right)_{loss\,approach} = \frac{P_{waste}}{P_{waste,\,rated}} \cdot \frac{\Delta \eta}{(1-\eta)} \tag{67}$$

If Equation 60 is solved for P_{waste}, then

$$P_{waste} = P_{shaft}\left(\frac{1}{\eta} - 1\right) \tag{68}$$

By extension, the rated waste power is

$$P_{waste,\,rated} = P_{shaft,\,rated}\left(\frac{1}{\eta_{rated}} - 1\right) \tag{69}$$

Again, if the assumed motor efficiency is the rated full-load efficiency $(\eta = \eta_{rated})$, then combining Equations 67 through 69 yields

$$\begin{aligned}\left(\frac{\Delta P_{in}}{P_{in,\,rated}}\right)_{loss\,approach} &= \frac{P_{shaft}}{P_{shaft,\,rated}} \cdot \frac{\Delta \eta}{(1-\eta)} \\ &= LF \cdot \frac{\Delta \eta}{(1-\eta)}\end{aligned} \tag{70}$$

Equation 70 is similar to Equation 64, except the load factor LF contextualizes the uncertainty in input power. Note that this is a best-case uncertainty because it neglects all errors in the model and uncertainties in the model parameters except for the uncertainty associated with motor efficiency.

3.3.1.2. Estimating Input Power Directly

A similar treatment can be done to determine the resilience of the Slip Method or Current Method from uncertainty in motor efficiency. Unlike the loss approach, the Slip or Current

methods of estimating motor power *directly* estimate the load factor, from which input power can be determined.

$$\left(P_{in}\right)_{direct\ approach} = LF \cdot \left(\frac{P_{shaft,\ full\ load}}{\eta}\right) \tag{71}$$

The partial derivative with respect to motor efficiency is

$$\left(\frac{\partial P_{in}}{\partial \eta}\right)_{direct\ approach} = LF \cdot P_{shaft,\ full\ load} \cdot \frac{(-1)}{\eta^2} \tag{72}$$

If it is assumed that the Slip or Current model is perfect (no errors) and all the parameters have zero uncertainty except for the motor efficiency, then the absolute uncertainty in input power is

$$\left(\Delta P_{in}\right)_{direct\ approach} = \sqrt{\left(\frac{\partial P_{in}}{\partial \eta} \cdot \Delta \eta\right)^2} = \left|\frac{\partial P_{in}}{\partial \eta} \cdot \Delta \eta\right| \tag{73}$$

Dividing the absolute uncertainty by the input power gives the relative uncertainty of the input power a model—such as the Slip or Current method—that uses the direct approach:

$$\left(\frac{\Delta P_{in}}{P_{in}}\right)_{direct\ approach} = \frac{\Delta \eta}{\eta} \tag{74}$$

As done earlier, it is useful to compare the uncertainty in input power to the rated input power. If the assumed motor efficiency is the rated full-load efficiency $(\eta = \eta_{rated})$, then

$$\left(\frac{\Delta P_{in}}{P_{in,\ rated}}\right)_{direct\ approach} = LF \cdot \frac{\Delta \eta}{\eta} \tag{75}$$

Again, note that this is a best-case uncertainty because it ignores any errors in the model and it also neglects all uncertainties in the model except for the uncertainty associated with motor efficiency.

3.3.1.3. Summary

Compare the effect on input power uncertainty (normalized to the rated input power) from uncertainty in efficiency between the loss approach and direct approach:

$$\left(\frac{\Delta P_{in}}{P_{in,\,rated}}\right)_{loss\,approach} = LF \cdot \frac{\Delta \eta}{(1-\eta)} \tag{76}$$

$$\left(\frac{\Delta P_{in}}{P_{in,\,rated}}\right)_{direct\,approach} = LF \cdot \frac{\Delta \eta}{\eta} \tag{77}$$

By comparing Equation 76 with Equation 77, we can conclude that the direct approach (e.g., slip or Current Method) is much more resilient from the effect of motor efficiency uncertainty than the motor loss method. Figure 5 compares the uncertainty in each method's power prediction at fully-load and half-loaded conditions if a motor's efficiency is 85%.

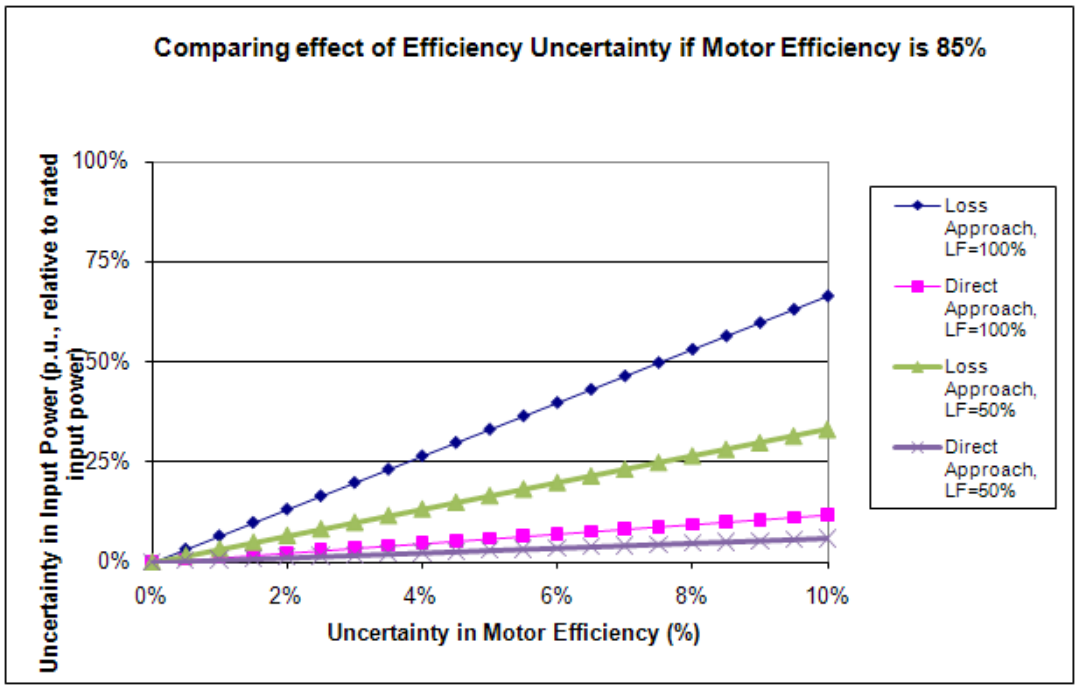

Figure 5: Comparing the effect of efficiency uncertainty on motor input power uncertainty if motor efficiency is 85%.

Recall that it is desired that motor input power be determined within ±20% of the nominal input power (Table 1). Also note that running motor efficiency in the field is an unknown quantity. Even at full-load, a motor with a nameplate efficiency of 85.5% is allowed by NEMA to have a running full-load efficiency of 82.5% (NEMA 2006, sec. 12.58.2). Hsu et al. recommend a ±10% efficiency uncertainty with using the nameplate method for motors loaded between 50% and 100% (1998, 122). Therefore it should be recognized that the loss approach is handicapped from uncertainty in motor efficiency values.

3.3.2. Investigating the Uncertainty of the Slip Method

Recall the basic slip model gives the percent motor load as:

$$LF = \frac{N_{sync} - N_{shaft}}{N_{sync} - N_{shaft,\,Full\,Load}} \tag{78}$$

The literature warns about the uncertainty of the full-load shaft speed. That will be investigated next, followed by an investigation of all of the Slip Method's parameters.

3.3.2.1. Considering only Shaft Speed Uncertainty

Nameplate full-load speed suffers from high uncertainties. First of all, manufacturers usually round their nameplate speed information to the nearest 5 RPM (EASA 1999, 18). That is small relative to the full-load speed, however it is rather large compared to the slip speed. Even more concerning is that NEMA gives motor manufacturers a large tolerance in the reporting of the full-load speed: the actual full-load speed can vary from the nameplate full-load speed by ±20% of the difference between the synchronous and rated speed (Revelt 1997, 2). If the motor is rewound, the tolerance will likely be even greater because rewinding may change the full-load speed from the nameplate value (Gopalakrishnan et al. 2006, 51).

If it assumed that the Slip Method model is perfect and all measurements are error-free except for the nameplate full-load shaft speed, then the uncertainty in motor load factor LF is[20]

$$\Delta LF = \sqrt{\left(\frac{\partial LF}{\partial N_{shaft,FL}} \cdot \Delta N_{shaft,FL} \right)^2} \tag{79}$$

where

$$\frac{\partial LF}{\partial N_{shaft,FL}} = \frac{N_{sync} - N_{shaft}}{(N_{sync} - N_{shaft,FL})^2} \tag{80}$$

using the load factor Equation 78.

NEMA MG 1-2006 states that "[t]he variation from the nameplate or published data speed of alternating-current, single-phase and polyphase, medium[21] motors shall not exceed 20 percent of the difference between synchronous speed and rated speed when measured at rated voltage, frequency, and load and with an ambient temperature of 25 ºC" (NEMA 2006, sec. 12.46). This

[20] Using the Kline-McClintock propagation-of-error method (Holman 2001, 51-53).

[21] A full classification of polyphase medium induction motors is available in NEMA MG-1 Section 10.32. At the least, medium motors include motors sized from 1.5 hp to 125 hp (NEMA 2006, 10.32.4).

gives an uncertainty in full-load shaft speed of

$$\Delta N_{shaft,FL} = (0.2)\cdot(N_{sync} - N_{shaft,FL}) \tag{81}$$

Combining Equations 78 and 79 through 81 gives

$$\begin{aligned}\Delta LF &= (0.2)\cdot\frac{N_{sync} - N_{shaft}}{N_{sync} - N_{shaft,FL}} \\ &= (0.2)\cdot LF\end{aligned} \tag{82}$$

It can be shown that if rated nameplate shaft power and motor efficiency have zero uncertainty, then applying the propagation-of-uncertainty method to Equation 11 yields

$$\Delta P_{in} = \frac{\Delta LF \cdot P_{rated}}{\eta_{motor}} \tag{83}$$

The performance requirement stated in objective statement (see Table 1) calls for

$$\Delta P_{in} \leq (0.20)\cdot P_{rated} \tag{84}$$

For a typical motor efficiency η_{motor} of 85%, combining Equations 82 through 84 gives the region that satisfies the performance requirement:

$$LF \leq \frac{0.2}{0.2}\cdot(0.85) = 0.85 \tag{85}$$

To summarize, if it assumed that the Slip Method model is perfect and the parameter uncertainties are zero except for the uncertainty in nameplate full-load shaft speed that is allowed by NEMA, then the Slip Method satisfies the the objective statement's performance requirement (Equation 84) for load factors $LF \leq 85\%$.

3.3.2.2. Considering Uncertainty in All Parameters in the Slip Method

In order to better understand the effect of the various parameters and their respective uncertainties on the model, an uncertainty analysis was done using the error propagation method:

$$\Delta LF \approx \left[\left(\frac{\partial LF}{\partial N_{shaft}} \cdot \Delta N_{shaft} \right)^2 + \left(\frac{\partial LF}{\partial N_{shaft,\,Full\,Load}} \cdot \Delta N_{shaft,\,Full\,Load} \right)^2 + \left(\frac{\partial LF}{\partial N_{sync}} \cdot \Delta N_{sync} \right)^2 \right]^{1/2} \quad (86)$$

where ΔLF is the uncertainty in the percent motor load LF, ΔN_{shaft} is the uncertainty in measured shaft speed N_{shaft}, and $\Delta N_{shaft,\,full\,load}$ is the uncertainty in full load (rated) shaft speed $N_{shaft,\,full\,load}$.

Figure 6 shows the relative uncertainty in the estimated load factor plotted as a function of normalized motor load factor. The only difference between the two curves is that one represents an 1800 RPM motor (with a full load speed of 1760 RPM) and the other curve represents a 3600 RPM motor (with a full load speed of 3510 RPM). Both curves have a synchronous shaft speed uncertainty of 0 RPM, a nameplate full-load shaft speed uncertainty of 5 RPM, and a measured shaft speed uncertainty of 1 RPM.

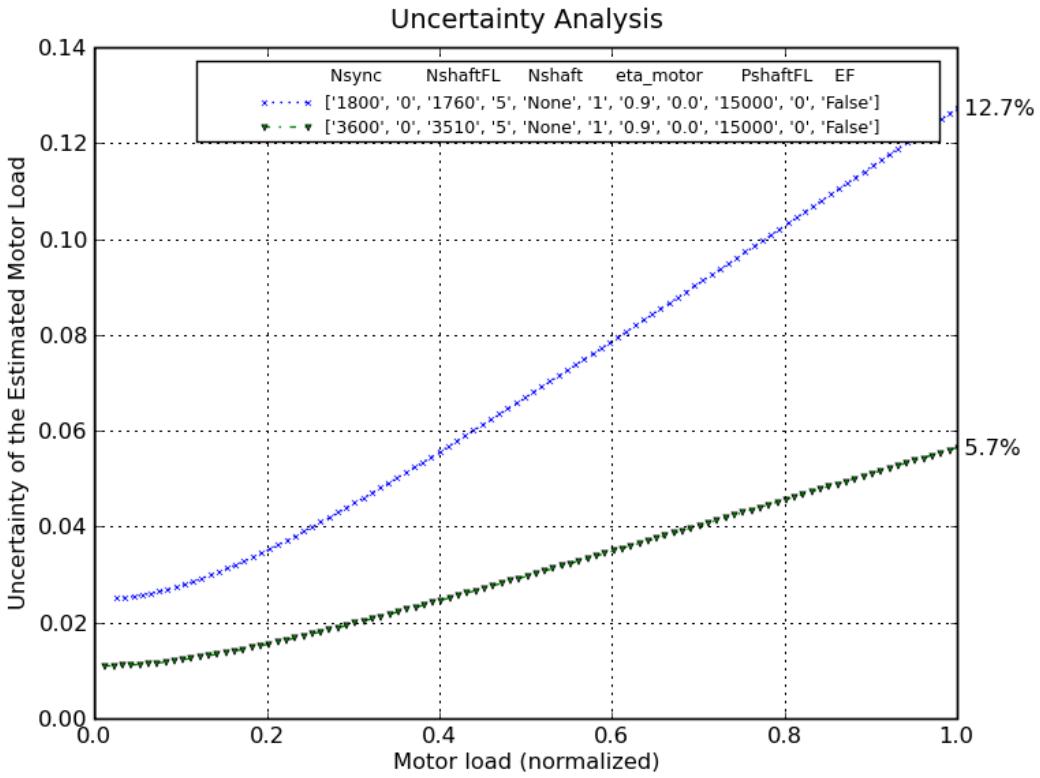

Figure 6: Relative uncertainty of estimated load as a function of load for a 1800 RPM motor and 3600 RPM motor.

Modifying the uncertainty values results in different uncertainty curve behavior. For example, Figure 7 shows the uncertainty behavior if the 1800 RPM motor has a 0 RPM synchronous speed uncertainty, 2 RPM full-load shaft speed uncertainty, and a 2 RPM measured shaft speed uncertainty; and if the 3600 RPM motor has a 0 RPM synchronous speed uncertainty, 10 RPM full-load shaft speed uncertainty, and a 2 RPM measured shaft speed uncertainty.

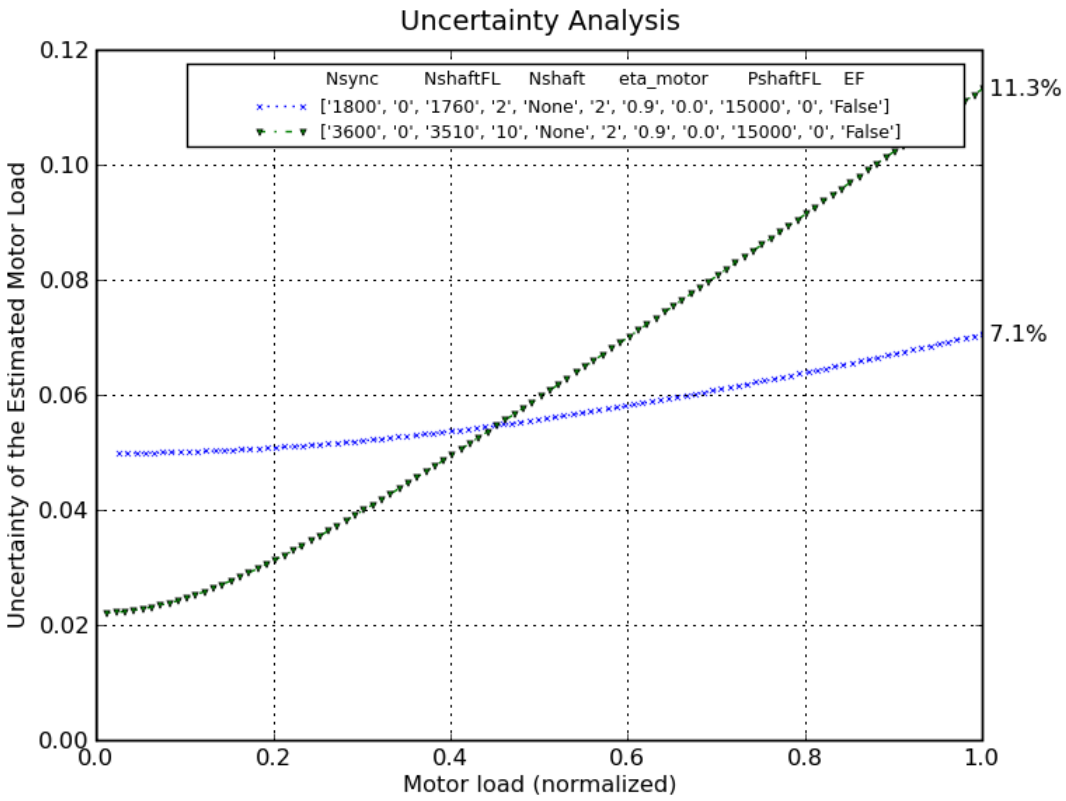

Figure 7: Effect of changing various parameter uncertainties.

While no conclusions were made from the plots from this particular uncertainty analysis, it is reported here for completeness.

4. EXPERIMENTS AND DATA ANALYSIS

4.1. STATISTICAL METRICS

In order to evaluate the load factor or input power prediction methods, several statistical metrics are used. In this investigation, the residual is defined as the predicted value minus the actual or measured value:

$$Residual = Predicted\ Value - Measured\ Value \tag{87}$$

The Mean Bias Error (MBE) is determined by

$$MBE = \frac{\sum_{i=1}^{n} Residual_i}{n} \tag{88}$$

where i is a dummy variable and n is the number of data points.

The root mean square error (RMSE)[22] is defined as

$$RMSE = \left(\frac{\sum_{i=1}^{n} Residual_i^2}{n-k} \right)^{1/2} \tag{89}$$

where i is a dummy variable, n is the number of data points. When used in regression, k is the number of regression coefficients (including the intercept if it is allowed to be nonzero) (Chiulli 1999, 274). When the predicted value is not determined from regression, $k = 1$.

When used to evaluate motor input power, the RMSE has units of power (e.g. kW). In order for easy evaluation across multiple motors (no matter their size), the RMSE is normalized by dividing by the nominal input power of the motor:

[22] When used in regression, the RMSE is often referred to as the standard error of the regression (SER) or the standard error of the estimate.

$$RMSE_{pu} = \frac{RMSE}{P_{nominal\,input}} = \frac{RMSE \cdot \eta_{motor,\,nameplate}}{P_{shaft,\,nameplate}} \tag{90}$$

This percent unit (p.u.) metric allows easy comparison to the requirements of the present research.

Confidence intervals for the population mean can be established with

$$MBE \pm z \cdot (SE_{mean}) = MBE \pm z \cdot \frac{\sigma}{\sqrt{n}} \tag{91}$$

where MBE is the mean bias error, $z = 1.96$ for the 95% confidence level, and the standard error of the mean is the ratio of the sample standard deviation σ and the square root of the sample size n (Miles and Shevlin 2001, 9). For small samples sizes (e.g. $n < 30$), the z statistic is replaced with Student's t value, which is determined by the $n-k$ degrees of freedom and the desired significance level.

Confidence intervals for coefficients of regression parameters can be established with

$$Coefficient\ Value \pm t \cdot SE_{regression\ parameter} \tag{92}$$

where the standard error of the regression parameter $SE_{regression\ parameter}$ is given for each regression parameter by regression packages and the Student's t value is determined by the $n-k$ degrees of freedom and the desired significance level (Weisberg 2005, 32-33).

Confidence intervals for a predicted value at a specific value (x_0) can be determined by

$$Prediction \pm t \cdot RMSE \cdot \left(1 + \frac{1}{n} + \frac{(x_0 - \bar{x})^2}{\sum_{i=1}^{n} (x_i - \bar{x})^2} \right)^{1/2} \tag{93}$$

where $\bar{x}$ is the average value. The last term in the square root is often much smaller than the other terms, which suggests it can be ignored. Indeed, using $\pm 2 \cdot RMSE$ provides an approximate confidence interval (at the 95% confidence level) for future predictions (Wilks 2006, 194-195; Chiulli 1999, 275).

4.2. SLIP AND CURRENT METHOD ANALYSIS USING MANUFACTURER PERFORMANCE DATA

Recall in Section 2.2.3.1. that Gopalakrishnan et al. reported a regression-improved form of the Slip Method that incorporated a motor's nameplate voltage. Hsu notes that a modified version of the Slip method in conjunction with other nameplate values and built-in statistical data can improve the accuracy for a targeted group of motors (Hsu et al. 1998, 120). It was conjectured that other nameplate parameters—such as nameplate horsepower, nameplate synchronous speed, nameplate power factor, locked rotor code, and NEMA design code—might additionally be able to improve these methods. Before conducting expensive motor experiments in the laboratory, it seemed expedient to acquire motor performance data and determine what parameters—if any—were of interest in improving the Slip and Current Methods.

While such motor performance data may be obtained manually by experimentation, some motor manufacturers provide them on their websites. Unfortunately, some manufacturers limit the distribution of the motor performance data by requiring an email request, which is daunting if one would like to obtain performance data for hundreds of motors. Other manufacturers provide the data as curves on a graph which are difficult to convert to machine-readable numbers. Baldor Electric Company and Reliance Electric are two motor manufacturers that provide motor performance data on their websites. Although Baldor acquired Reliance in 2007, each brand had unique motors and the performance data was provided in different formats. In order to acquire the Baldor data, a Python script was created to spider through their motor HTML pages, download the motor specifications and performance data, and parse the data into a HDF5-format database. Acquiring the Reliance motor data took significantly more work than for the Baldor data because they stored their data in PDF-format files and used multiple data schemes for storing their data. Web spidering, data parsing, and data analysis was done with the Python language—which was extended with SciPy/NumPy for array manipulation, PyTables for database interfacing, and Matplotlib for plotting graphs (Jones et al. 2009; Alted and Vilata 2009; Hunter 2009).

Data for 720 Baldor motors was obtained, but this was reduced to 350 motor data sets for motors

equal to or greater than 5 HP. Data for 2023 Reliance motors was obtained, however only 1377 of these motors contained parseable motor performance data. Of these, only 556 Reliance motors were between 5 and 75 horsepower, had synchronous speeds not less than 1200 RPM, and did not have glaring errors[23] in the performance data.

Unfortunately, some of the motor performance data was repetitious. Figure 8 shows the average residual error for each motor using the basic Slip Method described in Equation 78. Upon zooming in (see Figure 9), it is apparent that many motors share identical average residual values.

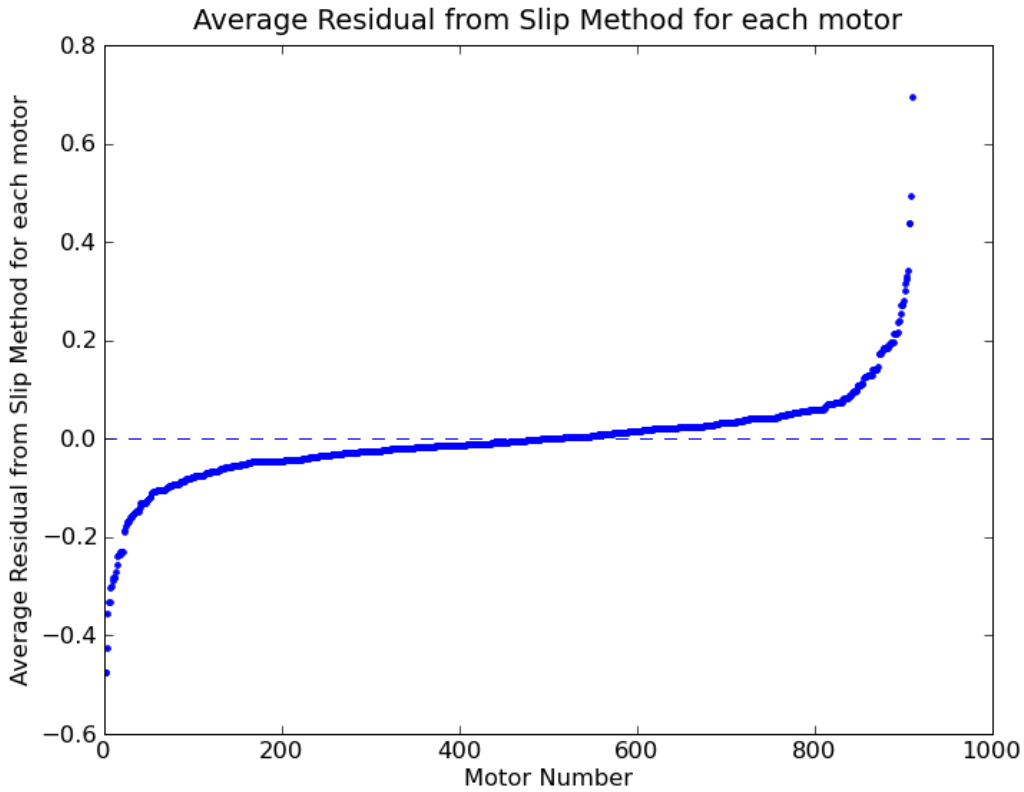

Figure 8: Average residual from Slip Method for each motor.

[23] Eleven Reliance motors were rejected for "glaring errors" (e.g., measured shaft speed was greater than rated synchronous speed).

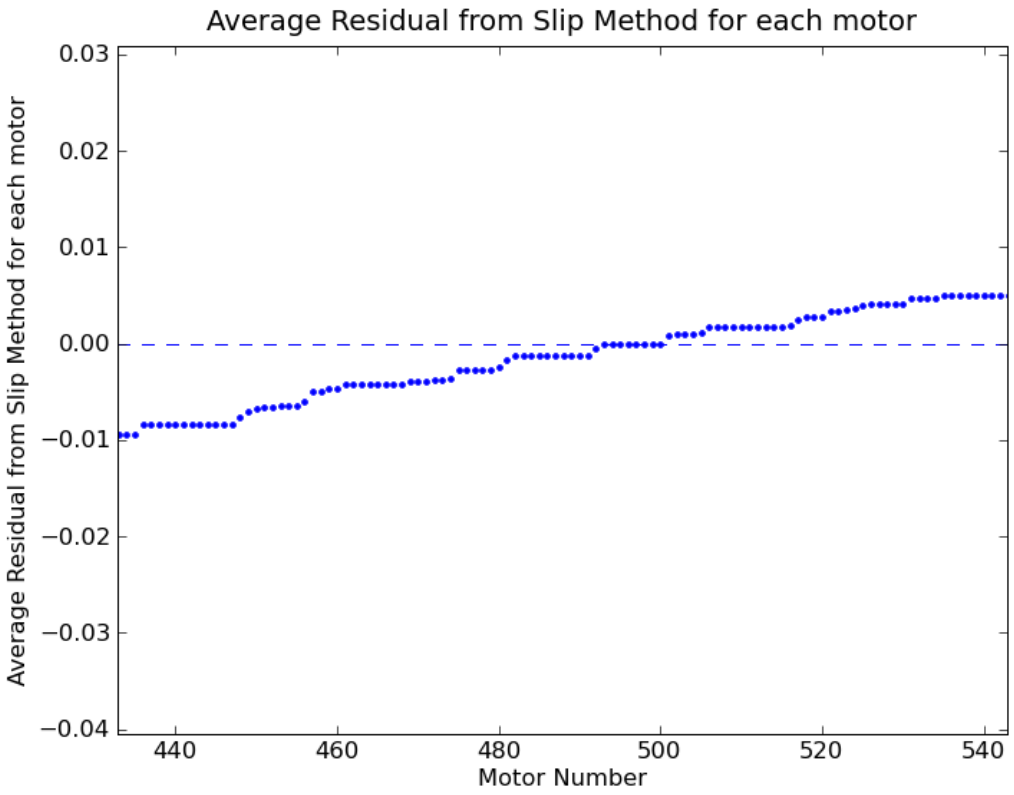

Figure 9: Average residual from Slip Method for each motor (zoomed in).

In order to remove the superfluous motors, a consolidation function that considers a motor's residuals and nameplate values and attempts to group quasi-identical motors together was created. Consolidating quasi-identical motors further reduced the Baldor and Reliance data to a population of 550 motors.

Using the motor performance data, the Slip Method and Current Method were used to predict the motor's load factor. The residuals are defined as the predicted load factors minus the actual values. The error bars correspond to a 95% confidence level that the population mean bias error is within the limits.

4.2.1. Slip Method

Recall the Slip Method of estimating motor load:

$$LF = \frac{N_{sync} - N_{shaft}}{N_{sync} - N_{shaft,\ Full\ Load}} \tag{94}$$

4.2.1.1. Slip Method Residuals as a Function of Various Nameplate Parameters

Each plot shows the mean bias error and the standard deviation. Each mean bias error data point is bounded by limit bars which represents the interval that the population mean lies in at the 95% confidence level as determined by Equation 91. Beside each standard deviation data point is a number in parentheses which represents the number of motors in that data point. Figure 10 shows the Slip Method residuals as a function of rated horsepower. Not only is it difficult to discern a general trend that exists for both motor manufacturers, but each manufacturer does not appear to have its own trend (especially with such large error bars[24]). In fact, the same can be said for the Slip Method residuals as a function of other nameplate parameters, such as Nameplate Synchronous Speed (Figure 11), Nominal Power Factor (Figure 12).

[24] Unless otherwise stated, the error bars show the interval for which the population mean may lie at a 95% confidence level.

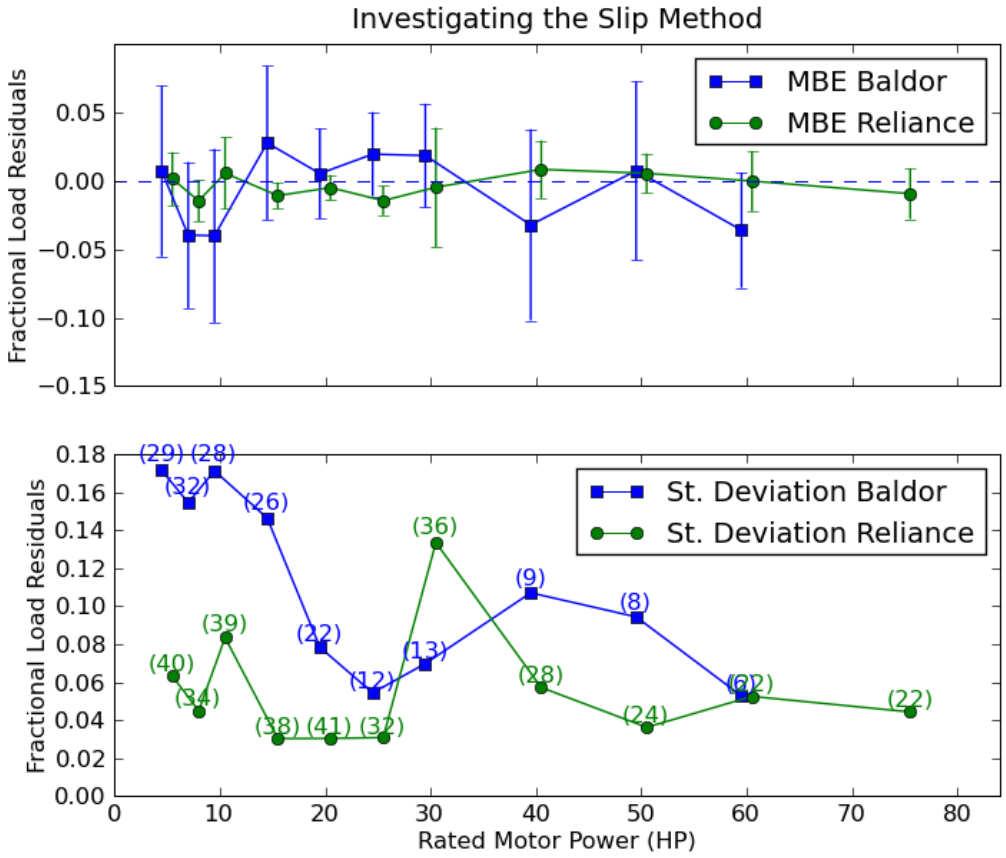

Figure 10: Slip Method residual as function of rated horsepower. In the plot, values have been shifted so that error bars don't overlap.

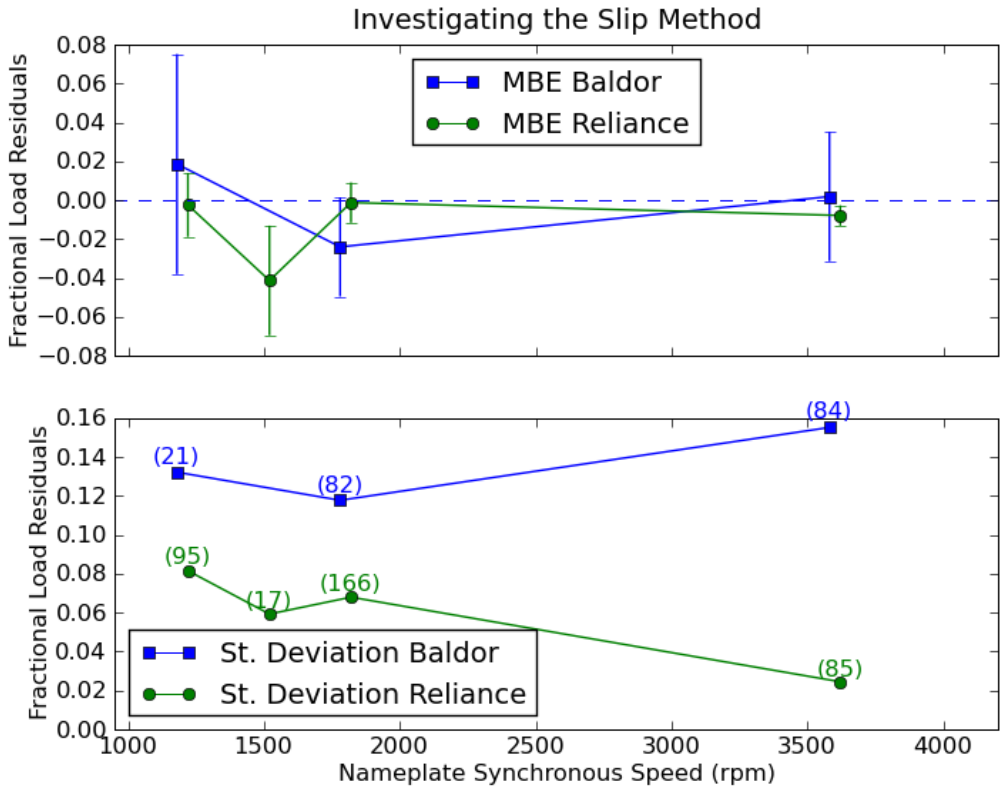

Figure 11: Slip Method residual as function of nameplate synchronous speed. In this plot, the values are shifted so that error bars do not overlap.

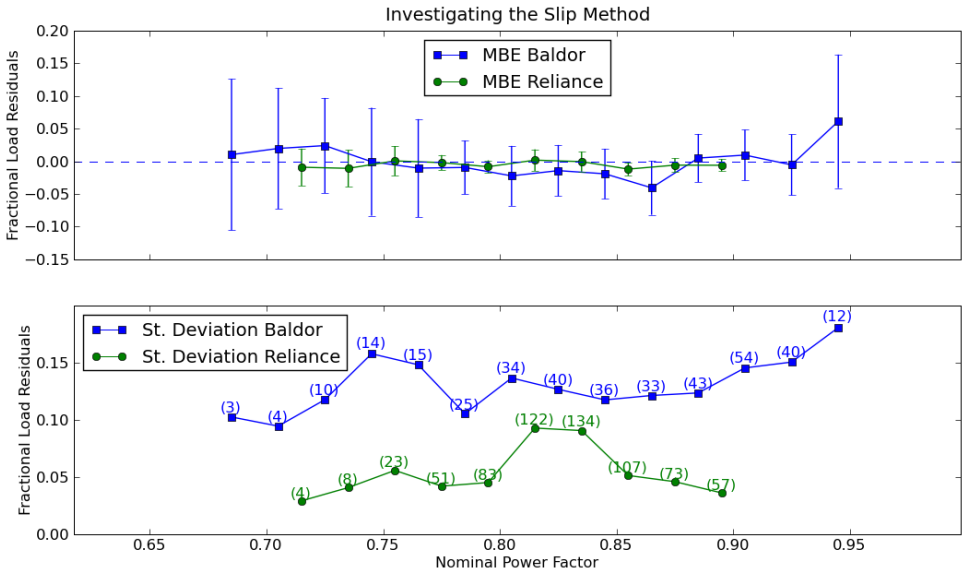

Figure 12: Slip Method residual as function of nameplate power factor.

4.2.1.2. Slip Method Residuals as a Function of the Predicted Variable

The previous plots do not show significant and consistent dependencies on the explored nameplate variables. However, when the Slip Method residuals are plotted against the predicted Slip Method variable, a trend is observed. Notice that Figure 13 shows both the Baldor and Reliance motors exhibit a somewhat U-shaped behavior[25]. Also notice the standard deviations for the Baldor motors are significantly higher than the Reliance motors. Possible causes for such discrepancies include different motor design schemes, different manufacturing procedures and allowed tolerances, and different testing laboratory procedures. Multiple attempts at contacting Baldor and Reliance for information regarding their motor testing procedures were futile.

Figure 14 shows the general trend for all motors, regardless of manufacturer.

[25] Without submitting evidence, I conjecture that the U-shape behavior in the Slip Method residuals may be due to the first order polynomial approximation that is applied to the steady-state portion of the motor's Torque-Speed curve. See Appendix A.

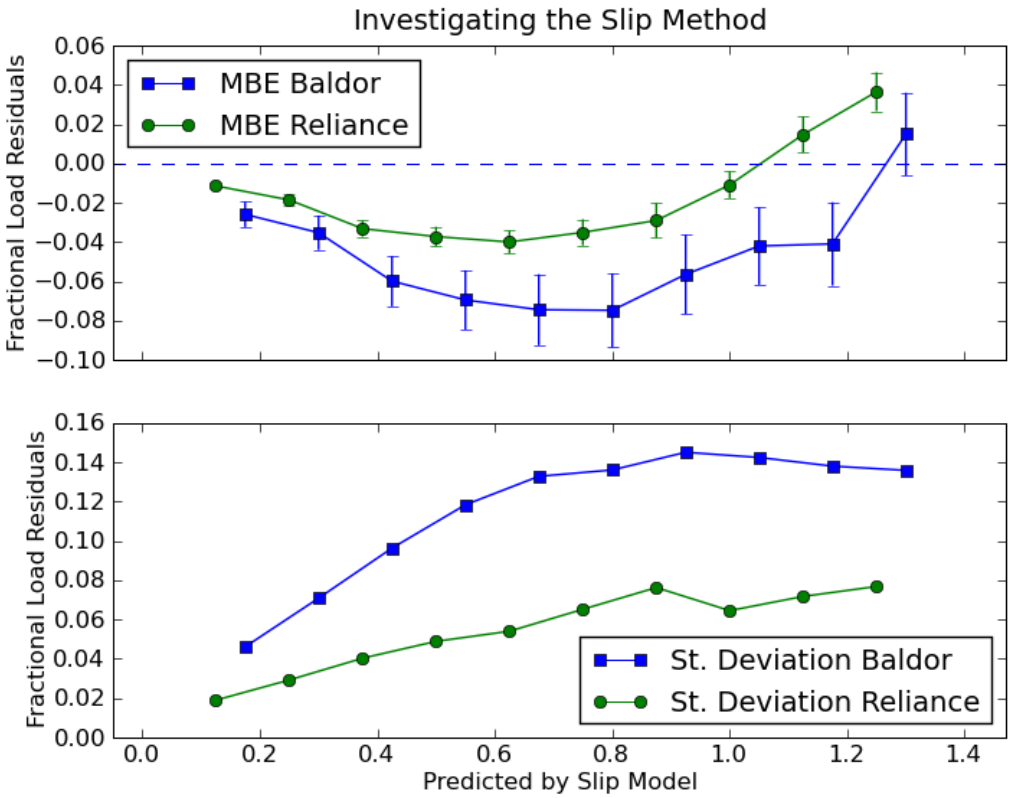

Figure 13: Slip Method residual as function of Slip Method prediction (contrasting Baldor and Reliance performance).

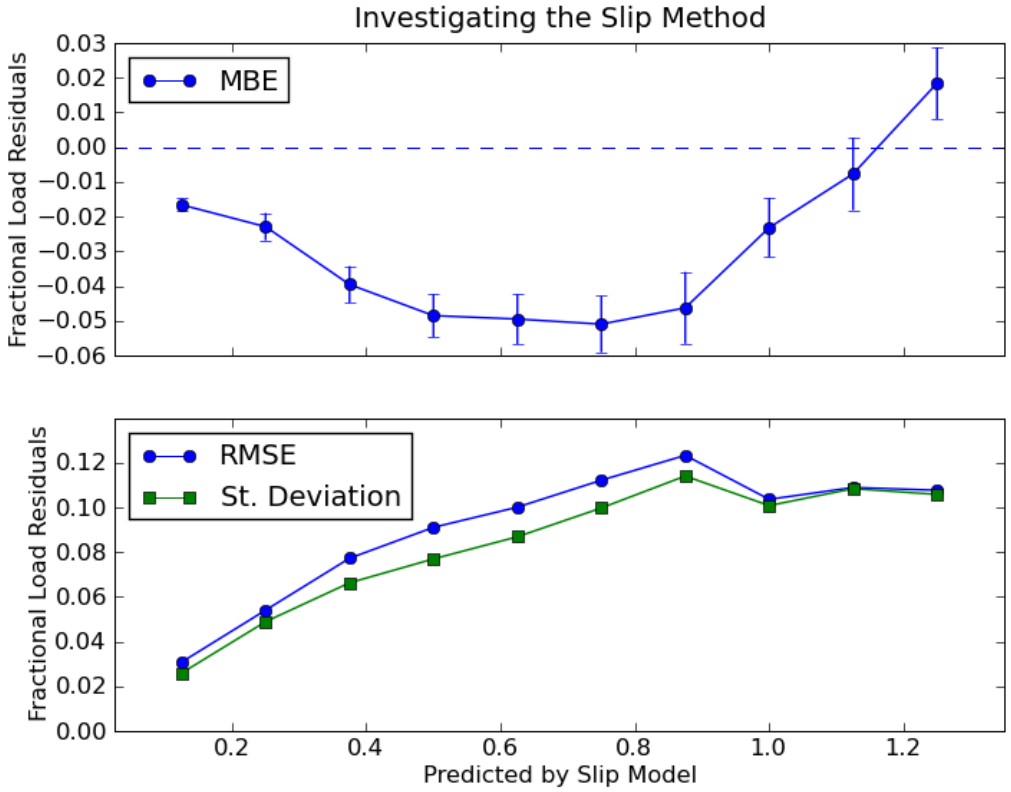

Figure 14: Slip Method residual as function of Slip Method prediction.

The RMSE for the Slip Method (Figure 14) gives an overall RMSE of 9.0%. Since the RMSE curve is above the standard deviation curve, Figure 14 suggests that the Slip Method may be improved using regression. In Figure 14, the load factor predicted by the Slip Method is compared to the actual load factor. Thus for this case the model is simply the load factor predicted by the basic Slip Method:

$$LF_{model} = LF_{slip} \tag{95}$$

where the predicted load factor of the motor using the basic Slip Method is

$$LF_{slip} = \frac{N_{sync} - N_{shaft}}{N_{sync} - N_{shaft,FL}} \tag{96}$$

In order to improve the prediction of the motor load factors, a second model is created which

corrects for the errors with a second-order polynomial:

$$\begin{aligned} LF_{model} &= LF_{slip} + Error \\ &= LF_{slip} + (a_2 \cdot LF_{slip}^2 + a_1 \cdot LF_{slip} + a_0) \\ &= a_2 \cdot LF_{slip}^2 + (a_1 + 1) \cdot LF_{slip} + a_0 \end{aligned} \tag{97}$$

A linear regression using the second-order polynomial (Equation 97) with the predicted slip load factor and the measured load factor on both the Baldor and Reliance motors yielded the coefficients shown in Table 5.

Table 5: Coefficients for Equation 97 determined by regression of the Baldor and Reliance motor performance data.

Coefficient	Value	St. Error of the Coefficient	Confidence Interval[26]
a_0	-0.006	0.004	±0.01
a_1	0.196	0.013	±0.03
a_2	-0.167	0.010	±0.02

Figure 15 shows the regression-improved Slip Method using the coefficients in Table 5 and Equation 97. Notice that the RMSE curve now essentially follows the standard deviation curve. Using the regression-improved Slip Method, the overall RMSE goes to 8.2% (from 9.0% without the regressed residuals). This regression applied equal weights to the data points. A more sophisticated approach could assign increased weights for the higher loads. The given regression used a composite of the Baldor/Reliance data. Recall Figure 13 which shows distinct behavior for the two studied manufacturers. Reduced RMSEs should be realized if manufacturer specific regression curves are generated.

[26] Confidence interval is determined using Equation 92 at the 95% confidence level.

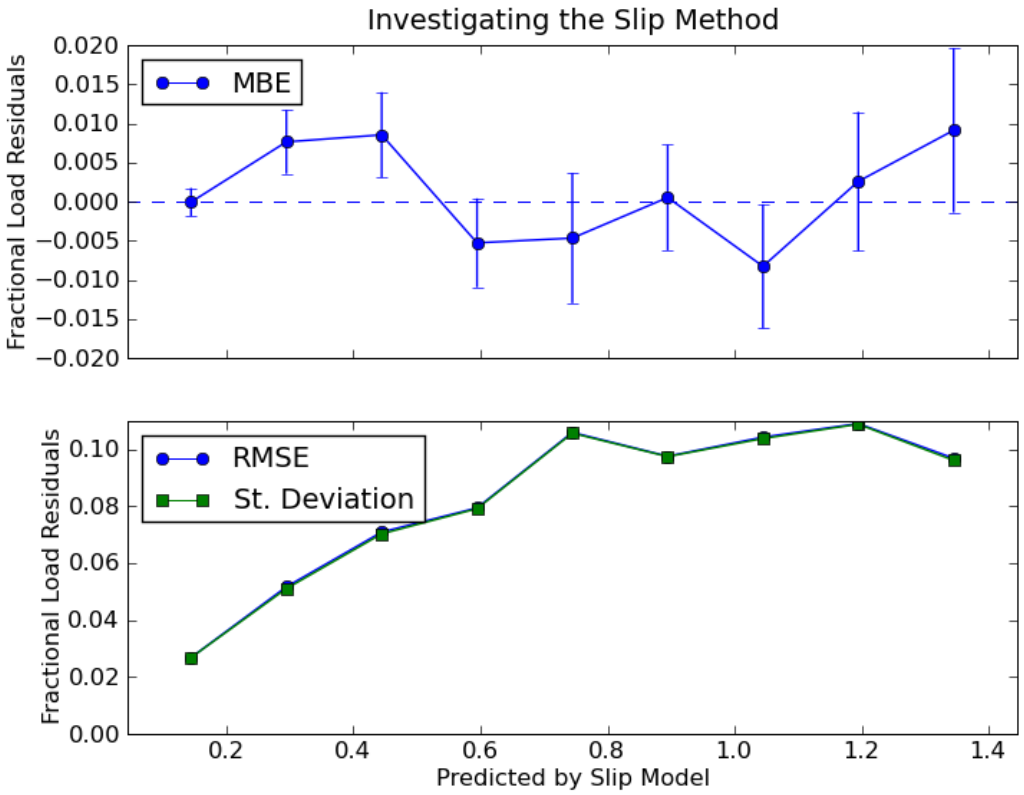

Figure 15: Regression of Slip Method residual as function of Slip Method prediction.

4.2.2. Current Method

4.2.2.1. Assuming No-Load Current is Zero

Recall the simplest Current Method, where the no-load current is assumed to be 0:

$$LF = \frac{I - I_{No\ Load}}{I_{Full\ Load} - I_{No\ Load}} = \frac{I}{I_{Full\ Load}} \tag{98}$$

Figure 16 plots the load fraction residuals for the Current Method (with $I_{No\ Load} = 0$) using all of the Baldor/Reliance data. Compare Figure 16 (the Current Method) with Figure 14 (the Slip

Method). Notice that above 70% load the RMSE and standard deviation for the Current Method is less than the Slip Method.

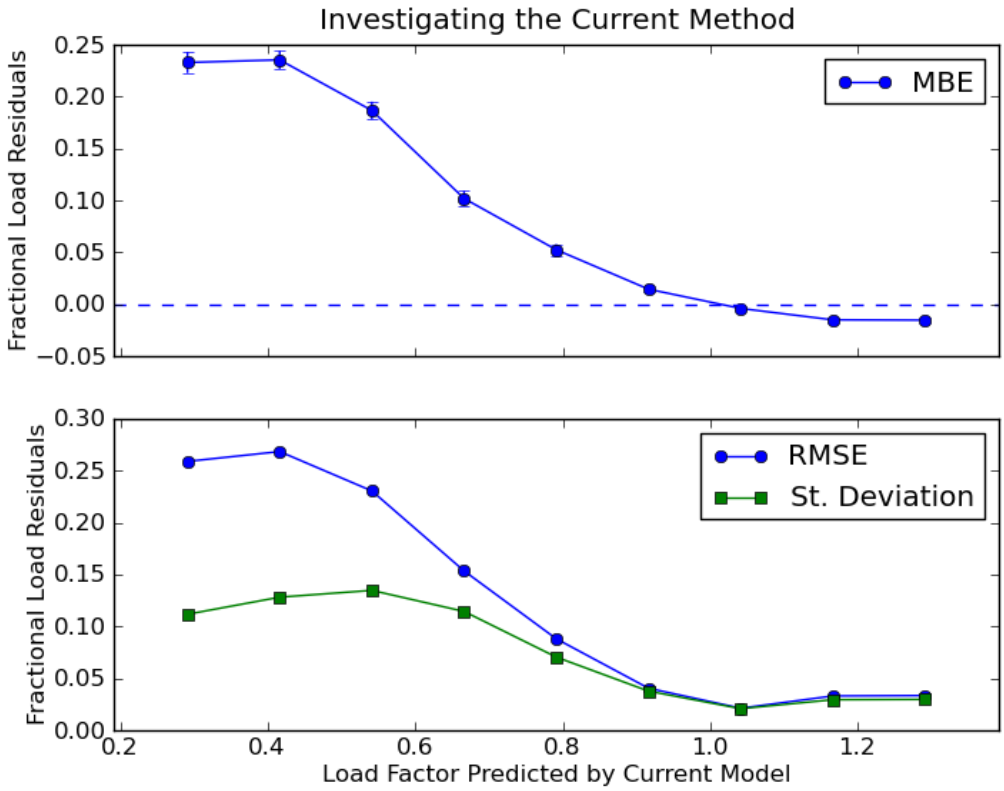

Figure 16: Current Method residual as function of Current Method prediction.

Recall that various nameplate parameters were not able to improve the Slip Method for the Baldor and Reliance motors. However, the Current Method residuals seem to have slightly more dependence on some nameplate values. For example, notice the dependence of the Current Method residuals on the Nominal Power Factor (Figure 17) and Nameplate Synchronous Speed (Figure 18). Also notice the large dependence of the Current Method residuals on the motor manufacturer.

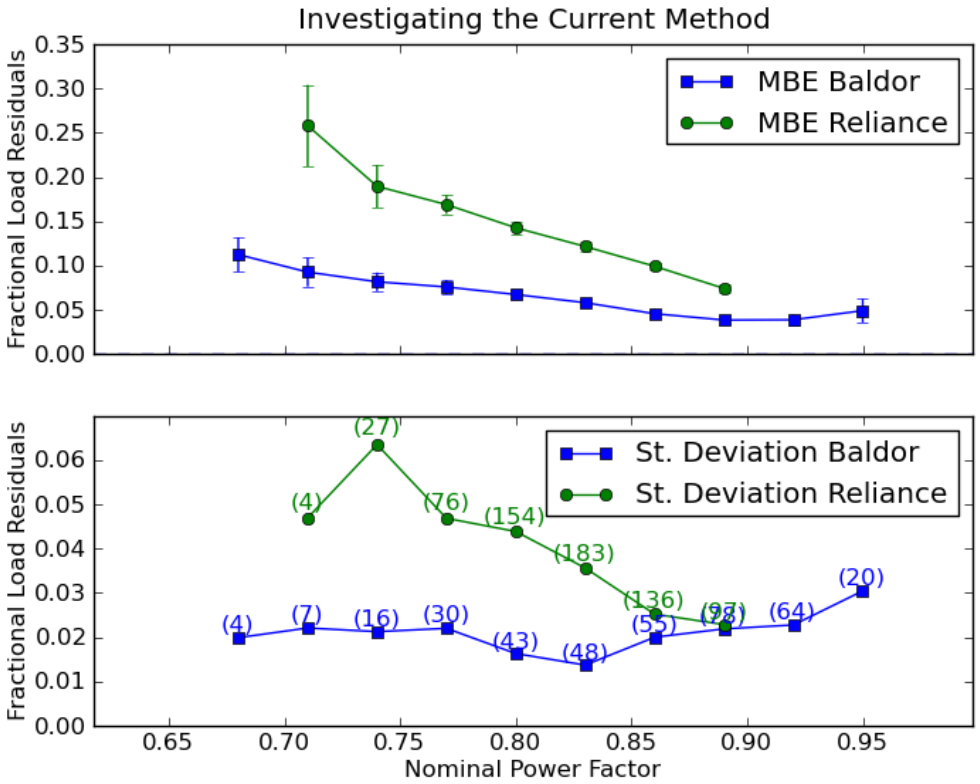

Figure 17: Current Method residual as function of nominal power factor.

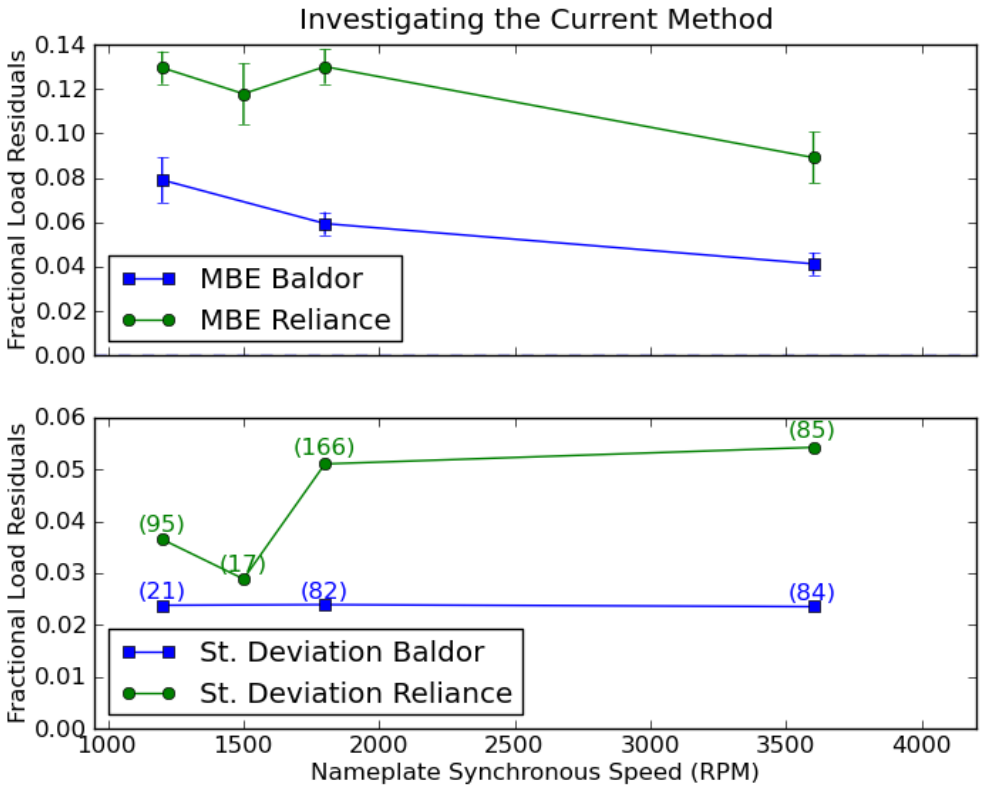

Figure 18: Current Method residual as function of nameplate synchronous speed.

4.2.2.2. Estimating No-Load Current

The Current Method can be improved if an estimate of the no-load current can be made. Often times, the no-load current is assumed to be a certain fraction of the full-load current:

$$I_{No\ Load} = k \cdot I_{Full\ Load} \tag{99}$$

where k is some fraction (Nailen 1994, 36).

Various authors give rough estimates for the no-load fraction, ranging from 25% to 40% (Holmquist, Rooks, and Richter 2004, 245; Gopalakrishnan et al. 2006, 40; Penrose 2004). The lower the horsepower and higher the number of poles, the higher the no-load current if harmonics and differing voltage is not present (Electrical Apparatus 2007, 6).

Figure 19 shows the Current Method residuals with various *k*-values applied to the Baldor/Reliance motor data. Notice that a k-value of 0.3 seems to have the lowest RMSE for this data set.

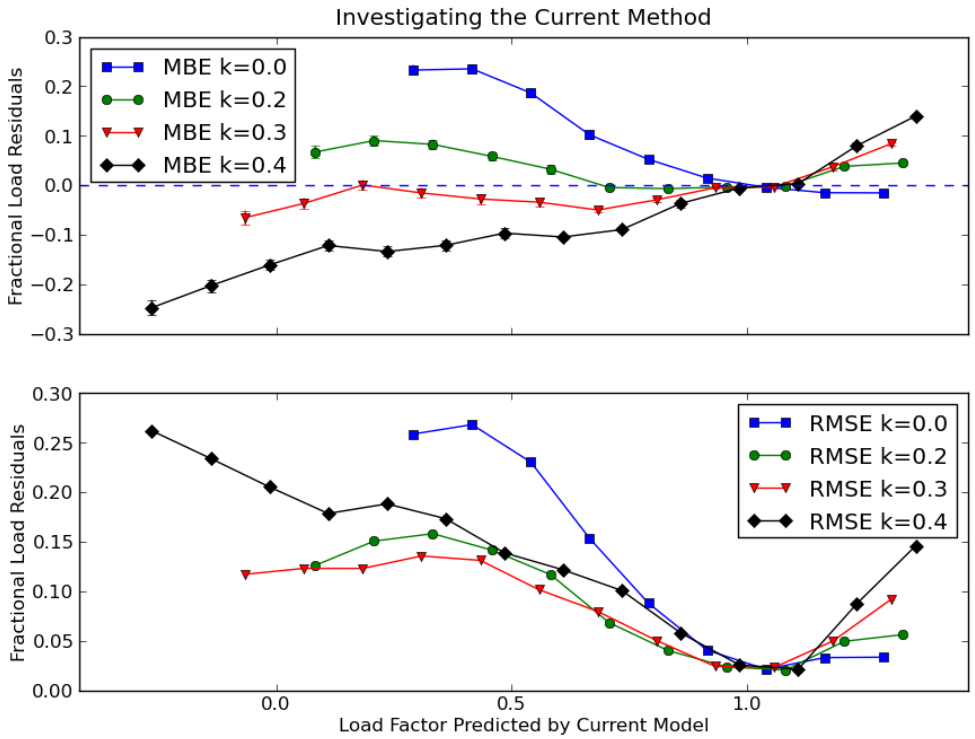

Figure 19: Current Method residual as function of Current Method with various k-values.

Figure 20 shows the application of the Current Method with a *k*=0.3 to the Baldor/Reliance data. Further improvement may be realized by predicted the k-value from nameplate parameters, such as horsepower and synchronous speed.

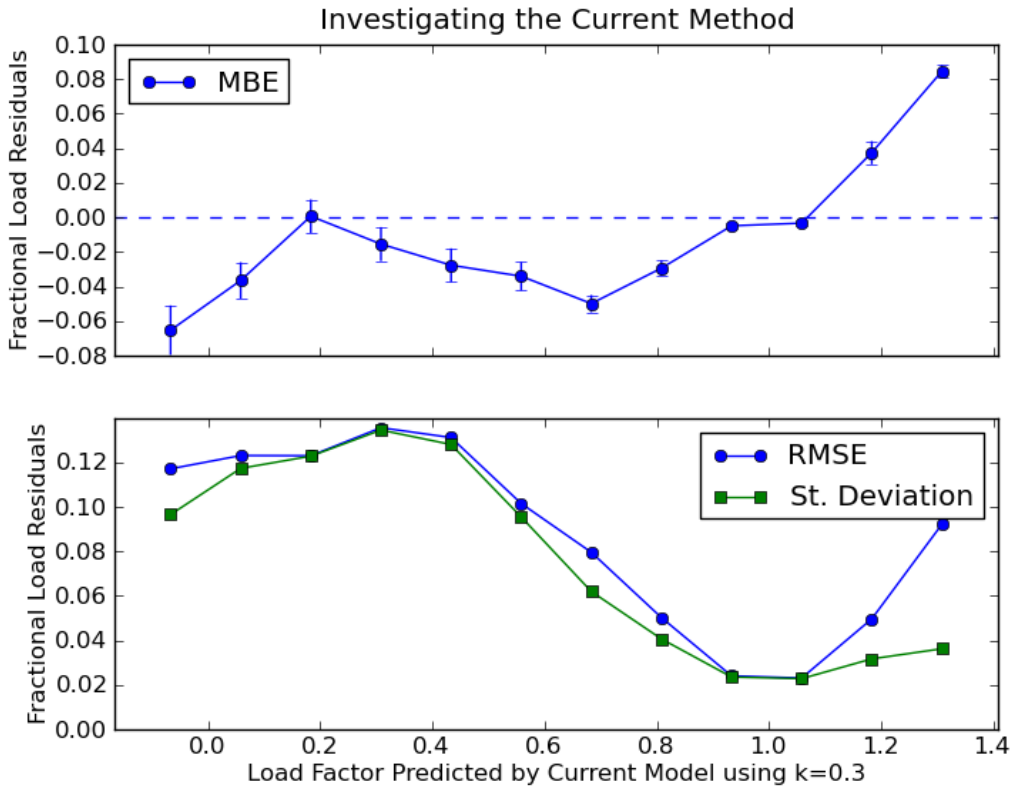

Figure 20: Current Method residuals as a function of Current Method with k=0.3

4.2.3. Comparison of Power Prediction Methods

In Sections 4.2.1. and 4.2.2., the performance of the Slip and Current Methods of estimating motor load factors has been considered. However, the real objective is motor power estimation, not load factor estimation. Migrating from motor load factor to motor input power requires an efficiency estimate. In the following plots and statistical metrics, the motor's running efficiency estimate is assumed to be the nameplate efficiency. Since it is input power—not load factor—that is being sought after here, the performance of the $V{\cdot}I{\cdot}PF{\cdot}\sqrt{3}$ method will also be shown. In the motor input power prediction context, the motor census for the Baldor/Reliance motors was 459 motors (instead of 550) because some motors did not have the required efficiency information.

Recall, the input power predicted by the Current Method is

$$P_{in} = \frac{I - I_{No\ Load}}{I_{Full\ Load} - I_{No\ Load}} \cdot \left(\frac{P_{shaft,rated}}{\eta_{motor}} \right) \tag{100}$$

In the following plot and statistical metrics, the no-load current is assumed to be zero: $I_{No\ Load} = 0$.

It follows that motor input power from the $V \cdot I \cdot PF \cdot \sqrt{3}$ method is

$$P_{in} = V \cdot I \cdot PF \cdot \sqrt{3} \tag{101}$$

In the following plot and statistical metrics, the supply voltage is assumed to be the motor's rated value and the power factor is either the rated value or 1.

The input power predicted by the Slip Method (including the torque factor) is given by

$$P_{in} = \frac{N_{sync} - N_{shaft}}{N_{sync,rated} - N_{shaft,rated}} \cdot \left(\frac{N_{shaft}}{N_{shaft,rated}} \right) \cdot \left(\frac{P_{shaft,rated}}{\eta_{motor}} \right) \tag{102}$$

Figure 21 shows the performance of the Current Method, $V \cdot I \cdot PF \cdot \sqrt{3}$, and Slip Method at predicting motor input power as a function of the normalized motor input power; Table 6 summarizes the performance of each method across all loads. The predicted input power—and input power residuals—have been normalized to each motor's nominal input power $P_{in,nominal} = P_{shaft,rated} / \eta_{rated}$. In Figure 21, the Current Method gives lower RMSE_pu values than using $V \cdot I \cdot PF \cdot \sqrt{3}$ to estimate motor input power.[27] Also notice that the Slip Method gives lower RMSE_pu than the Current Method at lower loads; at higher loads, the Current Method gives lower RMSE_pu values. The point of intersection is about 68% of the normalized predicted input power. Across all normalized predicted input power values, the Current Method and Slip Method give comparable RMSE_pu values: 10.0% and 9.9%, respectively. The Slip Method used in Figure 21 and Table 6 incorporate the torque factor $N_{shaft} / N_{shaft,rated}$. If that factor is neglected, the MBE_pu decreases by 0.2% points (i.e., moves further away from 0) and

[27] Although below 60% of the normalized predicted input power, using $V \cdot I \cdot PF \cdot \sqrt{3}$ with nameplate power factor gives similar RMSE_pu values.

the RMSE_pu increases by 0.2% points. Such a minor deterioration explains why the torque factor is often ignored in hand calculations.

Table 6: Comparison of Current Method, $V{\cdot}I{\cdot}PF{\cdot}\sqrt{3}$, and Slip Method at predicting input power for the Baldor/Reliance motors.

Method for Predicting Motor Input Power	MBE_pu	RMSE_pu
Current Method (k=0, Efficiency=Nameplate)	5.4%	10.0%
$V{\cdot}I{\cdot}PF{\cdot}\sqrt{3}$ (PF=Nameplate)	8.5%	18.6%
$V{\cdot}I{\cdot}PF{\cdot}\sqrt{3}$ (PF=1)	22.9%	27.6%
Slip Method (with Torque Factor, Efficiency=Nameplate)	-3.2%	9.9%

It should be noted that this data analysis does not consider under/over-voltage or voltage imbalance conditions.

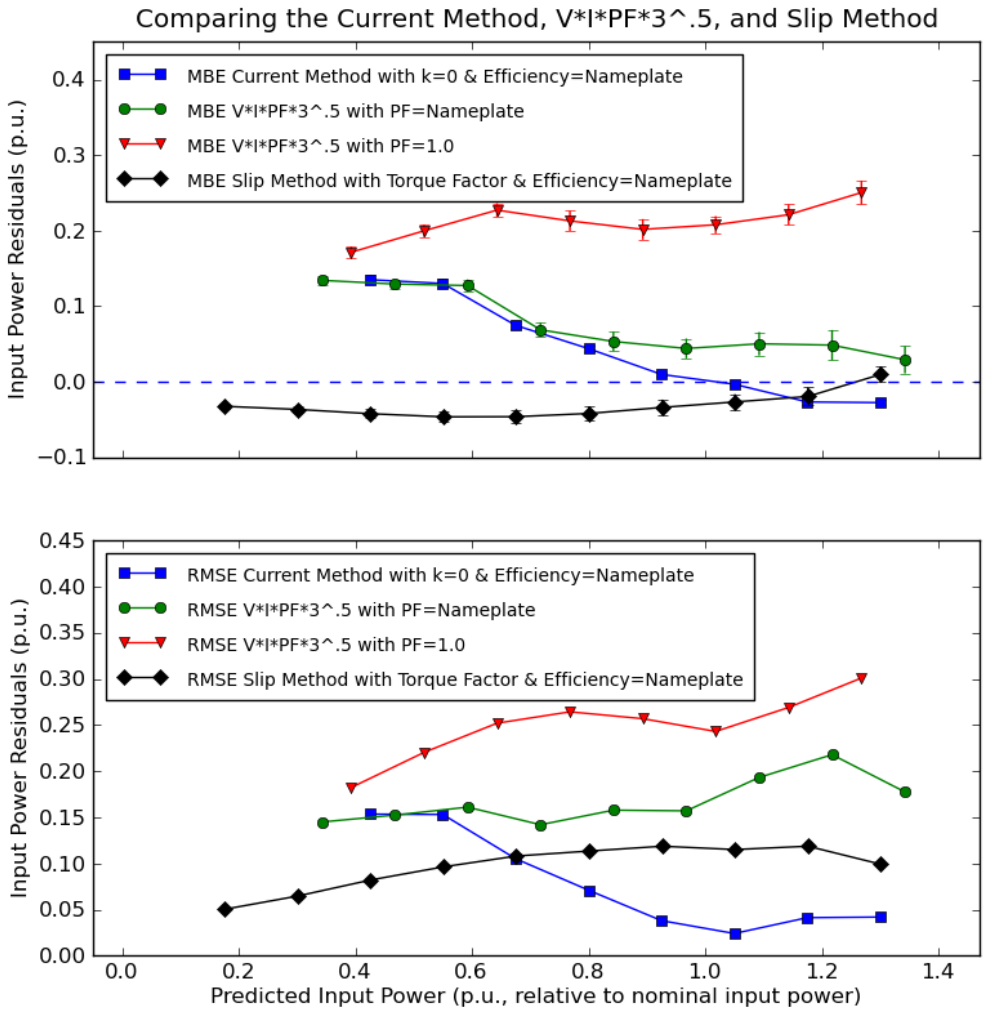

Figure 21: MBE_pu and RMSE_pu of residuals from predicting motor input power using the Current Method, $V \cdot I \cdot PF \cdot \sqrt{3}$, and Slip Method.

4.2.4. ORMEL Evaluation

Recall that ORMEL is an algorithm that estimates motor load factor and motor efficiency. ORMEL is implemented in the MotorMaster+ 4.0 motor managing software (Washington State University Cooperative Extension Energy Program 2003, 58). A limited subset of the Baldor

motors—21 motors ranging from 10 to 40 HP—was used to compare the Slip Method of estimating motor load factor and the ORMEL method of estimating motor load factor. Since the manufacturer's performance data was specified at the 25%, 50%, 75%, and 100% load factor levels, the Slip Method and ORMEL algorithm were also compared at these levels. The actual supply voltage was assumed to be at the nameplate rated voltage[28]. These assumptions allowed easy comparison between the manufacturer's performance data, Slip Method prediction, and ORMEL algorithm prediction.

The load factor for the Slip Method was calculated as

$$LF_{slip} = \frac{N_{sync} - N_{shaft}}{N_{sync} - N_{shaft,\,FL}} \tag{103}$$

The load factor predicted from the ORMEL algorithm was determined by specifying the nameplate parameters (see Figure 22) and the measured shaft speed (see Figure 23) in MotorMaster+ 4.0. The load factor residuals were determined by subtracting the measured load factor from the predicted load factor.

[28] Changing the supply voltage in ORMEL did not effect the predicted load factor or motor efficiency. It is well-known that supply voltage has a strong effect on motor slip, so any method such as the Slip Method or ORMEL algorithm that relies on shaft speed is vulnerable to an effect from supply voltage. The voltage-compensated Slip Method (Equation 19) attempts to correct for this, but from my limited observation the ORMEL method doesn't. Whether this was an error on my part, an ORMEL design limitation, or a MotorMaster+ software bug is not known.

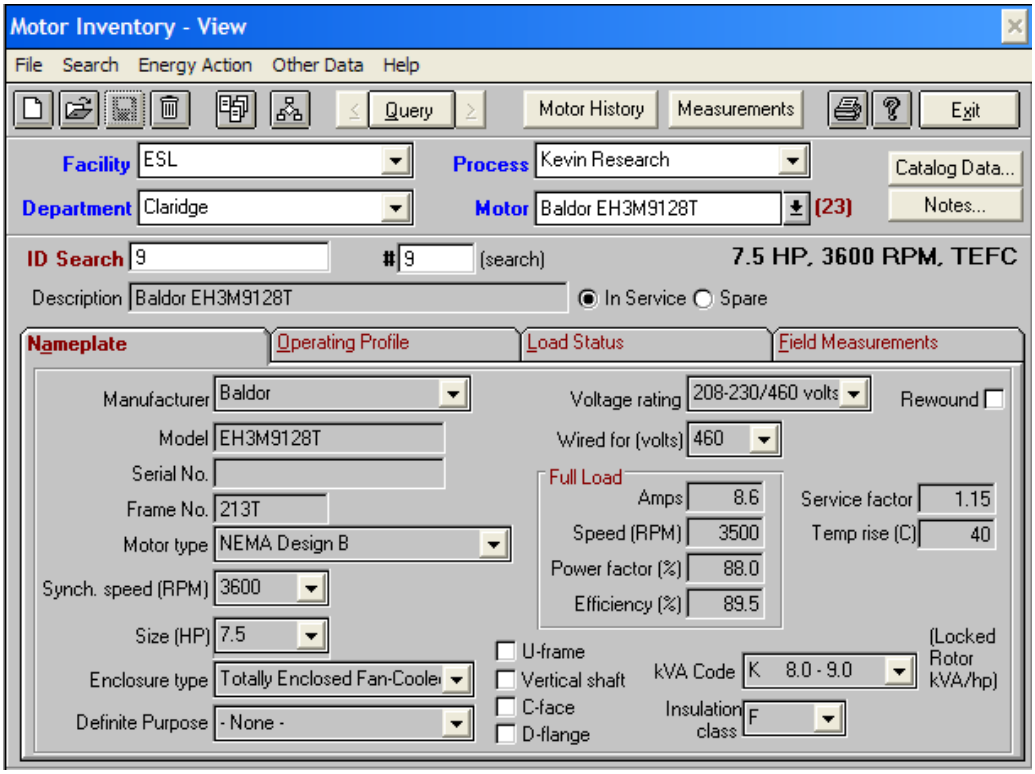

Figure 22: Screenshot of the Nameplate tab in MotorMaster+ 4.0.

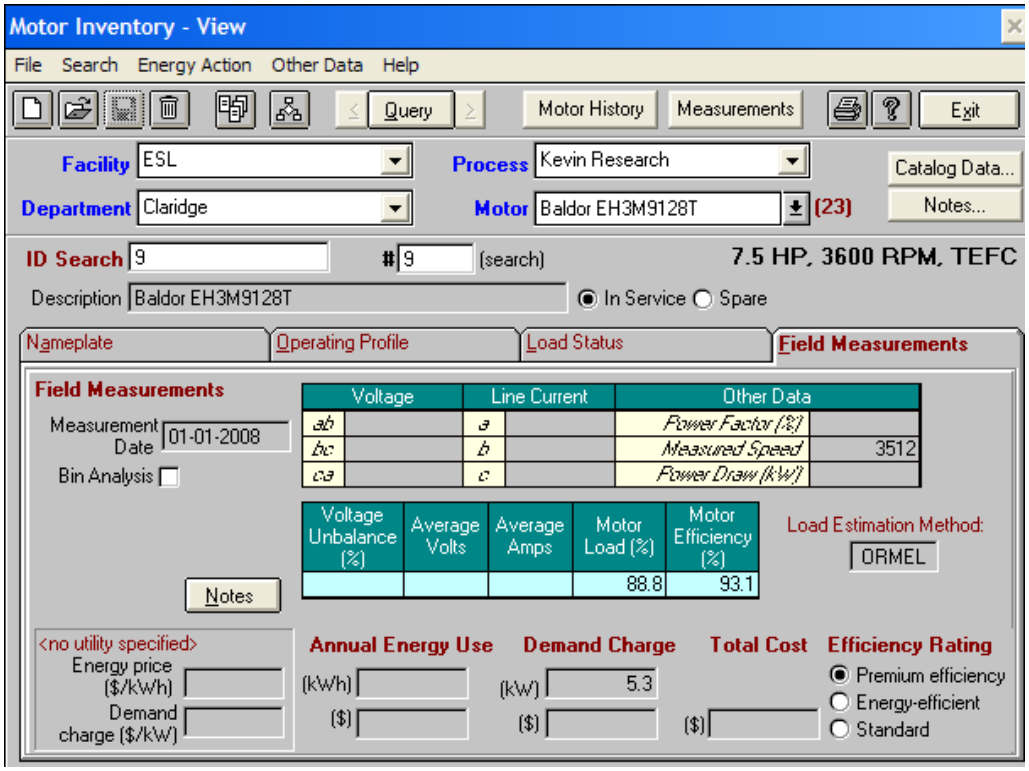

Figure 23: Screenshot of the Field Measurements tab in MotorMaster+ 4.0.

However, the ultimate goal is to estimate motor input power, not motor load factor. The motor input power from each method was determined by

$$P_{in} = \frac{LF \cdot P_{shaft,\,rated}}{\eta} \tag{104}$$

where the load factor LF was predicted from each method and rated shaft power $P_{shaft,\,rated}$ is determined from the motor's nameplate.

When calculating input power using the Slip Method, motor efficiency η was estimated to be the rated (nameplate) efficiency. When calculating input power using ORMEL, the efficiency value specified from the ORMEL algorithm was used. The motor input power residuals were determined by subtracting the measured input power from the predicted input power. These motor input power residuals were then normalized by dividing by each motor's nominal input power.

Table 7 shows the RMSE of the residuals from each method's prediction of motor load factors and motor input power for the 21 sampled motors. Notice that ORMEL does slightly better than the Slip Method for predicting load factor, but that the Slip Method has a slight improvement over ORMEL for predicting input power. It is surprising that predicting input power is slightly better performed with the Slip Method (along with assuming motor efficiency is the nameplate efficiency) than the ORMEL algorithm (which gives its own motor efficiency prediction).

Table 7: Comparison of predicting motor load factor using Slip Method and ORMEL for 21 sampled motors.

	RMSE of Residuals for	
	Load Factor	**Input Power (p.u., relative to nominal input power)**
Slip Method	7.6%	8.0%
ORMEL	7.0%	8.6%

The inconsistent behavior in Table 7 can be explained by plotting the error in the efficiency values used to predict input power. Figure 24 shows the error—when compared to the measured value—of assuming the nameplate efficiency value and using the efficiency value predicted by the ORMEL algorithm. Notice that assuming the nameplate efficiency value for the motor efficiency gives improved performance over using the ORMEL-predicted efficiency value for load factors at or above 50%. A satisfactory explanation for this behavior is not available[29].

[29] Notice that in the screenshots of MotorMaster+ 4.0 shown earlier, the predicted efficiency at the given shaft speed was 93.1% (see Figure 23), despite the fact that a nameplate full-load efficiency of 89.5% was specified in the Nameplate tab (see Figure 22).

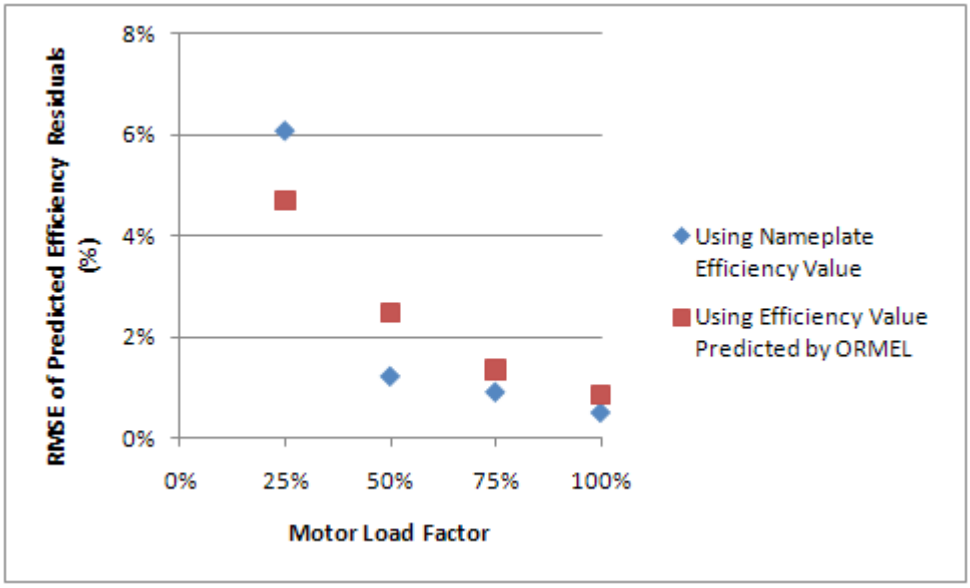

Figure 24: RMSE of predicted efficiency residuals (%) vs. motor load factor using the nameplate efficiency value and the ORMEL-predicted efficiency value on the 21 sampled motors.

In summary—using a sample of 21 Baldor motors—ORMEL was not found to have significantly improved load factor and input power predictive abilities over the Slip Method. Furthermore, at least for the sampled motors, assuming the nameplate efficiency for running motor efficiency gave improved performance over the efficiency predicted by ORMEL.

4.3. TEMPERATURE-BASED APPROACH FOR MOTOR POWER ESTIMATION

The principles of the loss method of estimating motor load factor were developed earlier in Section 3.2. In order to determine the effectiveness of this method, experiments were performed on two motors. The purpose of these experiments was to determine the motor thermal coefficients, refine the loss model by investigating temperature measurement techniques, and to assess the use of this approach for estimating motor input power.

4.3.1. Experiment Setup

4.3.1.1. Motor Setup

The experiments were performed at the Energy Systems Laboratory's Riverside Testing Facility, which is located on the Riverside Campus of Texas A&M University. Table 8 gives details of the tested motors.

Table 8: Tested motors.

Motor #	Manufacturer	Model	Rated Power (HP)	Voltage (V)	Full Load Speed (RPM)	Full Load Current (A)	Nameplate Efficiency	Enclosure
1	Leland-Faraday	LFI-86075	7.5	230/460	1148 (6 poles)	21.3/10.7	85%	ODP
2	Leland-Faraday	LFI-84100	10	230/460	1725 (4 poles)	27/13.5	85%	ODP

4.3.1.1.1. Motor #1

This 7.5 HP motor is part of the laboratory's Blue Chamber. A fan provided the load for the motor, while a damper allowed load adjustment. A wide range of loads was desired. In order to increase the motor's loading, a secondary fan was positioned to blow into the intake of the fan that was coupled with the motor under investigation. The secondary fan's speed was adjusted with a VFD. Although motor #1 could be wired for both 230 V and 460 V supply voltages, the experiment was conducted with the motor connected exclusively to a 480 V supply voltage. Figures 25 and 26 show the setup for motor #1. Figure 27 shows the secondary fan used to increase the load on motor #1.

Figure 25: Motor #1 surrounded by expanded metal.

Figure 26: Motor and fan enclosure. An adjustable damper is located at the discharge of the fan (at the top).

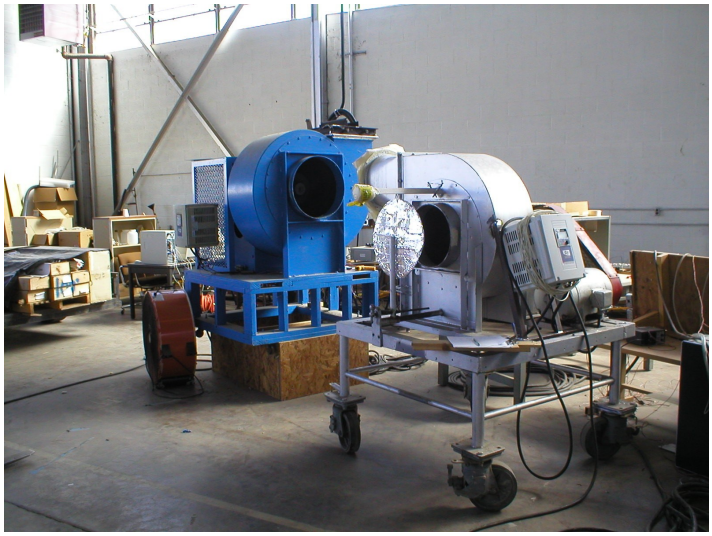

Figure 27: A secondary fan (the silver fan) allowed higher loads to be imposed on the motor under investigation.

4.3.1.1.2. Motor #2

This 10 HP Leland-Faraday motor was acquired from the laboratory's storage. The age of the motor is not known, but its manufacturer is no longer in business, at least under that name. However, upon opening the wiring box, it became apparent that the motor had never been run before. The motor accepted both 230 V and 460 V voltage supplies; data was taken at both voltages.

A fan and fan enclosure structure was available, but it lacked a shaft, bearings, sheaves, belts, method to mount/adjust the motor, structural reinforcement, air flow control, wiring, and a guard to prevent safety hazards with the rotating shafts and belts. Using the Riverside Testing Facility's equipment (drillpress, plasma cutter, MIG welder, and oxy-acetylene torch) and advice from Lab Manager Kelly Milligan, the various parts were created and acquired. The sheaves, bushings, shaft, belts, and 480 volt electrical plug were purchased; the rest of the materials (e.g. steel angle, steel plate, expanded metal, and wood) were acquired from scrap at the Riverside Testing Facility. Figure 28 shows the completed setup for motor #2.

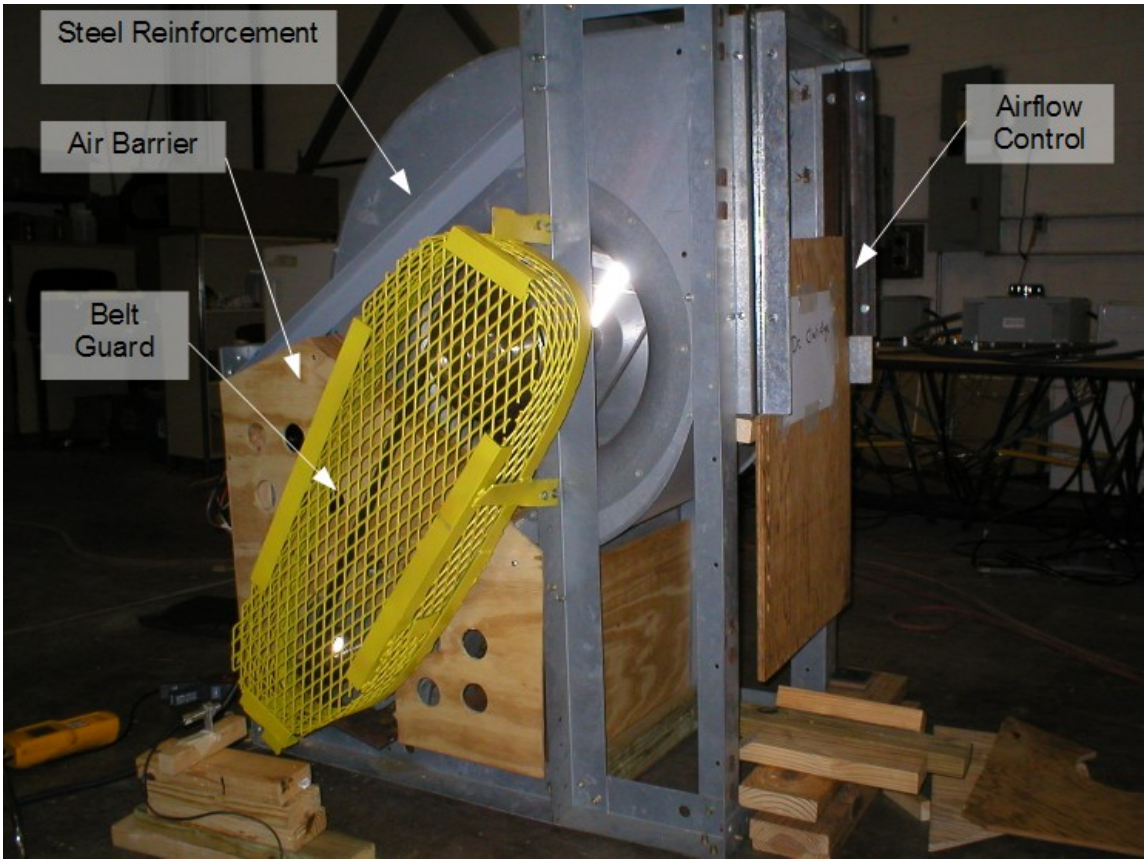

Figure 28: The completed setup for Motor #2.

Figure 29: Airflow control used a gate (shown in the closed position).

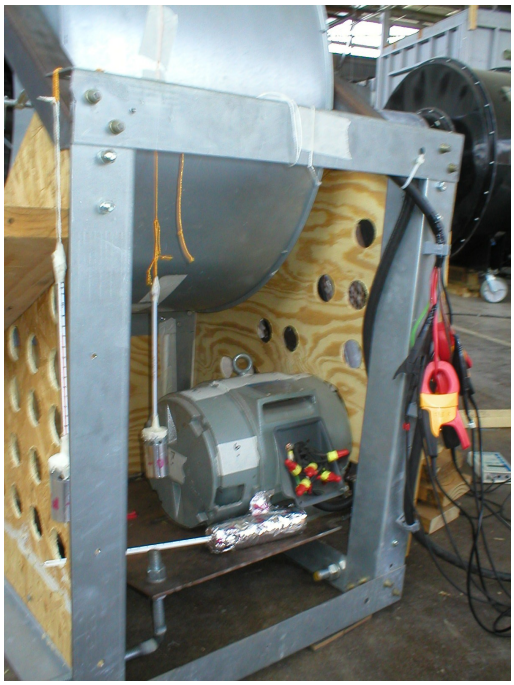

Figure 30: The compartment for Motor #2.

Of specific concern was the airflow from the fan affecting the cooling characteristics of the motor. More specifically, we didn't want the motor's cooling characteristics to vary when the airflow is varied. So in an attempt to shield the motor from the fan's airflow, partitions were created for 3 sides of the motor (as shown in Figures 29 and 30). From a superficial manual inspection, the partitions seemed to isolate the motor from the fan's airflow; however, later it will be shown that in the analysis of the motor data the fan airflow has a slight effect on the cooling properties of the motor.

Figure 29 shows the airflow control and the rear of the setup. In Figure 30, notice the mechanism used to adjust the motor base plate. This adjustment became invaluable when installing various pulley sizes. Notice two “ambient” air temperature values are taken: one outside the motor compartment and one inside the compartment. On average, the air temperatures differed about 5 °F, but at the extreme the air temperature reading inside the compartment was 11 °F higher than outside. The 2” holes in the paneling surrounding the motor compartment allow some cross ventilation for motor cooling.

This motor (Motor #2) ran significantly hotter than the last motor: surface temperatures of about 140-150 ºF were measured when running at about 75% load. It is reasonable that this motor will have higher temperatures than the other motor, due to having a greater nominal horsepower and smaller frame size. However, I was not expecting such high motor temperatures. Furthermore, the compartment has reduced the motor's access to cool air. Figure 31 shows the locations for surface temperature measurement.

In the experimental portion of the heat-loss model I'm assuming no or negligible heat loss from the motor's control volume via conduction. The base of the motor was once measured to be 130 ºF and the baseplate from 100 to 130 ºF. Therefore the baseplate behaved as a heat-sink but it's not accounted for in the experimental model.

Figure 31: Motor #2 with seven demarcated locations for IR temperature measurement. Masking tape was used in order to reduce errors from mis-specified emissivities. On the left-hand corner is the inside "ambient" air temperature thermometer which was only used for diagnostics.

4.3.1.2. Instrumentation

4.3.1.2.1. Electrical Measurements

Electrical measurements were measured using a Fluke 435 Power Quality Analyzer. The measured electrical variables included real power, power factor, current in three phases, and voltage for three phases. For each motor condition, electrical measurements were taken four times so that an average could be calculated. The phasor diagram provided by the meter was carefully checked in order to ensure proper clamp setup, since a single clamp installed in reverse can cause erroneous measurements.[30] According to the Fluke 435 specifications, the accuracy of the power measurements (not including errors in the current clamps) are 1% of the displayed value ±10 Watts (Fluke Corp. 2006, 8).

4.3.1.2.2. Shaft Speed Measurements

Shaft speed measurements for Motor #1 (Leland Faraday 7.5 HP) were taken using a Monarch ACT-3 tachometer. The manufacturer specifications claim a tachometer accuracy of ±0.0015% of the reading or ±½ of the displayed resolution; for shaft speeds greater than 1000 RPM the unit displays speeds with a resolution of 0.1 RPM (Monarch Instrument 2005, 2).

Shaft speed measurements for Motor #2 (Leland Faraday 10 HP) were taken using a Monarch TACH-4A tachometer. The manufacturer specifications claim a tachometer accuracy of ±0.1 RPM of the reading at the relevant speed range (Monarch Instrument 2009). In order to get an accurate shaft speed measurement, the unit recorded the minimum and maximum shaft speeds over a 10 second period. This was done for a total of 4 times for each input power condition. The average of these 8 shaft speed measurements was taken as the shaft speed measurement.

Per the manufacturer's instructions, the accuracy of both instruments were nominally verified by aiming the tachometer at a fluorescent light and ensuring that the tachometer displayed a “speed” of 7200±2 RPM (Monarch Instrument 2009).

[30] Experiment data from several days had to be discarded because one of the amperage clamps was reversed. From then on, the phasor diagram provided by the Fluke 435 was frequently checked.

4.3.1.2.3. Temperature Measurements

Both motors had Open Drip-Proof (ODP) enclosures, therefore they drew air in and expelled air via various vents. A mercury-in-glass thermometer was attached to measure the expelled air temperature; another mercury-in-glass thermometer measured the ambient air temperature. The mercury-in-glass thermometer scale allowed readings within 0.5 °F.

It was desired to measure the air temperature of the expelled air from the motor without radiation errors from the environment or the motor itself. Toward this end, a radiation shield was constructed consisting of metal pipe blocked off at both ends. Two holes were drilled into the pipe to allow air passage. In order to mitigate radiation or conduction heat transfer into the pipe, the pipe was completely wrapped with two layers of rubber insulation tape and two layers of thermal control membrane. Figure 32 shows the radiation shield construction and Figure 33 shows the positioning of the shield.

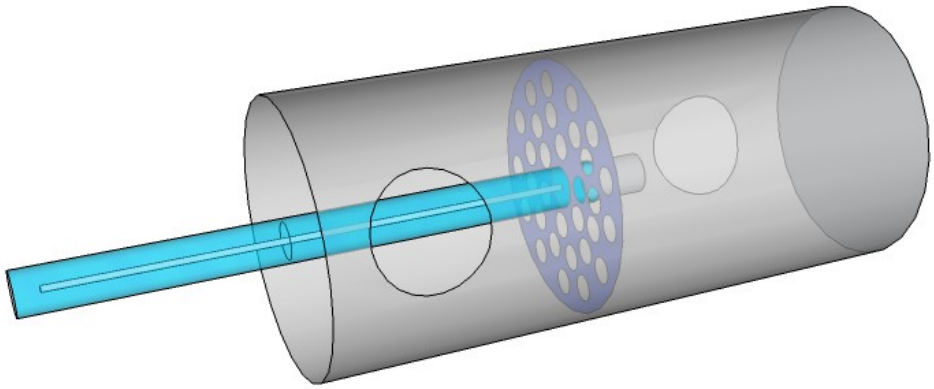

Figure 32: Radiation shield consisted of pipe blocked off at both ends, two holes drilled into pipe for air passage, porous support for thermometer, and layers of insulation wrapping the pipe.

Figure 33: The radiation shield was positioned so that ejected air from the motor blew directly into the intake hole of the radiation shield.

The thermometers were designed for full-immersion, although Figure 33 shows that the thermometer is only partially exposed to the ejected air from the motor that enters the radiation shield. In order to help account for the mismatch between the full-immersion thermometer and the partial-immersion application, an emergent-stem correction was applied:

$$Correction_{stem} = \beta \cdot N \left(T_{bulb} - T_{emergent} \right) \tag{105}$$

where $Correction_{stem}$ is added to the indicated temperature value, $\beta = 0.000016$ for mercury on the Celsius scale, N is the distance in degrees from the indicated temperature and the temperature discontinuity, T_{bulb} is the temperature of the bulb and approximated by the indicated temperature, and $T_{emergent}$ is the average temperature of the emergent portion of the liquid column. Since T_{bulb} is not known, it is approximated with the indicated temperature. $T_{emergent}$ is determined by placing a second thermometer with its bulb located halfway between

the temperature discontinuity and the indicated temperature on the thermometer of interest (Benedict 1984, 47-48). It is recognized that this method for stem correction is approximate: Nicholas estimates a ±10% accuracy for the correction value (1999, 13-126). In the motor experiment, the minimum stem correction was 0.04 ºC (0.06 ºF), the average stem correction applied was 0.09 ºC (0.17 ºF), and the maximum stem correction was 0.23 ºC (0.42 ºF).

The temperature of the motor surfaces was measured using a Fluke 62 Mini IR Thermometer. The pre-set emissivity of Fluke 62 Mini was 0.95; as recommended by the instrument manufacturer, masking tape was placed over the desired temperature measurement locations on the motor surface (Fluke Corp. 2005a, 2). Locations for spot temperature measurements using the IR thermometer were demarcated on the motor surface; 5 locations on the first motor and 7 on the second. Not only did the IR thermometer display the last measured temperature, but it also displayed the maximum temperature that was measured while the trigger was depressed. Therefore this feature allowed "scanning" the surface of the motor to acquire the maximum temperature detected during the scan. In order to make the "scanning" measurements repeatable, two paths were created on the motor surface, one of which was on the motor's endcap. Measurements were taken about 4 inches above the motor surface; that corresponds to a measurement spot of a 0.5 inch diameter circle (Fluke Corp. 2005a, 2).

For point measurements, the Fluke 62 Mini has a display resolution of 0.5 ºF; for path/scanning measurements, the display resolution is 1 ºF. In the relevant temperature range, the Fluke 62 Mini has a stated accuracy of ±3 ºF or ±1.5% of reading,[31] whichever is greater. However, as will be discussed shortly, repeatability may be more relevant since all measured temperatures—whether from the mercury-in-glass thermometers or IR thermometer—were reset to a reference measurement. The Fluke 62 Mini's stated repeatability is ±0.5% of reading or ±2 ºF, whichever is greater (Fluke Corp. 2005b, 2). Confidence levels for the accuracy and repeatability claims were not provided in the specifications.

Recall that the temperature approach for estimating motor power is based on temperature differentials. Therefore, it is the difference of temperature, not the temperature value itself that is of primary importance. In order to "calibrate" the instrumentation, temperature measurements

[31] It seems counter intuitive to apply a percentage to a temperature value from a non-absolute temperature scale, such as the Fahrenheit scale.

using the mercury-in-glass thermometers and the Fluke 62 IR thermometer were taken when the motor and surroundings were in thermal equilibrium, such as in the morning before any equipment was turned on. The ambient air temperature measurement was taken as the reference value; the difference between it and the other equilibrium temperature measurements was computed. In this way a correction constant would be applied to subsequent measurements using that instrumentation. For example, an average correction constant of -1.6 ºF and -0.81 ºF was applied to the ejection air temperature measurements and Fluke IR temperature measurements, respectively.

No attempt was made to measure the "surrounding surface temperature" T_{surr} of the surfaces around the motor. In these experiment analysis, the "surrounding surface temperature" T_{surr} was assumed to be the same as the ambient air temperature T_{∞}.

4.3.1.3. Test Procedure

Due to the amount of time required to warm up the motor (~ 3 hours), experiments were conducted around-the-clock in order to take advantage of the hot motor. In general, the procedure was conducted as follows.

1. Determine the desired input power value to be measured. Adjust the airflow amount until the desired input power is displayed on the Fluke 435. For motor #1, airflow adjustment was effected by damper position and adjusting the VFD speed on the loading fan. For motor #2, airflow adjustment was effected by damper position and pulley size.
2. Give motor time to achieve steady-state. The amount of time necessary varied depending on the amount of change in input power, and was determined by periodic temperature measurements. The criteria I used to determine when the steady-state condition had been reached was when the motor surface temperature—relative to the ambient temperature—was constant for 30 minutes. If the motor started out cold, I would wait a minimum of 3 hours. A warm motor was given a minimum of 1 hour to achieve steady state; a cold motor was given a minimum of 3 hours to achieve steady-state operation. It should be noted that the amount of time need to achieve steady-state depended on the change in power level: changing the input power from 2.5 kW to 5 kW took longer than going from 4.8 kW to 5 kW.

3. Record measurements:
    1. Measure electrical measurements. The measured electrical variables included real power, power factor, current in three phases, and line-to-line voltage between three phases. Each value was measured 4 times so that an average value could be calculated later.
    2. Measure shaft speed.
    3. Measure ambient air temperature.
    4. Measure motor temperatures. First, the temperature of the ejected air was measured using the liquid-in-glass thermometer. Secondly, 7 point locations on the motor enclosure were measured three times using the Fluke 62 IR thermometer. Finally, the 2 paths were scanned three times using the Fluke 62 IR.
4. Return to Step 1.

4.3.2. Data Analysis

4.3.2.1. Regression Approach

Recall from Section 3.2.5. the motor loss approach for estimating a motor's input power for an open motor, assuming no conduction from the shaft and motor base:

$$P_{input} = \frac{C_{conv} N_{shaft}^{C_{speed}} (T_s - T_\infty)}{1-\eta_{motor}} + \frac{C_{rad}\sigma (T_s^4 - T_{surr}^4)}{1-\eta_{motor}} + \frac{C_{through} N_{shaft} (\rho c_p)(T_{air,out} - T_\infty)}{1-\eta_{motor}} \qquad (106)$$

where shaft speed N_{shaft} is estimated using the synchronous speed of the motor, motor surface temperature T_s is a representative temperature, ambient air temperature is determined using the respective liquid-in-glass thermometer described earlier, the surrounding surface temperature T_{surr} is assumed to be the ambient temperature, the density and specific heat of air are taken at standard air conditions, the ejected air temperature $T_{air,out}$ is determined using the respective liquid-in-glass thermometer described earlier. The various constants C in Equation 106 are determined by regression.

Motor efficiency was never measured, but rather it was estimated using existing efficiency curves acquired from the literature. For example, the literature and the Baldor/Reliance motor

data gave motor efficiency as a function of motor speed, enclosure type, nominal power, and load factor. The chosen curve is then adjusted to match the nameplate motor efficiency at the 100% load factor by adding a constant. If the estimated efficiency curve differs from the actual efficiency curve, then the regression coefficients may correct for this. However, that is undesirable because then the thermal coefficients would contain efficiency information which may not hold across other motors.

In this preliminary investigation, the thermal performance of the motor when driven by a VFD is not reported. Running the motor without a VFD simplifies the experiment, because VFD efficiency and the decrease in motor efficiency due to a non-sinusoidal signal do not need to be accounted. Furthermore, the regression of the exponent coefficient C_{speed} could be ignored or held as a harmless constant. Since this investigation does not include VFD motors, C_{speed} is held as 1 and is not subject to regression.

From the point of the regression, Equation 106 can be written as a linear combination of three dimensions—external convection, external radiation, and internal convection:

$$P_{input,motor} = C_1 \cdot X_1 + C_2 \cdot X_2 + C_3 \cdot X_3 + C_{constant} \tag{107}$$

where

$$\begin{aligned} X_1 &= \frac{N_{shaft}^{C_{speed}} (T_s - T_\infty)}{1 - \eta_{motor}}, \\ X_2 &= \frac{\sigma (T_s^4 - T_{surr}^4)}{1 - \eta_{motor}}, \text{ and} \\ X_3 &= \frac{N_{shaft} (\rho c_p) (T_{air,out} - T_\infty)}{1 - \eta_{motor}}. \end{aligned} \tag{108}$$

The subscripts on the coefficients (conv, rad, and internal) have been replaced with numbers because in this analysis the various dimensions are being explored and possibly removed. The $C_{constant}$ term is sometimes included, although it's unclear what a constant term would physically represent. Chatterjee and Hadi note that "[i]n any regression model, unless there is strong theoretical reason, a constant should always be included even if the term is statistically not

significant. The constant represents the base or background level of the response variable" (2006, 64). It could be argued that a constant should not be included because it does not have a physical basis and it is determined solely by regression. On the other hand, if the original 3-dimensional (external convection, external radiation, and internal convection) temperature-based model is reduced to a model with one or two dimensions, then the coefficients lose their pithy physical meanings. In other words, if a regression coefficient goes from representing the product of the convection heat transfer coefficient and the respective surface area to merely being a fitted regression coefficient that incorporates other information (such as external radiation or internal convection), then it may not be a stretch to include a nonzero constant that does not have an elegant physical meaning. In any case, in the event that $C_{constant}$ is undesired it can easily be set to zero in these regressions.

4.3.2.2. Motor Loading

For Motor #1, temperature and electrical data for the motor running across-the-line (ATL) at 17 load points was measured at 480 Volts. As shown in Figure 34, Motor #1 was loaded from about 30% to 60% load factor. The 30% load factor was achieved by fully closing the damper and turning off the secondary loading fan. The 60% load factor was achieved by fully opening the damper and running the secondary loading fan at 60 Hz. It is useful to consider the standard deviation of the measured input power, since the standard deviation can be considered the Standard Error (or RMSE) from a mean model (e.g., the only parameter is the mean of the measured input power) (Chiulli 1999, 275). For motor #1, the standard deviation of the measured input power (i.e., standard error or RMSE from a mean model) was 701 Watts or 11% when normalized to the nominal input power of the motor.

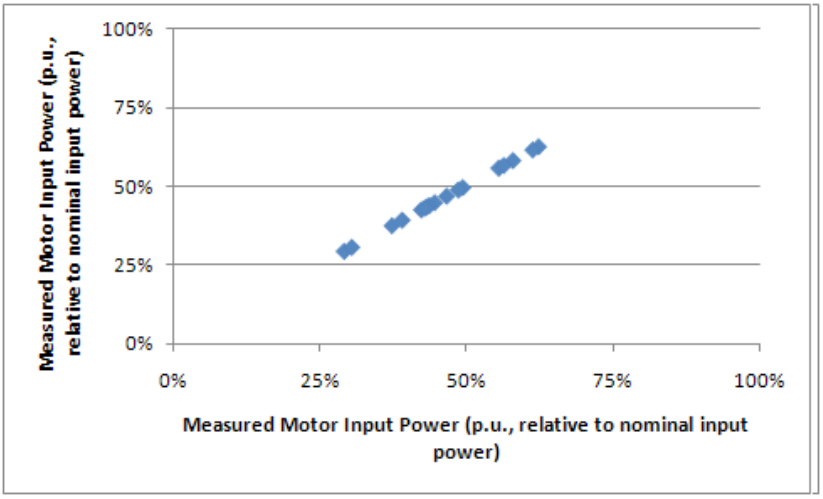

Figure 34: Motor #1: Measured Input Power (p.u.) vs. Measured Input Power (p.u.).

For Motor #2, temperature and electrical data for the motor running ATL at 39 load points was measured; 21 of the points used a 480 V supply voltage and the other 21 used a 240 V supply voltage. As shown in Figure 35, Motor #2 was loaded from 20% to a little over 100% load factor. The 20% load factor was achieved by fully closing the damper and using the 4.15 inch pulley on the motor shaft. The 100% load was achieved by partially opening the damper and using the 6.15 inch pulley on the motor shaft. (No secondary loading fan was applied to Motor #2). The standard deviation of the measured input power (i.e., RMSE from a mean model) was 1911 Watts or 22% when normalized to the nominal input power of the motor.

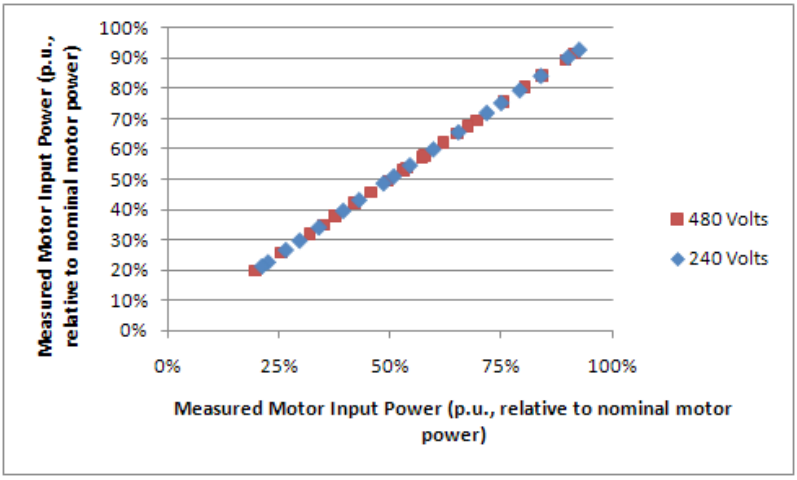

Figure 35: Motor #2: Measured Input Power (p.u.) vs. Measured Input Power (p.u.).

Not only is the standard deviation of the measured input power (i.e., RMSE from a mean model) useful in assessing the range of motor loads that a motor was subject to, but it also can serve as an upper bound of the residual errors when applying regression. For example, residual regression errors above 22% should not be expected for Motor #2.

4.3.2.3. Heat Transfer Components

Before conducting regression with the various variables, it is instructive to plot how the various independent combined variables (external convection, external radiation, and internal radiation) relate to the dependent variable (measured input power). In Figures 36 through 38, note that two trendlines are shown: one of them is forced through the origin, while the other one includes a constant to allow for nonzero intersection with the y-axis. From a superficial inspection of the figures, the three heat transfer modes (external convection, external radiation, internal convection) seem to behave similarly.

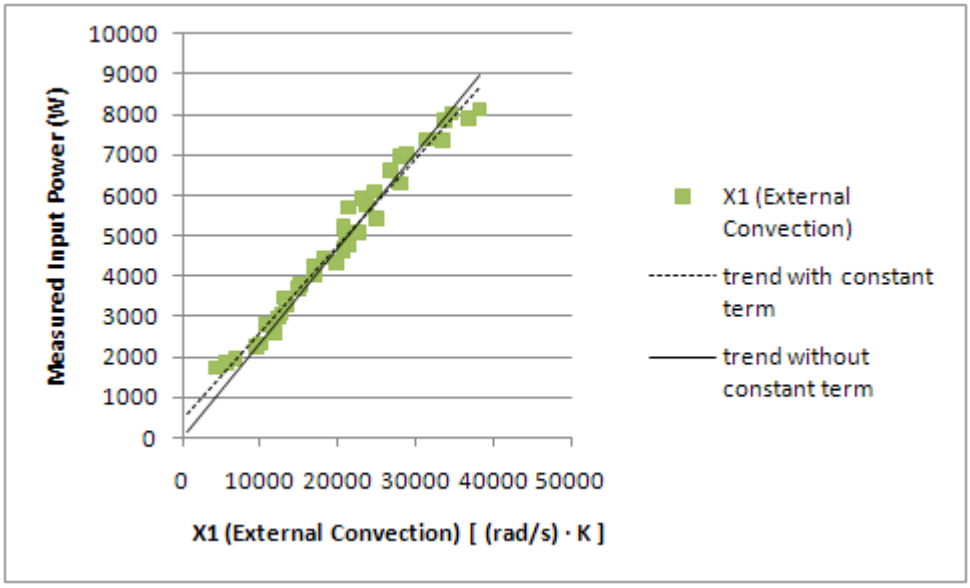

Figure 36: Motor #2: Measured Input Power vs. X1 (External Convection).

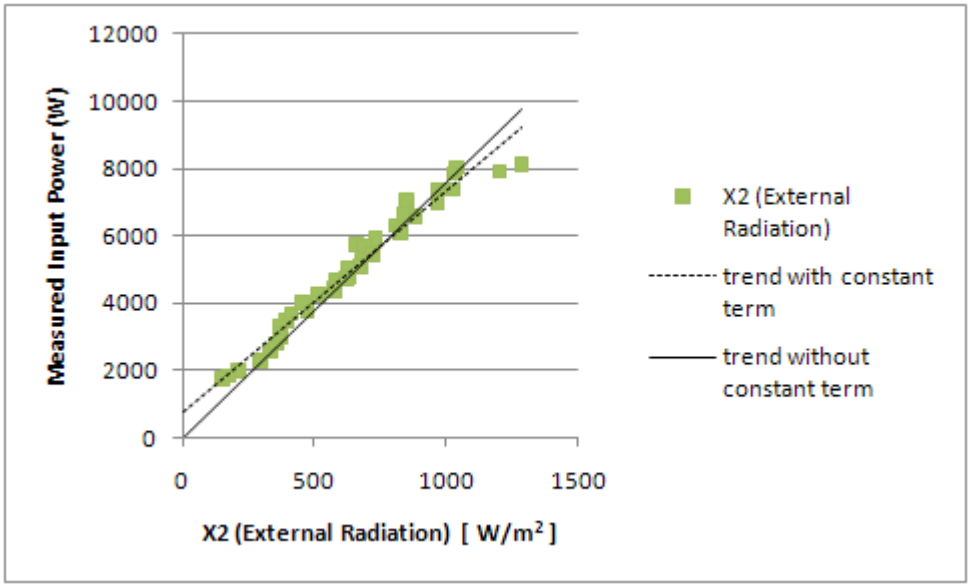

Figure 37: Motor #2: Measured Input Power vs. X2 (External Radiation).

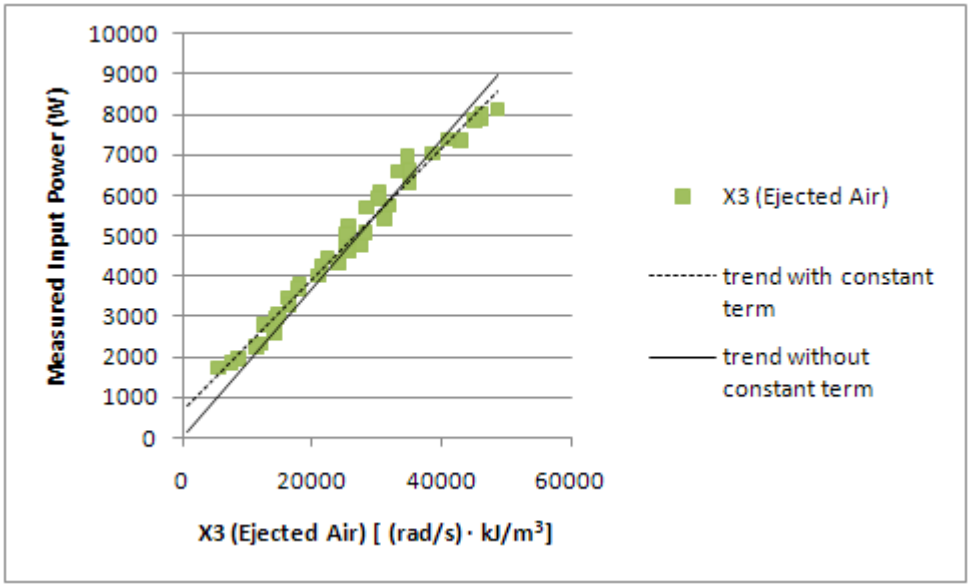

Figure 38: Motor #2: Measured Input Power vs. X3 (Ejected Air/Internal Convection).

It is instructive to consider the independence of the dimensions X1, X2, and X3 (which represent external convection, external radiation, and internal convection, respectively). Ideally, the dimensions are algebraically independent (Chatterjee and Ali S. Hadi 2006, 88).

Table 9 shows how the various dimensions compare with the predicted variable P (Power) and each other. The R-correlation values shown in this table assume a non-zero y-axis (Input Power) intercept. The high R values suggest that the dimensions are collinear.

Table 9: Correlation R-matrix of the predicted variable (P=Power) and predictor variables (X1, X2, and X3).

	Motor #1 (17 data points)				**Motor #2 (39 data points)**			
	Input Power	**X1**	**X2**	**X3**	**Input Power**	**X1**	**X2**	**X3**
Input Power	1.00				1.00			
X1	0.95	1.00			0.99	1.00		
X2	0.95	1.00	1.00		1.00	0.98	1.00	
X3	0.92	0.98	0.97	1.00	0.99	0.98	0.99	1.00

Recall from Equation 108 that the dimensions X1 and X2 use the same temperature values: surface temperature T_s and ambient temperature T_∞ (the surrounding surface temperature is not measured, so the ambient temperature is used as a proxy). Therefore it is not surprising that these two dimensions share a high correlation R value. While complete orthogonality between all the dimensions is not necessarily expected, the correlations given in Table 9 demonstrate that the dimensions are very closely aligned. "In most regression applications the predictor variables are not orthogonal. Usually, the lack of orthogonality is not serious enough to affect the analysis. However, in some situations the predictor variables are so strongly interrelated that the regression results are ambiguous" (Chatterjee and Ali S. Hadi 2006, 221).

Although the high correlations between the predictor variables is shown in Table 9 and demonstrates collinearity, the proper way for checking for multicollinearity is by iterating through the various variables to see how well the other variables predict it (Miles and Shevlin 2001, 129). This is shown in Table 10. The high R and R^2 values demonstrate that at least one variable may be able to be dropped, since the vast majority of the information in each variable can be predicted by the others. It should be mentioned that some correlation between the various dimensions is expected, since it seems reasonable that motors with a lot of wasted power will reject heat via multiple heat transfer modes.

Table 10: Checking for multicollinearity.

		Motor #1 (17 points)		**Motor #2 (39 points)**	
Predicted Variable	**Predictor Variable**	**R**	**R^2**	**R**	**R^2**
X1 (external convection)	X2 & X3	1.00	1.00	1.00	1.00
X2 (external radiation)	X1 & X3	1.00	1.00	0.99	0.98
X3 (internal heat transfer)	X1 & X2	1.00	1.00	1.00	0.99

Although multicollinearity appears to be a problem, using the entire model (X1, X2, X3, and C) does give good predictions of motor input power, with an RMSE of 257 Watts and an RMSE_pu of 2.9%. The Measured Input Power versus Predicted Input Power is compared in Figure 39 and

the Residuals are shown in Figure 40. The regression coefficients for X1, X2, X3, and C are 0.90, -5.8, 0.81, and 536, respectively. The negative coefficient for X2 is disappointing, since it clearly does not represent physical reality (radiation heat transfer should occur *from* the motor and not *to* the motor). Indeed, when algebraic signs of some of the coefficients are opposite that which is expected from the physical model, multicollinearity is to be suspected (Chatterjee and Ali S. Hadi 2006, 233). One solution to multicollinearity is to remove dimensions, although it may not be obvious which dimension to remove (Weisberg 2005, 216).

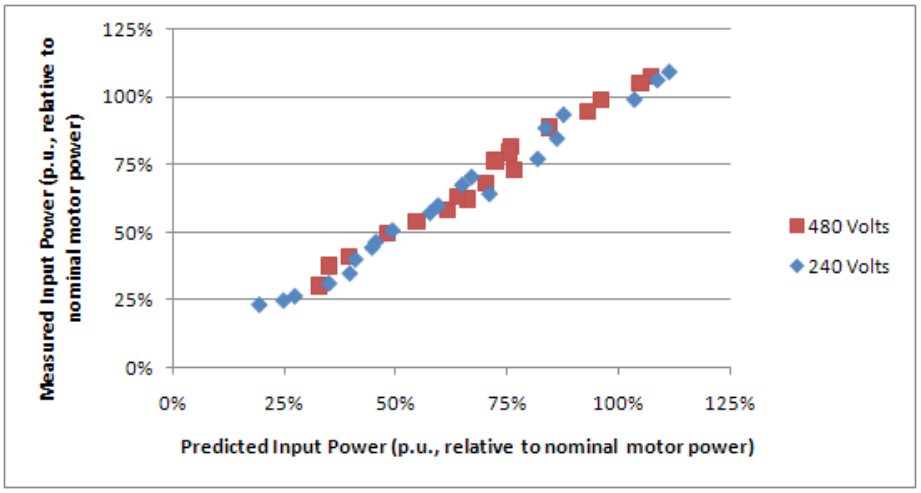

Figure 39: Measured Input Power (p.u.) vs. Predicted Input Power (p.u.) for regression with X1,X2,X3, & C on Motor #2.

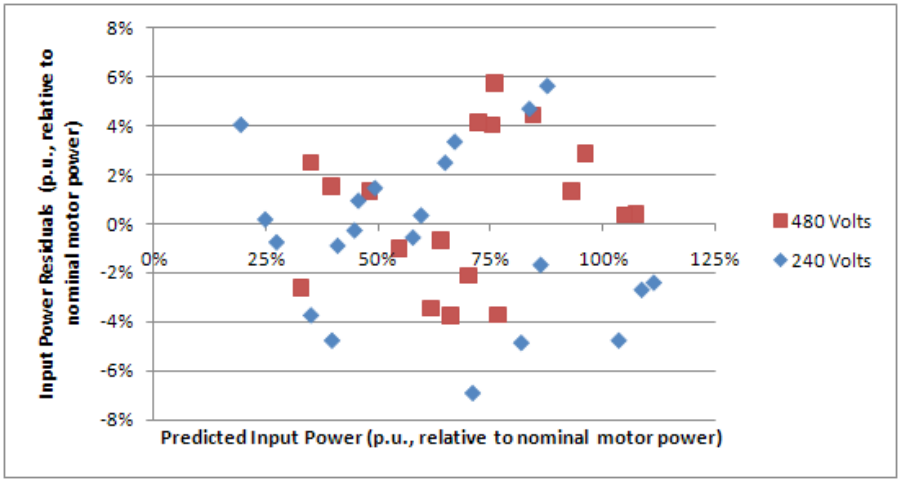

Figure 40: Measured Input Power (p.u.) vs. Predicted Input Power Residuals (p.u.) for regression with X1, X2, X3 & C on Motor #2.

In Figure 40, two clumps can be seen for the 480 V points. Upon further investigation, it seems like the clumps for 480 V are delineated by pulley size (see Figure 41). This may suggest that the fan's airflow has somehow affected the motor's cooling, despite the steps taken to isolate the motor from the fan's airflow.

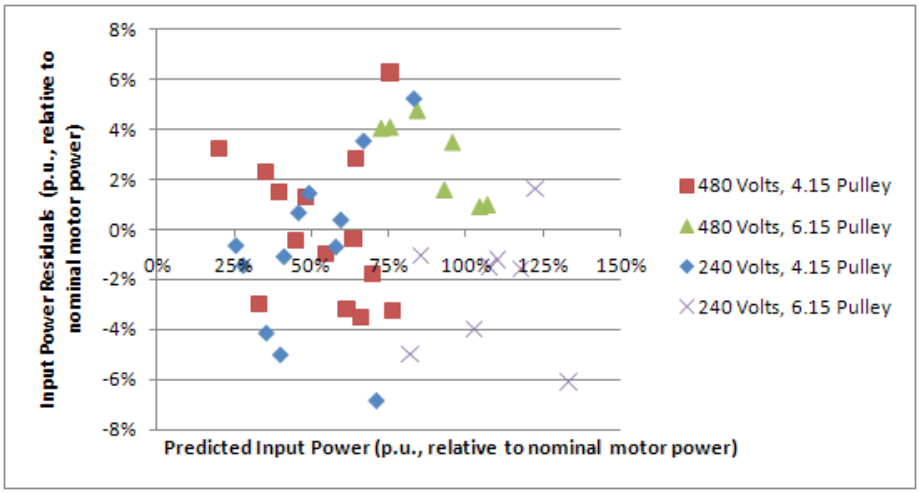

Figure 41: Measured Input Power (p.u.) vs. Predicted Input Power Residuals (p.u.) for regression with X1, X2, X3 & C and categorized by pulley size on Motor #2.

However, a closer look at Figure 41 shows that there may other factors at work. While it is evident that the pulley size accounts for some of the variation, there is marked contrast with the behavior within the same pulley size across the two supply voltages (e.g., 240 V with 4.15" Pulley is separate from 480 V with 4.15" Pulley). On the surface, it's not obvious why the nominal voltage would effect the thermal behavior of the motor.

Figures 42 and 43 show the current and voltage unbalance for Motor #2, respectively. Notice that the 460 V points suffer higher current unbalance than the 230 V data points.[32] The literature states that current unbalance decreases motor efficiency and increases motor temperature (Nadel et al. 2002, 2; Lobodovsky 2007, 274). That could help explain the delineation by voltage in Figure 41. Another difference between the 230 V and 460 V datapoints is the percent over-voltage. While Figure 43 does show voltage unbalance—which is comparable between the two nominal voltages—it also shows the over-voltage in the electrical supply (e.g., at the "460" V nominal voltage, the average measured voltage was 476 V). It's difficult to predict the effect of over-voltage on motor efficiency because its effect will depend on the motor load fraction and the type of motor (ASHRAE 2000c, 40.2; Emadi 2005, 140). In any case, the varying current unbalance and the varying over-voltage may explain some of the behavior in Figure 41.

[32] Indeed, a student's t test at the 5% significance level confirms that the 460 V datapoints suffer higher current unbalance than the 230 V datapoints.

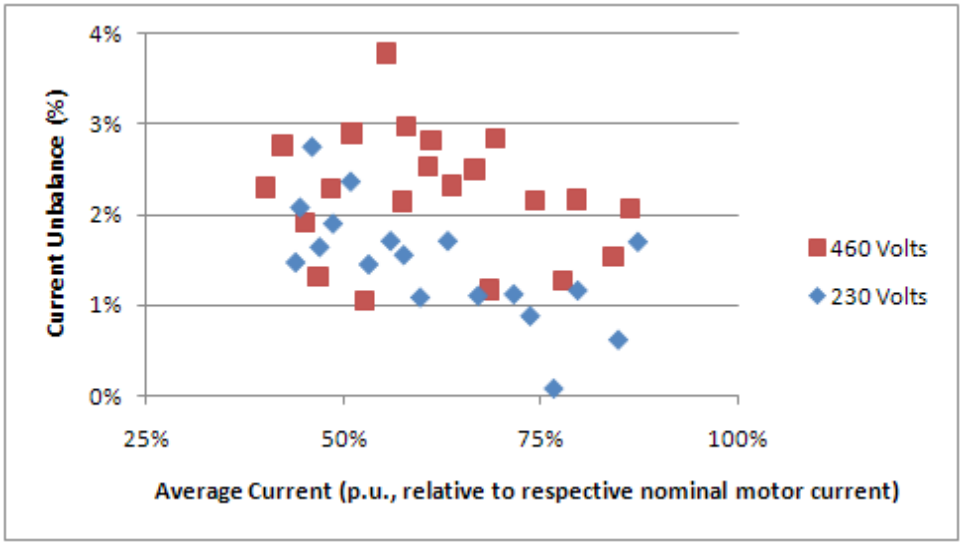

Figure 42: Current Unbalance vs. Average Current for Motor #2.

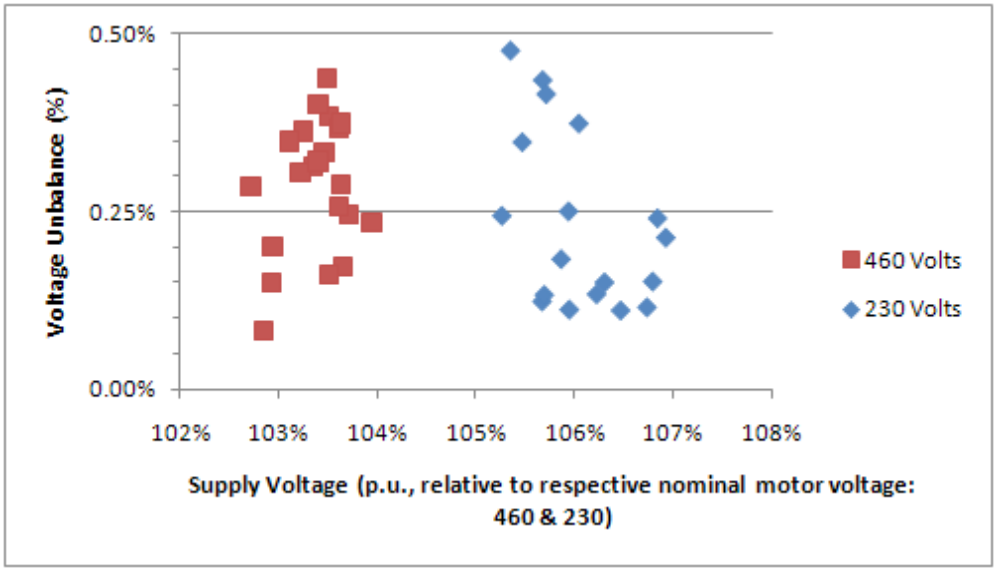

Figure 43: Voltage Unbalance vs. Supply Voltage normalized to Nominal Value for Motor #2.

Various combinations of the regression variables are explored and summarized in Table 11. Unfortunately, every regression that includes X2 (the external radiation dimension) gives a negative value for it's coefficient, except for when the regression is solely in terms of it with or

without a constant. This may be because radiation heat transfer does not play as strong a role as some of the other heat transfer modes, as mentioned earlier in the literature review of heat transfer behavior with motors. To be fair, the data collection of pertinent variables regarding the radiation mode is limited: view factors have not been considered and surrounding surface temperatures have not been measured but rather assumed to be at the ambient temperature.

Table 11: Dimension combination summary for 480/240 V data using Outside Ambient Temp and Average Surface Temp and a constant for Motor #2.

Variables	**Ambient Temp.**	**Surface Temp.**	**RMSE (W)**	**RMSE_pu**	**Notes:**
X1 X2 X3 C	Outside	Average	252	2.9%	X2 coeff. is neg.
X1 X2 C	Outside	Average	303	3.5%	X2 coeff. is neg.
X2 X3 C	Outside	Average	264	3.0%	X2 coeff. is neg.
X1 X3 C	Outside	Average	273	3.1%	
X1 C	Outside	Average	301	3.4%	
X2 C	Outside	Average	341	3.9%	
X3 C	Outside	Average	270	3.1%	

In Table 11, notice that regression using “X3 C” (i.e. internal convection and a constant) is just about as accurate as including all of the dimensions and a constant (X1 X2 X3 C). Table 12 is similar to Table 11 except constants are not included in the regressions. The Errors increase appreciably due to the poorer fit with the data.

Table 12: Dimension combination summary for 480/240 V data using Outside Ambient Temp and Average Surface Temp and without a constant for Motor #2.

Variables	**Ambient Temp.**	**Surface Temp.**	**RMSE (W)**	**RMSE_pu**	**Notes:**
X1 X2 X3	Outside	Average	285	3.3%	X2 coeff. is neg.
X1 X2	Outside	Average	324	3.7%	X2 coeff. is neg.
X2 X3	Outside	Average	374	4.3%	X2 coeff. is neg.
X1 X3	Outside	Average	360	4.1%	
X1	Outside	Average	356	4.1%	
X2	Outside	Average	472	5.4%	
X3	Outside	Average	389	4.4%	

The development of the motor loss model assumes that heat transfer occurs from the motor to the environment via various heat transfer modes. In the operation of a typical motor, it seems unlikely that heat transfer would occur in the opposite direction. Therefore, regressions that give a negative value for a dimension (i.e., heat transfer mode) may not reflect the actual physical phenomena. Such deviation from the expected physical model can demonstrate multicollinearity (Chatterjee and Ali S. Hadi 2006, 233). Notice in Tables 11 and 12 that the variable coefficients are positive only when the regression is done with a single dimension (and not combined with others), except for the regressions using “X1 X3 C” and “X1 X3”, respectively. These two regressions perform comparable to the single dimensions. This suggests that the Temperature Approach should focus on one dimension, instead of accounting for three different heat transfer modes.

4.3.2.4. Surface Temperature Location

In the previous regressions, the various component methods of heat transfer (external convection, external radiation, and heat transfer to the drawn in air) were examined and compared. The surface temperature used in the previous analysis was the average of the various motor surface temperatures. However, determining the average surface temperature measurement—especially if the measurements are point locations instead of paths—may not be practical for field use since demarcating the various regions for temperature measurement on the

motor surface may be difficult and not extend well across various motors. Therefore it seems prudent to examine the efficacy of the temperature measurement at various motor surface locations.

Recall that surface temperature measurements were taken at various locations and across two paths, as shown in Figure 44. In field applications, measurements that consolidate multiple locations—such as path or max/min measurements—may be preferred over spot measurements due to the difficulty in locating specific motor locations across many motors. Path A was composed of scanning along from Location #1 to #5. Path B was composed of scanning the end cap area around Location #7.

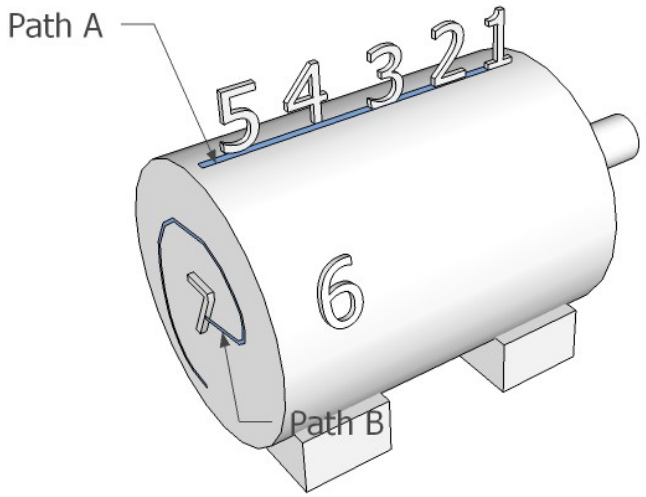

Figure 44: Surface temperature was measured at seven spot locations and over two paths on the motor enclosures.

The use of various surface locations to be the representative surface temperature is investigated. Each motor surface temperature location/path is iteratively used as the representative surface temperature input for both the "X1 C" regression and the "X1" regression. Reference Figure 44 for the surface temperature locations. Figure 45 is a plot of the RMSE_pu using various surface locations with the average motor surface temperature for the respected location; the plot shows how well various locations on the motor surface can predict motor input power using the "X1 C"

regression. Figure 46 is a similar plot, except it uses the X1 regression (i.e., y-intercept is forced to go through the origin).

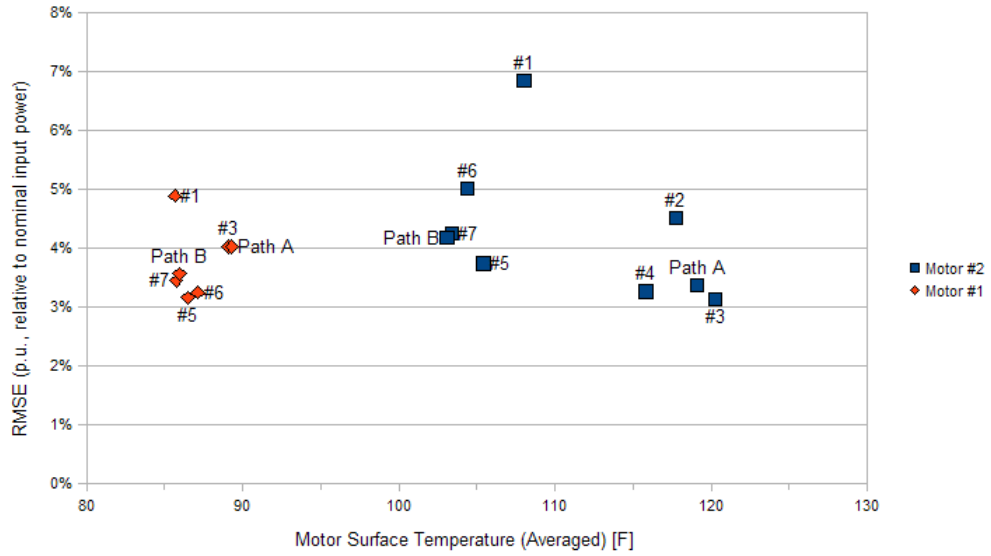

Figure 45: RMSE (p.u., relative to nominal input power) vs. Motor Surface Temperature (Averaged) [°F] using X1 C regression. This plot shows how well various motor surface locations predict motor input power when used as the representative surface temperature in a regression using X1 and C.

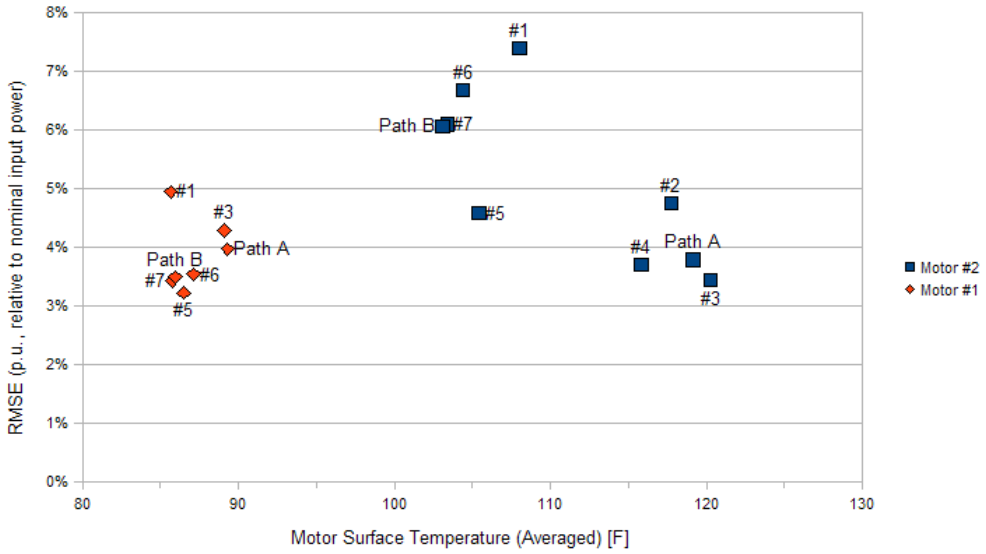

Figure 46: RMSE (p.u., relative to nominal input power) vs. Motor Surface Temperature (Averaged) [°F] using X1 regression. This plot shows how well various motor surface locations predict motor input power when used as the representative surface temperature in a regression using X1.

In both Figures 45 and 46, the surface temperatures for Motor #1 were significantly less than for Motor #2. This can be explained by recalling that Motor #1 was only loaded between 29% and 62% motor load fraction, whereas Motor #2 was loaded between 20% and 93% (see Figure 34 and 35, respectively). Furthermore, Motor #1 has a larger frame than Motor #2—and therefore has more external surface area—but has a smaller nominal horsepower.

In both Figures 45 and 46, the highest spot temperatures on the motor surface were obtained from Location #3, which is at the top center of the motor. It is not surprising that Path A—which runs directly over Location #3—has similar behavior. Similarly, Path B runs directly over Location #7, which explains its close agreement. The location that gives the highest RMSE for each motor is at Location #1, which is near the shaft end of the motor. The reasoning for this is unclear.

With Motor #1, little difference is seen when including—or not including—the intercept. Furthermore, the temperature distribution across the Motor #1's surface—at least at the measured

locations—does not vary as much as for Motor #2.

With Motor #2, the RMSE_pu for the cooler locations increase dramatically when the nonzero intercept is removed. That is clearly demonstrated in Figure 47, which shows the difference between the RMSE_pu predicted by X1 C and X1 for both motors. Recall that the original temperature approach model does not contain a nonzero y-intercept (see Equation 106), so the X1 regression is closer to the original model than X1 C. At least for motor #2, the hotter locations seem to provide performance that does not improve considerably when a constant (which has an ambiguous physical meaning) is included.

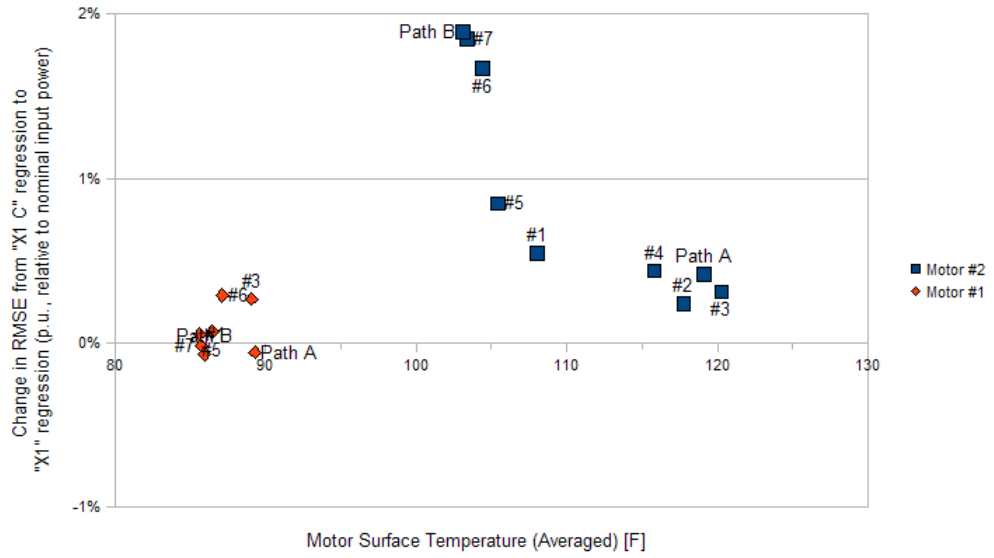

Figure 47: Change in RMSE from X1 C to X1 (p.u., relative to nominal input power) vs. Motor Surface Temperature (Averaged) [°F]. This plot shows how the RMSE_pu increase when the nonzero intercept is removed from the regression.

4.3.2.5. Comparison of Coefficients

It is instructive to compare the thermal performance between the two motors. Without doing any regression, Figures 48 and 49 show how the X1 (External Convection) dimension varies with the Measured Input Power. Figure 48 uses Path A as the representative surface temperature, whereas

Figure 49 uses Path B. Notice that motor #2 is loaded to a much greater range than motor #1. The slopes differ significantly between the motor #1 and motor #2. This could be because the motors have different cooling regimes; however, differences in motor setup should not be ignored (motor #1 was not as compartmentalized as motor #2). It should also be noted that the motors have two different synchronous speeds (1200 RPM and 1800 RPM), which will undoubtedly affect the motor cooling.

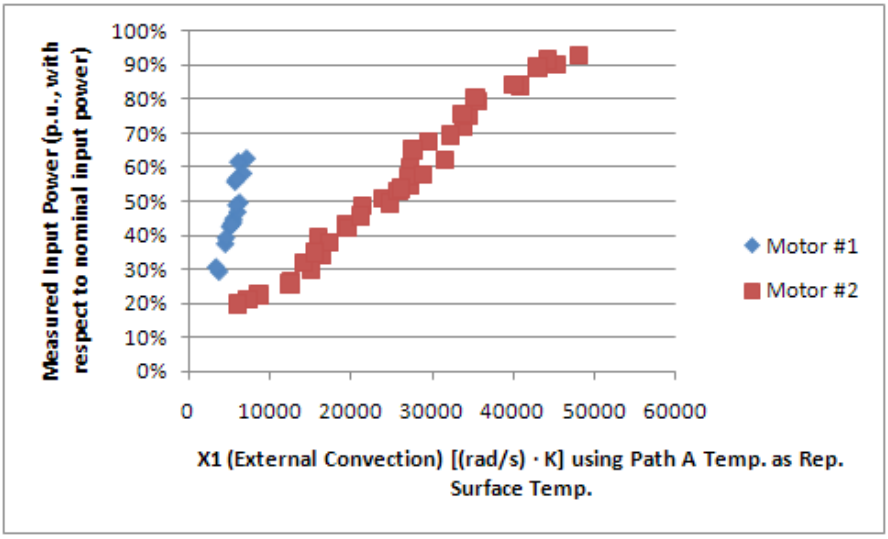

Figure 48: Measured Input Power (p.u., with respect to nominal input power) vs. X1 External Convection using Path A as the representative surface temperature.

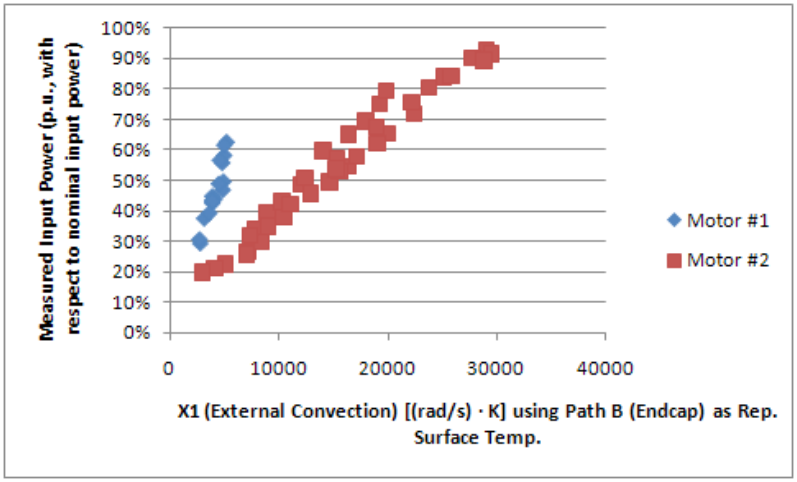

Figure 49: Measured Input Power (p.u., with respect to nominal input power) vs. X1 External Convection using Path B as the representative surface temperature.

Table 13 compares regressions using the X1 (External Convection) dimension for both Motor #1 and Motor #2. The representative surface temperature is either Path A or Path B. On average, the X1 coefficient for Motor #1 is about 2.7 times the corresponding value for Motor #2. Since Motor #1 is a 1200 RPM motor while Motor #2 is a 1800 RPM motor, it is expected that the slope—X1 coefficient value—for Motor #1 will be greater than for Motor #2 (recall Equation 108). However, it is evident that these two motors have differing cooling regimes, since—all things being equal—the X1 coefficient for Motor #1 would only be expected to be 1800/1200 = 1.5 times as great as the corresponding value for Motor #2. Table 13 also shows the regressions using the nonzero constant (X1 C). Allowing for a nonzero intercept improves the RMSE for Motor #2, but is negligible for Motor #1.[33]

[33] That may explain why the X1 coefficient for the "X1 C" regression for Motor #1 has such large confidence intervals.

Table 13: Comparison of regression of X1 (External Convection) between Motor #1 and Motor #2 using Path A and Path B as the representative surface temperature.

Model Variables	Rep. Surface Temp.	Motor	Coefficient Values with Confidence Interval[34]		Model Standard Error of the Estimate	
			Intercept	X1 Coefficient	Watts	p.u.[35]
X1	Path A	Motor #1	0	0.56 ± 0.02	261	4.0%
		Motor #2	0	0.19 ± 0.01	332	3.8%
	Path B	Motor #1	0	0.75 ± 0.03	230	3.5%
		Motor #2	0	0.30 ± 0.01	532	6.1%
X1 C	Path A	Motor #1	-279 ± 804	0.61 ± 0.14	265	4.0%
		Motor #2	410 ± 250	0.17 ± 0.01	295	3.4%
	Path B	Motor #1	-198 ± 681	0.79 ± 0.16	234	3.6%
		Motor #2	917 ± 282	0.26 ± 0.02	366	4.2%

Figure 50 compares the X3 Ejected Air dimension with measured input power for both motors. Its behavior is similar to the X1 External Convection behavior shown earlier in Figures 48 and 49.

[34] The confidence intervals for the intercept and X1 coefficients are determined by Equation 92 (page 60) at the 95% confidence level.

[35] With respect to the nominal motor input power.

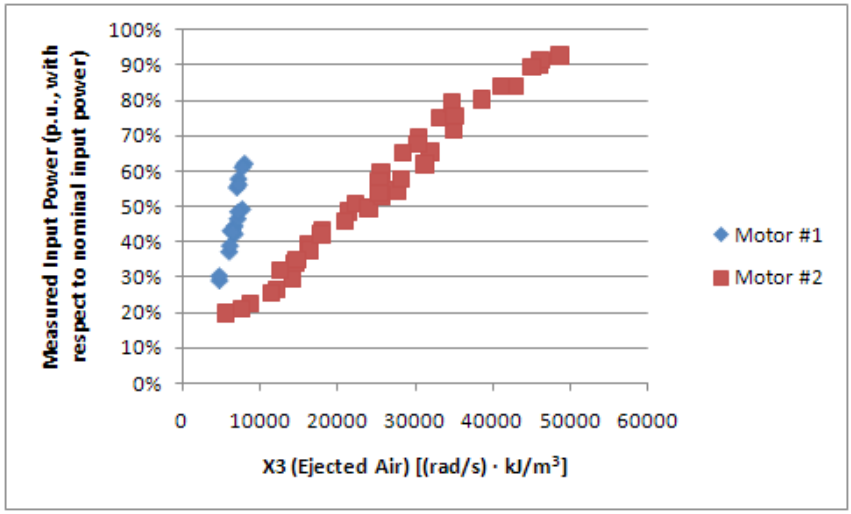

Figure 50: Measured Input Power (p.u., with respect to nominal input power) vs. X3 Ejected Air.

Table 14 compares regressions using the X3 (Ejected Air) dimension for both Motor #1 and #2. The X3 coefficient for Motor #1 is about 2.6 times the corresponding value for Motor #2. Including a nonzero constant in the regressions helps both motors, especially Motor #2. When comparing the performance of the X3 regression with X1 using Path A, the X3 regression does not do as well.

Table 14: Comparison of regression of X3 (Ejected Air) between Motor #1 and Motor #2.

Model Variables	**Motor**	**Coefficient Values with Confidence Interval[36]**		**Model Standard Error of the Estimate**	
		Intercept	**X3 Coefficient**	**Watts**	**p.u.[37]**
X3	Motor #1	0	0.46 ± 0.02	317	4.8%
	Motor #2	0	0.18 ± 0.01	389	4.4%
X3 C	Motor #1	-1369 ± 1076	0.66 ± 0.16	268	4.1%
	Motor #2	690 ± 217	0.16 ± 0.01	270	3.1%

[36] The confidence intervals for the intercept and X3 coefficients are determined by Equation 92 (page 60) at the 95% confidence level.

[37] With respect to the nominal motor input power.

4.3.2.6. Summary

Applying regression with multiple dimensions (i.e., using the full form of Equation 107) resulted in multicollinearity and nonphysical regression coefficients. This is not surprising since the heat transfer modes are not independent of each other. Only regressions using single dimensions provided valid coefficient values. In general, if a regression constant is included, an improvement is found in the model residuals, although it is unclear as to the physical significance of such a constant.

The use of various surface temperatures as the representative surface temperature was investigated. The choice of the best representative surface temperature is not simply the one that predicts the motor power with the least error. Rather, the practicality of the measurement is also considered. For example, motor temperature varies with location and it may be impractical to locate a desired location for temperature measurement. A measurement method that considers multiple motor surface locations or scanning a path on the motor surface may be more practical. Compared to Motor #2, Motor #1 had small degree of temperature variation and trends are not obvious. However, on both motors location #1 which is immediately adjacent to the exposed shaft provided the worst measurement location. If a constant is not included, the hotter locations on Motor #2 provide superior motor power predictions than the cooler locations. Path measurements—which may be more forgiving to measure—provided comparable performance to spot measurements.

The thermal behavior of the two motors differs considerably. Motor #1 had an X1 coefficient from using an X1 regression that was 2.7 times as great as the corresponding value for Motor #2. Motor #1 had an X3 coefficient from using a X3 regression that was 2.6 times as great as the corresponding value for Motor #2. Including constants in the regressions slightly improves Motor #1's performance and improves Motor #2's performance. However, as mentioned earlier, it's not clear what a constant physically represents.

So far we have shown that—given proper coefficients—motor input power can be estimated by measuring various motor temperatures. Recall that the regression coefficients are essentially heat transfer coefficients times various surface areas: external convection coefficient $C_{conv} = h A_{conv}$ and the external radiation coefficient $C_{rad} = \epsilon A_{rad}$. A model to predict these

coefficients—outside of testing for them—has yet to be developed. Such a model would likely be based on motor nameplate values, such as nominal shaft power, synchronous speed, frame size, and enclosure type.

This investigation has been able to show that—given proper coefficients—motor input power can be accurately estimated by measuring various motor temperatures. The RMSE (p.u., relative to the nominal input power) of the loss model when applied to the data is in the neighborhood of 4%. It should be noted that this RMSE is best case and does not reflect the uncertainties for applying this method in the field. Recall that the main regression equation—the motor input power equation shown in Equation 106—requires motor efficiency. However, motor efficiency depends on the motor's load factor—which is the quantity being sought. Therefore in these regressions—where the motor power is directly measured—the motor power is used to estimate the motor efficiency with the help of a generic motor efficiency vs. motor load curve. In the field this luxury is not generally available. Section 3.3.1. showed the vulnerability of the temperature based approach from motor efficiency uncertainty.

Furthermore, in this investigation, the motor coefficients are being solved for using the measured data. In the field, these values would have to be predicted from a not-yet-created model that is likely to be imperfect. Therefore the uncertainty in using the motor loss power estimation in the field will likely be greater than the RMSEs reported here.

4.4. PERFORMANCE OF SLIP AND CURRENT METHODS OF POWER ESTIMATION ON REAL MOTORS

The Slip and Current Methods of estimating ATL-driven motor power was discussed earlier in Section 4.2. That data analysis did not allow for an evaluation of VFD-driven motors with the VFD-Extended Slip Method developed earlier in Section 3.1. Furthermore, the performance of the Slip and Current Methods under real conditions (e.g., over/under-voltage, voltage imbalance, etc.) should be evaluated.

This section details non-thermal tests with Motor #1 and #2. These two motors were specified earlier in Section 4.3.1.1. In this context, these two motors were driven across-the-line and with

a VFD. The VFD used to drive both motors was a Toshiba Q7 33 KVA (30 HP) 480-V Adjustable Speed Drive.

Motor efficiency η_{motor} was not measured, rather an efficiency curve was assumed from the literature as detailed earlier. When driven by a VFD, a 1% drop is taken in motor efficiency (Wallbom-Carlson 1998, 31). VFD efficiency η_{VFD} was not measured; however, the VFD displayed output and input power and these values were recorded. VFD efficiency was taken as the ratio of the VFD-displayed output and input power. A polynomial curve was fitted to the VFD efficiency data points so that VFD efficiency could be estimated from the measured input power. For example, Figure 51 shows the VFD efficiency curve that was determined from the VFD efficiency data points.

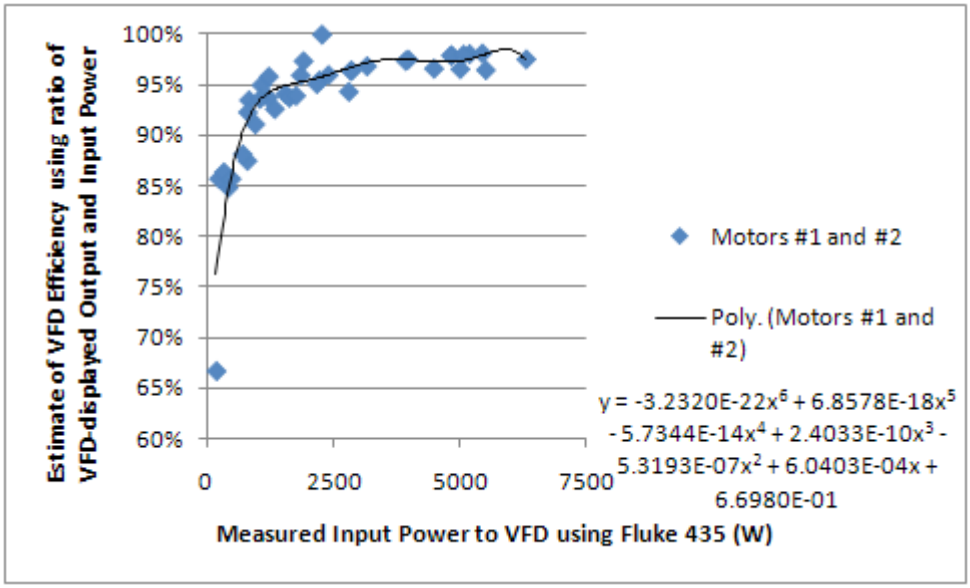

Figure 51: Estimate of VFD Efficiency using the ratio of VFD-displayed Output and Input Power.

4.4.1. VFD-Extended Slip Method

The VFD-Extended Slip Method was developed in Section 3.1.:

$$P_{in} = \frac{N_{sync} - N_{shaft}}{N_{sync,\,rated} - N_{shaft,\,rated}} \cdot \left(\frac{N_{shaft}}{N_{shaft,\,rated}} \right) \cdot \left(\frac{P_{shaft,\,rated}}{\eta_{motor} \cdot \eta_{VFD}} \right) \tag{109}$$

The shaft speed measurement N_{shaft} is detailed earlier in Section 4.3.1.2.2. The supply synchronous speed N_{sync} was determined by using Equation 1. Nameplate shaft power $P_{shaft,\,rated}$ and full-load shaft speed $N_{shaft,\,rated}$ were taken directly off the motors' nameplate and are detailed in Section 4.3.1.1. Figure 52 shows the performance of the VFD-extended Slip Method (Equation 109) on Motor #2. Note the general U-shape trend that was observed earlier in Section 4.2.1.2. applies to the VFD data as well. However, the data points with the VFD at 50 Hz seem to diverge from the trend at high loads. Also note the excessive overestimation of input power at low VFD speeds (i.e., 20 and 30 Hz). This may be due to a deviation from the constant V/Hz scheme that is assumed.

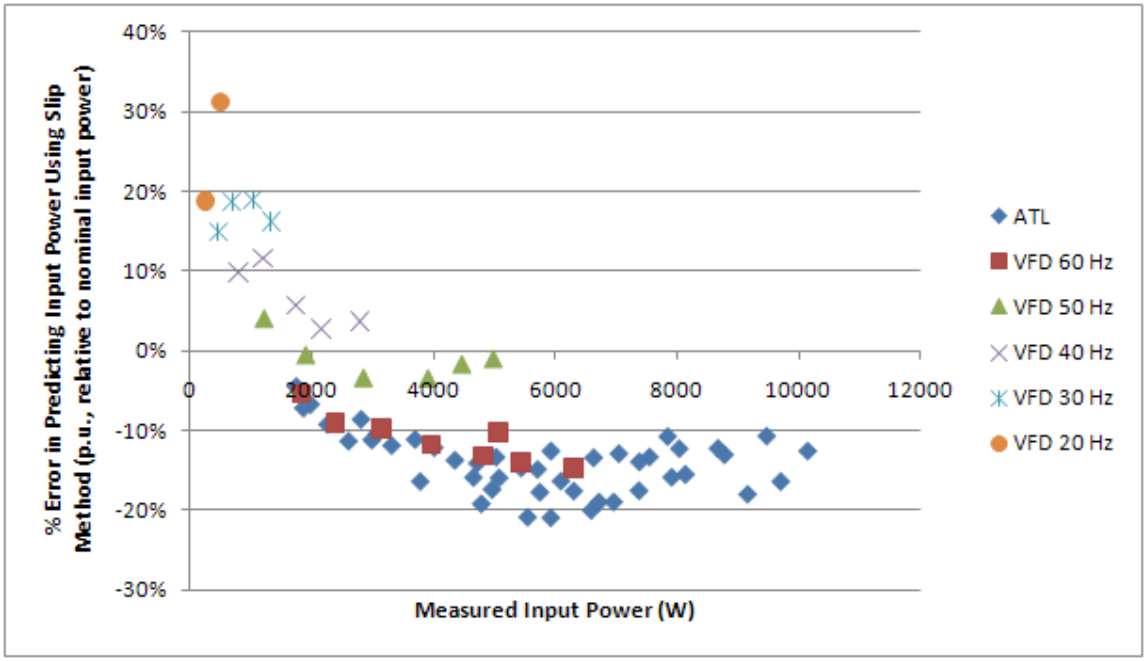

Figure 52: Percent error in predicting input power using VFD-Extended Slip Method (p.u., relative to nominal input power) using Motor #2.

Recall the voltage correction factor $(V/V_{rated})^2$ that is oftentimes included with the ATL Slip Method. In the development of the VFD-Extended Slip Method (Section 3.1.), the constant V/Hz assumption is used to convert that factor into $(N_{sync}/N_{sync,rated})^2$, which is eventually canceled out algebraically. Out of curiosity, the factor $(N_{sync}/N_{sync,rated})^2$ is temporarily tacked onto Equation 109, with the result shown in Figure 53. Notice that the VFD data points have a more uniform trend than in previous plots. In Figure 54, the factor $(N_{sync}/N_{sync,rated})^1$ is tacked on instead; this results in a compromise between the trends seen in Figures 52 and 53. Before too much is inferred from these Slip and Current charts, it should be recalled that at low loads and VFD speeds, efficiency may vary significantly and may not be properly accounted.

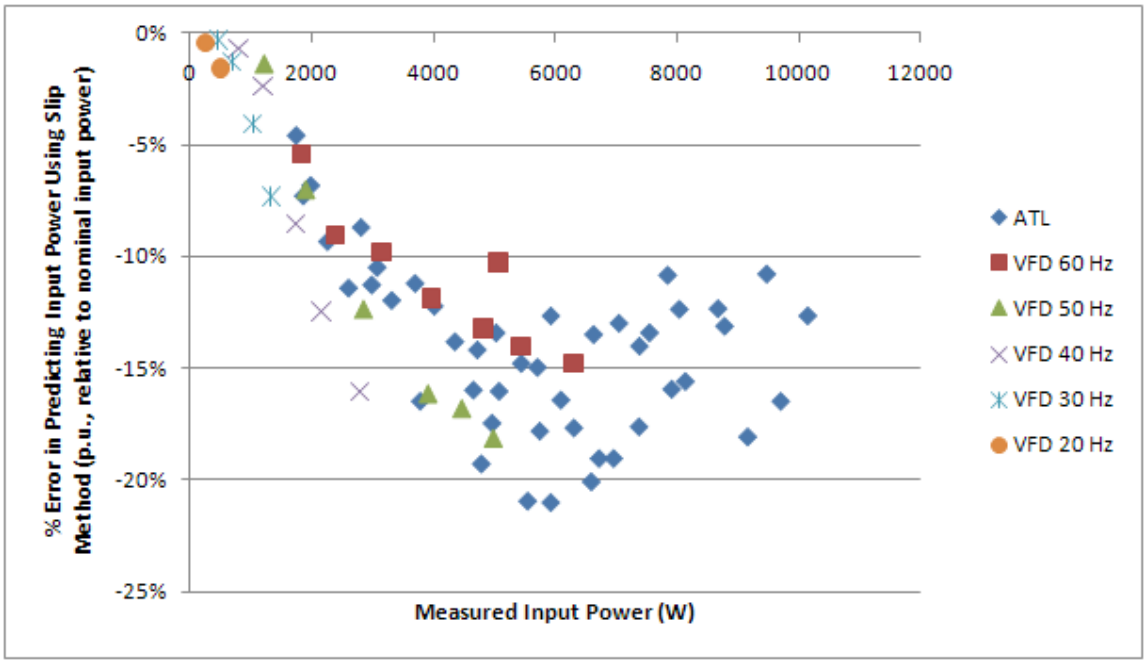

Figure 53: Percent error in predicting input power using VFD-Extended Slip Method with the voltage correction factor (N_sync / N_sync,rated)^2 tacked on (p.u., relative to nominal input power) using Motor #2.

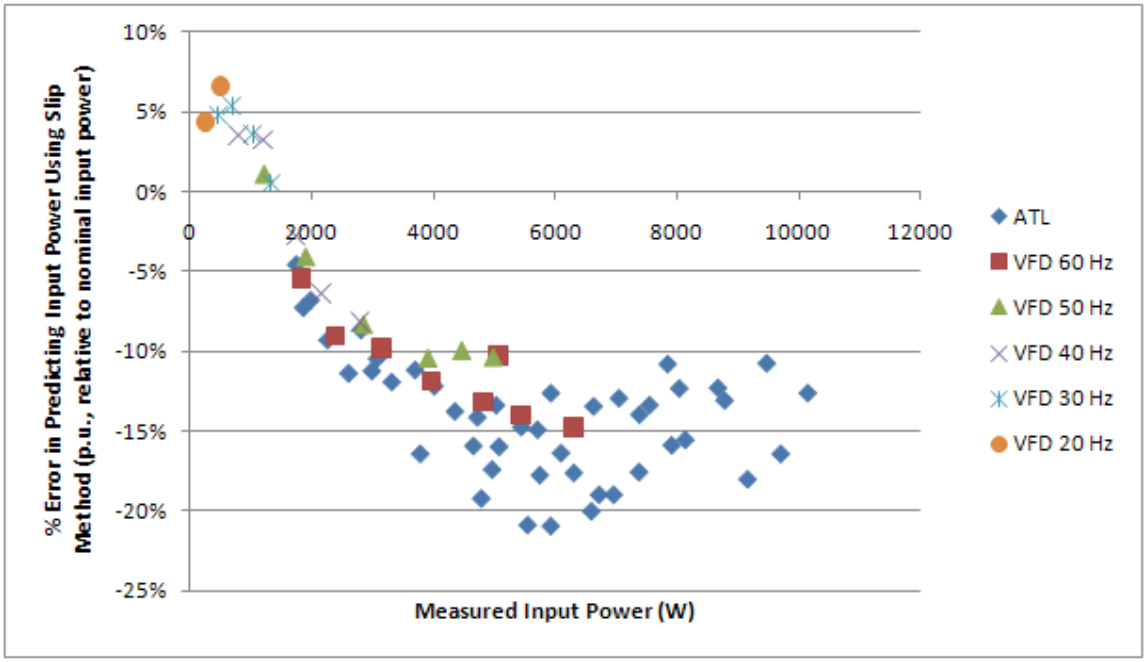

Figure 54: Percent error in predicting input power using VFD-Extended Slip Method with the voltage correction factor (N_sync / N_sync,rated)^1 tacked on (p.u., relative to nominal input power) using Motor #2.

In the previous plots, the ATL data points seem to have a much wider band than the VFD data points. Figure 55 plots only the ATL data points and classifies them by nominal voltage. Clearly, the 460 V data has less error than the 230 V data.

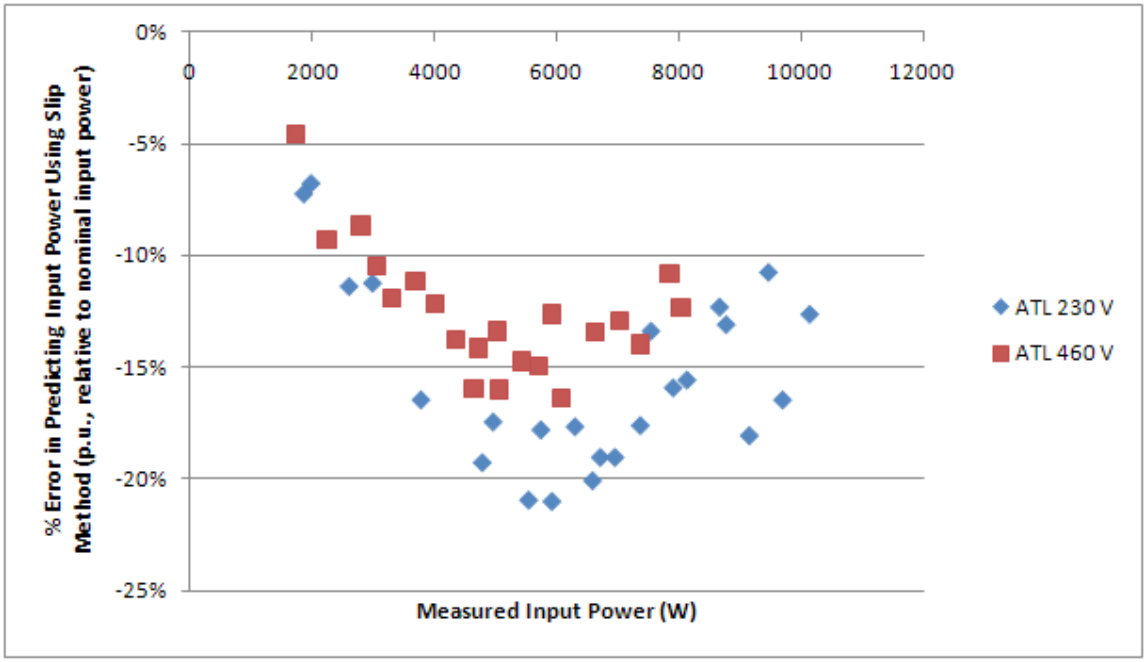

Figure 55: Percent error in predicting input power of the ATL data with the Slip Method (p.u., relative to nominal input power) for Motor #2.

Upon closer inspection of the data, the average supply voltage was greater than the nameplate voltage: the nominal 230 V data had an average supply voltage of 243±0.6 V and the nominal 460 V data had an average supply voltage of 477±0.7 V; both confidence intervals are at the 95% confidence level. Compared to the nominal nameplate voltages—230 V and 460 V—the measured voltages were 6% and 3% over the rated voltage specified on the motor, respectively. Recall the voltage compensation form of the Slip Method for motors driven ATL (earlier shown on page 27):

$$P_{input} = \frac{N_{sync,rated} - N_{shaft}}{N_{sync,rated} - N_{shaft,rated}} \cdot \frac{N_{shaft}}{N_{shaft,rated}} \cdot \frac{P_{shaft,rated}}{\eta_{motor}} \cdot \left(\frac{V_{stator}}{V_{stator,rated}} \right)^2 \quad (110)$$

Figure 56 shows the performance of Equation 110 when used to plot the ATL data, where $V_{stator,rated}$ is the nameplate's nominal voltage (230 V or 460 V) and V_{stator} is set to be the average of the supply voltage: 243 V and 477 V, respectively. When compared to the ATL performance without voltage compensation (Figure 55), Figure 56 shows marked improvement.

Furthermore, the difference between the 230 V and 460 V data is not as marked. Note that individual voltage measurements were not used in Equation 110; rather the averaged measured value was used. That approximates conditions in the field, where average site supply voltage may be known, but measuring voltage at each motor is undesired and tedious. Compensating for the average site voltage decreases the RMSE_pu of the predicted motor input power using the Slip Method on the ATL data from 14.7% to 10.0%.

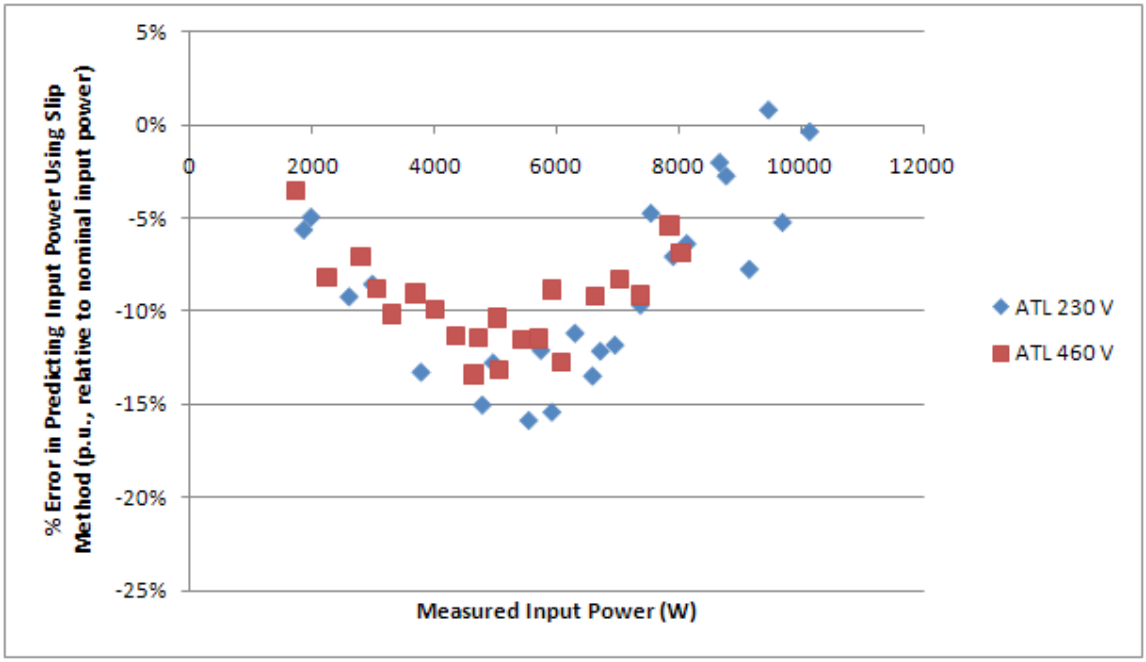

Figure 56: Percent error in predicting input power of the ATL data with the Voltage-Compensated Slip Method (p.u., relative to nominal input power) for Motor #2.

4.4.2. Current Method

Before investigating the Current Method, it is instructive to consider using

$$P_{input} = V \cdot I \cdot PF \cdot \sqrt{3} \tag{111}$$

with assumptions for voltage V and power factor PF. Figure 57 shows the performance of Equation 111 if the average on-site supply voltage is taken for voltage V and the nameplate

power factor is used for PF. A satisfactory explanation for the opposite trends of the ATL and VFD data has yet to be found. Indeed, at low load factors the power factor is also low; therefore the assumption of nameplate power factor could greatly overestimate the measured input power at low loads. It may be of interest to note that as measured input power is decreased, the current unbalance for VFD-driven motors significantly increases; whereas motors driven ATL do not find such a large increase.

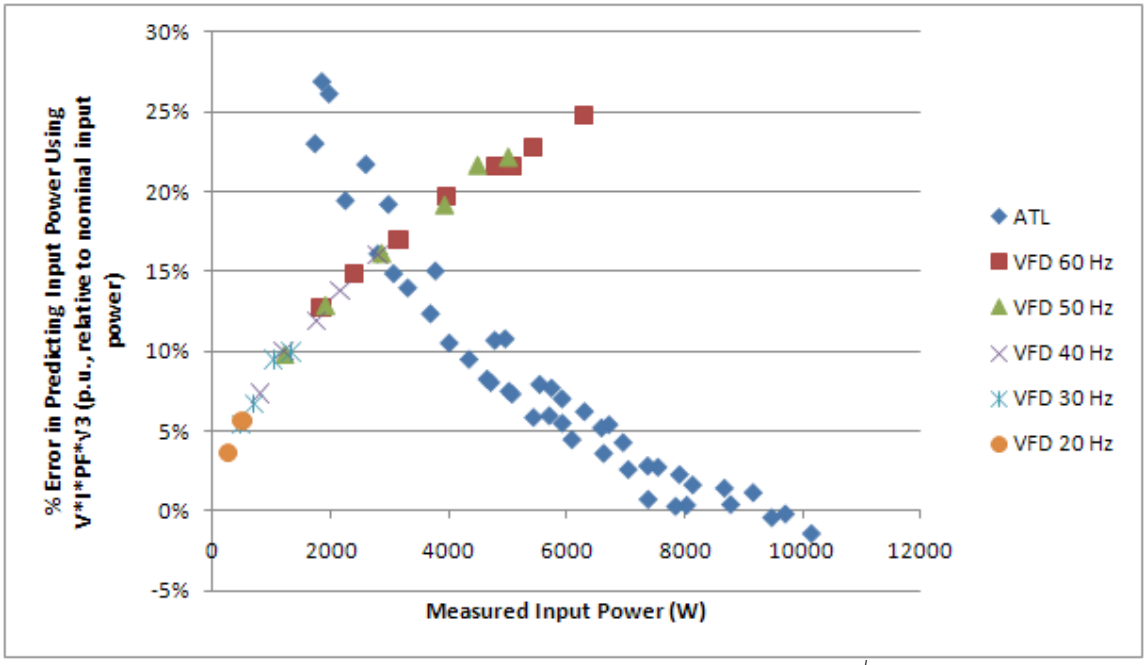

Figure 57: Percent error in predicting input power of the ATL data with V·I·PF·√3 (p.u., relative to nominal input power) for Motor #2.

No literature regarding the application of the Current Method to VFD-driven motors was located; therefore it is of interest to see how this method fares with VFD-driven motors. Also note that—unlike the Slip Method, where a VFD-Extended Equation has been given—the Current Method that is investigated here is the one used in the literature. Recall that the typical Current Method, when used to predict input power is given as:

$$P_{in} = \begin{cases} \dfrac{I - I_{No\ Load}}{I_{Full\ Load} - I_{No\ Load}} \cdot \left(\dfrac{P_{shaft,rated}}{\eta_{motor} \cdot \eta_{VFD}} \right), & \text{if } I \geq I_{NoLoad} \\ 0, & \text{if } I < I_{NoLoad} \end{cases} \quad (112)$$

Current was measured in all three phases upstream from the VFD (if present); the average of which was used for current I. Nameplate shaft power $P_{shaft,\,rated}$ and full-load current $I_{Full\ Load}$ were taken directly from the motors' nameplate. The No-Load Current $I_{No\ Load}$ was estimated as a fraction of the full-load current: $I_{No\ Load} = k \cdot I_{Full\ Load}$, where k is a fraction usually between 0 and 0.3. In order to avoid negative input power estimates caused when $I < I_{No\ Load}$, a minimum of zero is established for the predicted input power.

Several k values were investigated (e.g., 0, 0.1, 0.2, and 0.3). Using $k = 0$ provided the largest input power prediction errors; this condition is plotted for Motor #2 in Figure 58. Notice that the ATL datapoints and the VFD datapoints create distinct trends; below 2000 Watts (23% of the nominal input power), errors increase significantly. Using $k = 0.2$ provided the smallest input power prediction errors; this condition is shown for Motor #2 in Figure 59. In that plot, the VFD behavior diverges considerably from the ATL behavior, although the RMSE for the ATL and VFD errors are considerably less than with $k = 0$.

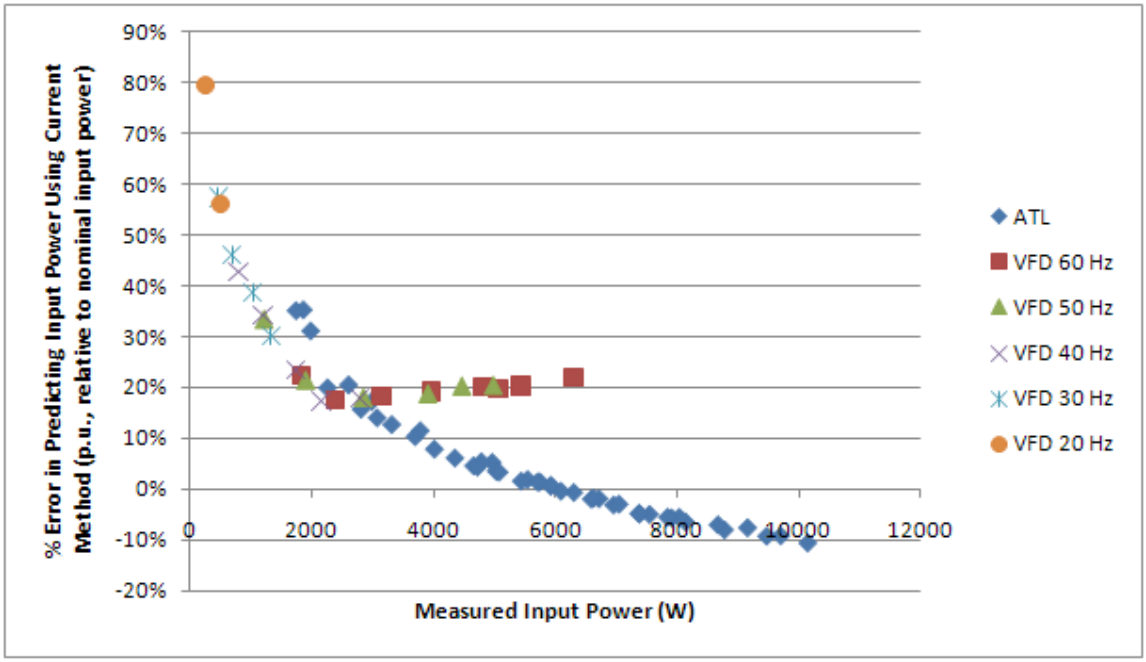

Figure 58: Percent error in predicting input power using Current Method with k=0 (p.u., relative to nominal input power) using Motor #2.

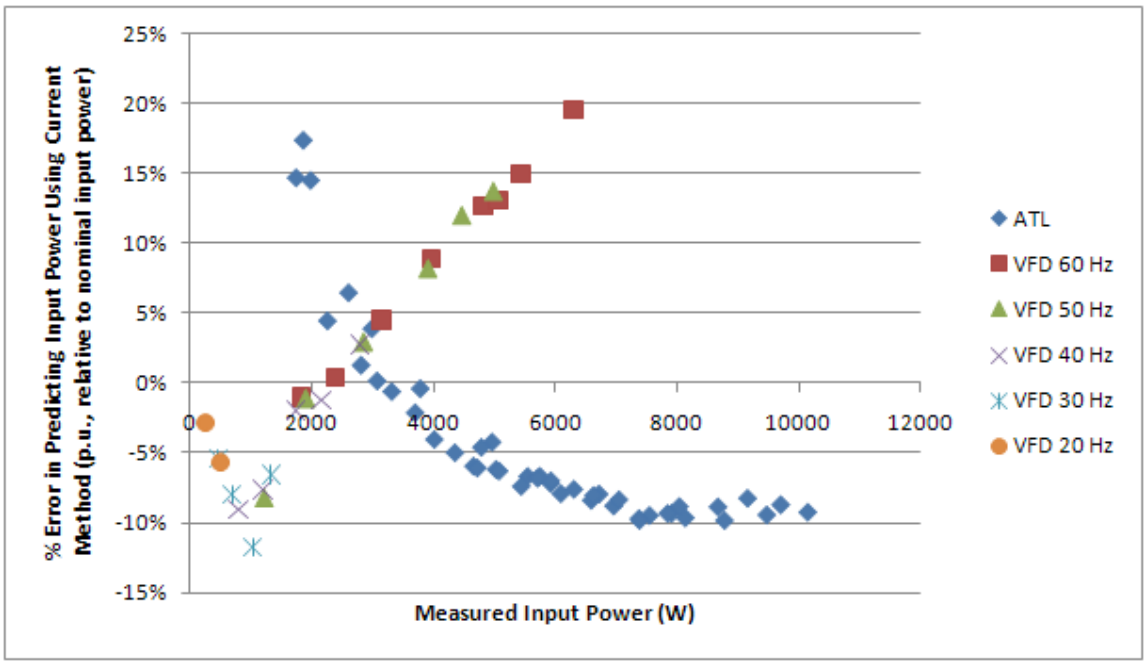

Figure 59: Percent error in predicting input power using Current Method with k=0.2 (p.u., relative to nominal input power) using Motor #2.

4.4.3. Summary

Table 15 compares the performance of variations of the Slip Method and Current Method over both motors. When driven ATL, the Slip Method performs worse than the Current Method; however, when the supply voltage is compensated for, the Slip Method is comparable to the Current Method. When the motors were driven by a VFD, a comparison of the performance of the Slip and Current Methods is difficult due to the effect of the choice of k-value.

Table 15: Comparison of RMSE_pu of the motor input power residuals for power prediction methods.

Method	**Constraint**	**Motor #1**		**Motor #2**	
		ATL	**VFD > 20 Hz**	**ATL**	**VFD > 20 Hz**
Slip Method	Using Eq. 109	20%	12%	15%	11%
	With direct Voltage Compensation (Eq. 110)	17%	N/A	10%	N/A
$V \cdot I \cdot PF \cdot \sqrt{3}$	$V = V_{site\ average}$ and $PF = PF_{rated}$	22%	19%	11%	17%
Current Method	$k = 0$	18%	24%	12%	29%
	$k = 0.2$	16%	14%	8%	9%

Recall the torque factor (the second factor in Equations 109 and 110) which is often missing from Slip Methods given in the literature. All of the presented Slip Method calculations (including those in Table 15) have included this factor. If that factor is neglected, the RMSE of the motor input power residuals for motor #1 and motor #2 increase about 1% point.

5. SUMMARY

Recall the objective of this research was to explore methods for rapid, safe, and non-invasive estimation of input power for motors used in commercial HVAC and pumping applications. Direct electrical measurement, Current Method (and $V \cdot I \cdot PF \cdot \sqrt{3}$), Slip Method, and a temperature approach to estimating motor input power have been investigated.

5.1. DIRECT ELECTRICAL MEASUREMENT

While direct electrical measurement using a wattmeter is the most accurate method of measuring motor input power, its setup time, invasiveness, and potential safety hazards limit its use for preliminary energy audits. Installed equipment—such as a chiller or VFD—may display input power. When such readings are readily available on installed equipment in the field, they are the preferred method for measuring input power in the preliminary energy audit context. This approach may also offer the ability to develop an input power profile over a time period by using data logging.

5.2. CURRENT METHOD

The usefulness of the Current Method in this investigation largely depends on the rapidness and safety of measuring current. Physical access to all three electrical phases is restricted in the field, thereby limiting the use of current clamps. Installed equipment—such as a chiller or VFD —may display average current.

With the 459 Baldor/Reliance motors, the Current Method (using k=0 and efficiency=nameplate) predicted normalized input power with a MBE_pu of 5.4% and a RMSE_pu of 10.0% (Section 4.2.3.). Furthermore, the Current Method may be a candidate for improved performance by using regression of the predicted variable (Section 4.2.2.). In addition, nameplate parameters (nameplate power factor and rated synchronous speed) and motor manufacturer were found to have a major impact on the Current Method errors. Recall that motor nameplates generally don't provide No Load Current values. For the Baldor/Reliance data set, it was shown that the best estimate for the No Load Current was 30% of the rated Full Load Current.

For Motor #1 and #2, the Current Method provided widely varying standard errors of the estimates: 16% and 8% for ATL using k=2, respectively (Table 15). When driven by a VFD, the Current Method (using k=2) provided RMSE_pu of 14% and 9%, respectively.

Recall a cousin to the Current Method is the use of $V_{site\,average} \cdot I \cdot PF_{rated} \cdot \sqrt{3}$ for motor input power estimation. This approach still requires current measurement, but dispenses with estimating no-load motor current which is required for the Current Method. With 459 Baldor/Reliance motors, using $V_{site\,average} \cdot I \cdot PF_{rated} \cdot \sqrt{3}$ performed worse than the Current Method using *k=0*, with a MBE_pu of 8.5% and RMSE_pu of 18.6% if the applied voltage is the rated voltage and nameplate power factor is assumed (Section 4.2.3.). The performance of $V_{site\,average} \cdot I \cdot PF_{rated} \cdot \sqrt{3}$ on motor #1 and #2 was mixed: for motors driven ATL using $V_{site\,average} \cdot I \cdot PF_{rated} \cdot \sqrt{3}$ provided comparable performance to the Current Method, which goes against the Baldor/Reliance findings found in Section 4.2.3. When driven by a VFD, using $V_{site\,average} \cdot I \cdot PF_{rated} \cdot \sqrt{3}$ on motor #1 and #2 provided improved errors from the Current Method (Section 4.4.3.); it is not known if that will extend to other VFD-driven motors. It is conceivable that using $V \cdot I \cdot PF \cdot \sqrt{3}$ may be of use when current information is available for motors without accessible nameplate information. If current information is available, it likely came from a VFD display. In such situations, the VFD effect on power factor would need to be investigated.

5.3. SLIP METHOD

If installed equipment does not readily display input power or average current, then the Slip Method for estimating motor input power is recommended if access to motor nameplate information and a shaft speed measurement is available. Shaft speed measurements should be done with a stroboscopic tachometer, which may measure shaft speed without the need for equipment shut-down to apply a marker to the shaft.

With the 459 Baldor/Reliance motors, the Slip Method (including the torque factor and using efficiency=nameplate) predicted normalized input power with a MBE_pu of -3.2% and a RMSE_pu of 9.9% (Section 4.2.3.). The Baldor/Reliance dataset investigation (Section 4.2.1.)

demonstrated that—while knowledge of non-shaft speed nameplate parameters does not improve the Slip Method's error—a recognizable trend exists for the Slip Method's residual from predicting the load factor. Adding an error-correction polynomial to the Slip Method reduced the RMSE of the predicted motor load factor from 9.0% to 8.2% for the Baldor/Reliance motor data. Further refinement may be possible if load factors are weighted and regression curves are generated per motor manufacturer.

The Slip Method was extended to VFD-driven motors (Section 3.1.) and tested on Motor #1 and Motor #2. Results from the two motor tests indicate that the VFD-extended Slip Method gives a RMSE_pu of the residual predicted input power for the two motors at 12% and 11%, respectively. When run ATL, the Slip Method was improved by accounting for the average site voltage; the RMSE_pu of the residual predicted input power for the two motors was reduced 3% and 5% points, respectively.

Neglecting the torque factor $N_{shaft}/N_{shaft,rated}$ resulted in a slight increase in error. With the Baldor/Reliance motors, neglecting the torque factor increased the RMSE_pu of the predicted normalized input power by 0.2% points (Section 4.2.3.). With motor #1 and #2, neglecting the torque factor increased the RMSE_pu of the predicted normalized power by 1% point (Section 4.4.3.).

5.4. ORMEL

Regarding ORMEL, an evaluation of its load factor prediction abilities with 21 Baldor motors suggests that it does not give significantly improved load factor residuals compared to the Slip Method (Section 4.2.4.). As far as measurements are concerned, ORMEL suffers from any measurement problems that the Slip Method has because it also requires a shaft speed measurement and nameplate full-load speed values, along with other nameplate parameters. Therefore, even if ORMEL has improved motor power prediction abilities over the Slip Method, its application in the preliminary energy audit context is limited to that of the Slip Method.

5.5. MOTOR TEMPERATURE APPROACH

If installed equipment does not display input power or average current, and if shaft speed measurements are impractical, then a temperature approach for estimating motor input power may be applicable. This approach requires various temperature measurements, motor efficiency, and at least one thermal constant which corresponds to the motor. Motor efficiency is the only nameplate value that is explicitly required. However, other nameplate information (e.g. insulation class, motor size, motor synchronous speed, etc.) may be useful in predicting values for the various constants.

A major disadvantage to the temperature approach for estimating motor power is the determination of motor efficiency. In Section 3.3.1. and Appendix B, it has been demonstrated that uncertainty in motor efficiency has a major effect on the uncertainty in input power with this method. Motor efficiency is also required for the Slip and Current Methods[38], but they are more resilient from the effect of motor efficiency uncertainty. A second disadvantage for this approach is that—until another model is created to predict the motor thermal constants from easily determined (e.g. nameplate) parameters—the motor constants must be experimentally determined for each motor. It has been demonstrated that thermal coefficients may vary significantly across motors (Section 4.3.2.5.).

This temperature-based approach was evaluated on Motor #1 and Motor #2. If a motor's thermal constants and running efficiency are known, then this method gives motor input power estimates with an RMSE_pu on the order of 4% for both motors (Table 13). That performance value should not be directly compared to other motor input power methods (e.g. Slip Method or Current Method) because it does not include errors from mis-specified motor running efficiency or motor thermal constants.

5.6. CONCLUSION

This investigation has evaluated, extended, and developed methods for input power estimation. It is useful to compare the methods with terms used in the objective statement. Table 16 summarizes motor input power estimation methods and gives qualitative estimates for

[38] Motor efficiency is not required for the wattmeter method or $V \cdot I \cdot PF \cdot \sqrt{3}$.

Table 16: Comparison of motor input power estimation methods.

Method	Primary Variable	Other Parameters	Field Condition	Time	Safety Risk	Invasiveness	Uncertainty
Direct measurement	Real Power	None	Displayed on installed equipment	Low	Low	Low	Low
			Application of wattmeter	High	High	High	
***V*·*I*·*PF*·√3**	Current	Voltage, Power Factor	Current is displayed on installed equipment	Low	Low	Low	Medium / High
			Application of current clamps	Medium	Medium	Medium	
Current Method	Current	Full-Load Current, No-Load Current, Efficiency	Current is displayed on installed equipment	Low	Low	Low	Medium
			Application of current clamps	Medium	Medium	Medium	
Slip Method	Shaft speed	Full-Load Shaft Speed, Efficiency	Shaft speed measurement does not require marker application	Low	Low	Low	Medium
			Shaft speed measurement requires marker application	Low	Low	Medium	
ORMEL	Shaft speed	Full-Load Shaft Speed, Full-Load Amps, Full-Load Power Factor, kVA code	Shaft speed measurement does not require marker application	Low	Low	Low	Medium
			Shaft speed measurement requires marker application	Low	Low	Medium	
Temperature Approach	Motor temperature	Reference temperature, Thermal coefficients, Efficiency	Motor enclosure is accessible	Low	Low	Low	High

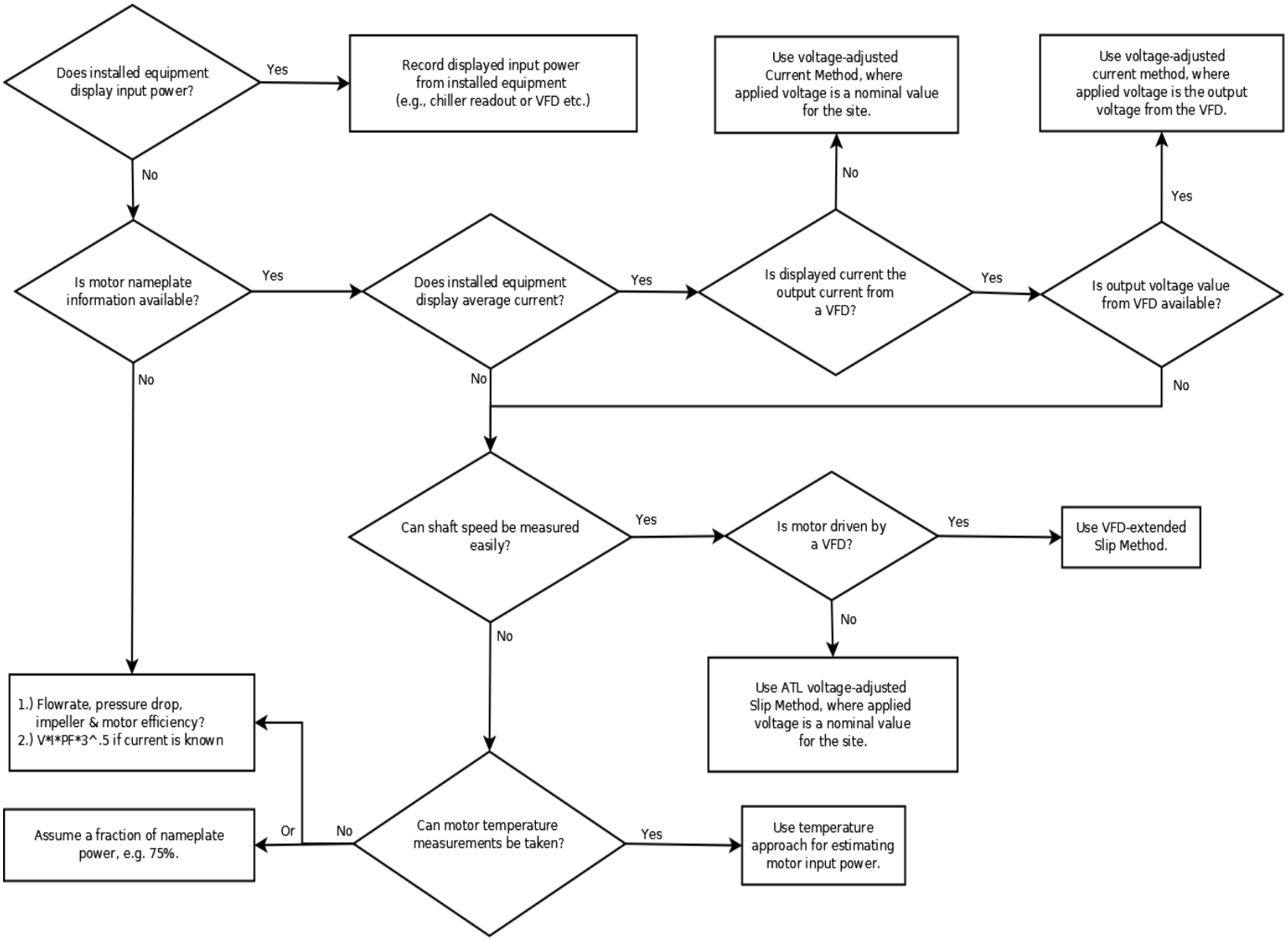

Figure 60: Flowchart for determining motor input power in building energy assessments.

setup/measurement time, safety risk, invasiveness, and input power uncertainty. For easy comparison, each performance dimension—Time, Safety Risk, Invasiveness, and Uncertainty—is an undesirable quality that should be minimized. It is recognized that Table 16 only offers coarse evaluations; that is due to the difficulty in assessing the methods. Even comparing input power uncertainty is not easy because of the differing assumptions that are used in the input power prediction methods. The construction of this summary table has been aided by a similarevaluation by Lu, Habetler, and Harley (2006, 931).

Figure 60 outlines a proposed flowchart for determining motor input power in the field. If installed equipment displays input power, then using that reading is preferred. Else if installed equipment displays average current, then the Current Method should be used. If installed equipment does not display input power or average current, the application of wattmeters or current clamps may be too time-consuming and invasive for the preliminary energy audit. In that case, if a shaft speed measurement is readily available, then the Slip Method is a satisfactory method for estimating motor input power. If a shaft speed measurement is not accessible, then the temperature approach may be of use. Finally, assuming a fraction of the nameplate power is a fallback method for estimating motor input power.

For situations where nameplate information is not available, it may be of use to investigate using $V \cdot I \cdot PF \cdot \sqrt{3}$ (if current is known) or consider a fluid power approach which accounts for the pressure drop and flowrate of the driven fluid, impeller efficiency, and motor efficiency. These two options are listed but have not been investigated.

5.7. FUTURE WORK

A survey of field conditions is necessary to further evaluate the motor input power methods. What percentage of HVAC motors can a stroboscopic tachometer directly read shaft speed without stopping[39] the motor? What percentage of installed equipment (e.g. VFDs) directly display input power without having to interface with a user-interface? What is the typical voltage variation—by time and location—in commercial buildings? Answers to all of these questions will help refine the direction for future research.

[39] Stopping the motor to apply a marker to the shaft is inconvenient for the energy auditor. Stroboscopic shaft measurements may not require stopping the motor to place a marker (Energy Ideas Clearinghouse 2007; Ramsay 1996, 71). The applicable prevalence of this claim should be evaluated.

More information may be gleaned from the Baldor/Reliance data set. Motor efficiency trends with the Baldor/Reliance motors may be useful to obtain. Power factor trends may be useful for the $V \cdot I \cdot PF \cdot \sqrt{3}$ method, which in this paper have been assumed to be constant.
For VFD-driven motors, anecdotal experience has demonstrated that some VFDs display current, voltage, and power factor; in these cases, a method using $V \cdot I \cdot PF \cdot \sqrt{3}$ should be investigated. Also note that only one VFD was tested; before too much is inferred from the VFD data, it would be prudent to consider other VFDs.

It has been shown that if certain motor thermal coefficients are known, then a motor's input power can be estimated via various motor temperature measurements. It has also been shown that the coefficients vary considerably between two motors. A model that predicts the coefficients should be created. If further experiments are performed using the temperature approach, it is suggested that motor efficiency be measured and not estimated from an efficiency vs. load curve. In addition, more refined temperature measurement of the air is needed, instead of using liquid-in-glass thermometers which provided 0.5 ºF intervals. It is also advised that the motor should be completely isolated from the fan's airflow; although steps were taken in this investigation toward this, diagnostic plots demonstrated that the fan's airflow affected the motor cooling. Furthermore, it may be desirable to have improved control over the ambient temperature. In the completed thermal experiments, the room temperature varied considerably (e.g. on one occasion, the ambient temperature dropped from 81 ºF to 76 ºF in one hour).

Most of these power prediction methods in this investigation require a value for a motor's running efficiency. The temperature-based approach requires accurate estimates for running efficiency that may not be provided from assuming the nameplate efficiency value. A complete understanding of how nameplate efficiency deviates from running efficiency is required.

REFERENCES

Agamloh, E.B. 2007. The partial load efficiency of induction motors. In *Record for the 42nd (2007) IEEE Industry Applications Conference*, 1460-1466. September 23. doi:10.1109/07IAS.2007.225.

Albers, T., and A.H. Bonnett. 2002. Motor temperature considerations for pulp and paper mill applications. *IEEE Transactions on Industry Applications* 38(6): 1701-1713. doi:10.1109/TIA.2002.805574.

Alted, F., and I. Vilata. *PyTables: Hierarchical Datasets in Python, Version 2.0.* http://www.pytables.org. Accessed October 2009.

Angers, P. 2003. Comparison between nameplate efficiency and actual measured efficiency for three-phase induction motors. In *Energy Efficiency in Motor Driven Systems*, 54-59. Berlin, Germany: Springer-Verlag.

ASHRAE. 2000a. Centrifugal pumps. In *2000 ASHRAE Handbook on HVAC Systems and Equipment*, 39.1 to 39.15. IP Edition. Atlanta, GA: ASHRAE.

ASHRAE. 2000b. Fans. In *2000 ASHRAE Handbook on HVAC Systems and Equipment*, 18.1 to 18.9. IP Edition. Atlanta, GA: ASHRAE.

ASHRAE. 2000c. Motors, motor controls, and variable-speed drives. In *2000 ASHRAE Handbook on HVAC Systems and Equipment*, 40.1 to 40.13. IP Edition. Atlanta, GA: ASHRAE.

ASHRAE. 2004. *Procedures for Commercial Building Energy Audits*. SP-56. Atlanta, GA: ASHRAE.

ASHRAE. 2005. Heat transfer. In *2005 ASHRAE Handbook on Fundamentals*, 3.1 to 3.35. IP Edition. Atlanta, GA: ASHRAE.

Astrom, J. 2004. Measurement of loss components in two induction machines and three types of frequency converters. M.S. Thesis, Chalmers University of Technology, Göteborg, Sweden. http://webfiles.portal.chalmers.se/et/MSc/AstromJohanMSc.pdf.

Auinger, H. 2001. Efficiency of electric motors under practical conditions. *Power Engineering Journal* 15(3): 163-167.

Barnes, M. 2003. *Practical Variable Speed Drives and Power Electronics*. Oxford, England: Newnes.

Bartos, F. 2001. The 3 (or more) faces of AC variable-speed drives. *Control Engineering* 48(11): 64.

Benedict, R.P. 1984. *Fundamentals of Temperature, Pressure, and Flow Measurements*. 3rd ed. New York: Wiley.

Bernier, M.A., and B. Bourret. 1999. Pumping energy and variable frequency drives. *ASHRAE Journal* 41(12): 37-40.

Boglietti, A., A. Cavagnino, M. Parvis, and A. Vallan. 2006. Evaluation of radiation thermal resistances in industrial motors. *IEEE Transactions on Industry Applications* 42(3): 688-693. doi:10.1109/TIA.2006.873655.

Boglietti, A., A. Cavagnino, and D. Staton. 2008. Determination of critical parameters in electrical machine thermal models. *IEEE Transactions on Industry Applications* 44(4): 1150-1159. doi:10.1109/TIA.2008.926233.

Boldea, I., and S. A. Nasar. 2002. *The Induction Machine Handbook*. Electric Power Engineering Series. Boca Raton, FL: CRC Press.

Bonnett, A.H. 1994. An update on AC induction motor efficiency. *IEEE Transactions on Industry Applications* 30(5): 1362-72. doi:10.1109/28.315251.

Bonnett, A.H. 2001. Operating temperature considerations and performance characteristics for IEEE 841 motors. *IEEE Transactions on Industry Applications* 37(4): 1120-1131. doi:10.1109/28.936405.

Bousbaine, A. 1999. Thermal modelling of induction motors based on accurate loss density distribution. *Electric Machines and Power Systems* 27(3): 311-24. doi:10.1080/073135699269325.

Capehart, B.L. 2000. Equipment Load Factors, Use Factors and Diversity Factors as well as a General Discussion of Energy Audit Procedures. http://www.ise.ufl.edu/capehart/papers/diversity.doc.

Capehart, B.L., and L.C. Capehart. 2007. Auditing: Improved accuracy. In *Encyclopedia of Energy Engineering and Technology*, 1:69-75. Vol. 1. Boca Raton, FL: CRC Press.

Chang, Y.T. 2006. Comparison of three types of induction motor control. In *2nd International Conference on Power Electronics Systems and Applications*, 209-219. Hong Kong, China: IEEE.

Chan, T. 2004. Beyond the affinity laws. *Engineered Systems* 21(8): 37-48.

Chatterjee, S., and A.S. Hadi. 2006. *Regression Analysis by Example*. 4th ed. Hoboken, NJ: Wiley-Interscience.

Chen, K., and R. Nailen. 2004. Motor efficiency and energy considerations. In *Handbook of Electric Motors*, 2nd ed., eds. H.A. Toliyat and G.B. Kliman, 185-188. Boca Raton, FL: CRC Press.

Chillet, C., R. Isnard, A.W. Hadi, and M. Brunello. 1990. Analysis and localization of losses in an induction machine using a calorimetric method. *Electric Machines and Power Systems* 18(1): 29-39.

Chiulli, R. 1999. *Quantitative Analysis: An Introduction*. Amsterdam, The Netherlands: Gordon and Breach Science Publishers.

da Costa Bortoni, E. 2007. Motor oversizing outlook. In *Proceedings of International Conference on Electrical Machines and Systems, Seoul, Korea*, 1385-1396. October 8. doi:10.1109/ICEMS.2007.4412067.

Domijan, A. Jr., and D. Czarkowski. 1997. Challenges in electrical power measurements of adjustable speed drives and motors. *ASHRAE Journal* 39(2): 32-41.

Douglass, John G. 1997. *Efficacy of methods for estimating in-service motor efficiency*. Olympia, WA: Washington State University Cooperative Extension Energy Program.

EASA. 1999. *Understanding Energy Efficient Motors*. Electrical Apparatus Service Association. http://easa.com/indus/ee_399.pdf.

Electrical Apparatus. 2007. Constant for full- to no-load? *Electrical Apparatus* 60(2): 6.

Elkor Technologies. 2006. *Introduction to Current Transformers*. Application Note. London, ON, Canada. http://www.elkor.net/pdfs/AN0305-Current_Transformers.pdf.

Emadi, A. 2005. *Energy-Efficient Electric Motors*. Third Edition. Electrical and Computer Engineering 122. New York: Marcel Dekker, Inc.

Energy Ideas Clearinghouse. 2007. *Calculating motor load: how much does it cost to take measurements from which we can calculate percent load on our motors?* Energy Solutions Database. Washington State University. http://www.energyexperts.org/energy_solutions/res_details.cfm?resourceID=2915&keyword=tach&sector=All. Accessed June 2008.

E Source. 1999. *Drivepower Technology Atlas*. E Source Technology Atlas Series. Boulder, CO: E Source, Inc.

Fluke Corp. 2005a. Application note: The Fluke 62 mini infrared thermometer. http://support.fluke.com/find-sales/Download/Asset/2517382_6250_ENG_A_W.PDF.

Fluke Corp. 2005b. *The Fluke 62 mini infrared thermometer*. Technical Data. Everett, WA. http://support.fluke.com/FInd-Sales/Download/Asset/2437622_6250_ENG_A_W.PDF.

Fluke Corp. 2006. *Fluke 430 series: Three-phase power quality analyzers*. Technical Data. Everett, WA. http://support.fluke.com/FInd-Sales/download/asset/2643006_6112_eng_a_w.pdf.

Gopalakrishnan, B., S. Chaudhari, P. Famouri, and R.W. Plummer. 2006. Facilitation for load based energy savings in three-phase squirrel cage induction motors. *Energy Engineering: Journal of the Association of Energy Engineers* 103(6): 37-64.

Guru, B.S., and H.R. Hiziroğlu. 2001. *Electric Machinery and Transformers*. 3rd ed. New York: Oxford University Press.

Haasl, T., and K. Heinemeier. 2006. *California commissioning guide: Existing buildings*. California Commissioning Collaborative. http://www.cacx.org/resources/documents/CA_Commissioning_Guide_Existing.pdf.

Hay, N., D. Lampard, S.J. Pickering, and T.F. Roylance. 1995. Air flow and heat transfer over the

ribbed surface of an externally cooled electric motor. In *Proceedings of the 1995 ASME/JSME Thermal Engineering Joint Conference, Part 1*, 1:321-326. Vol. 1. New York: ASME.

Hoffmeyer, W.R., W.J. Martiny, and J.H. Johnson. 2004. Induction motors--Polyphase and single-phase. In *Handbook of Electric Motors*, 2nd ed., eds. H.A. Toliyat and G.B. Kliman, 35-43. Boca Raton, FL: CRC Press.

Holman, J. P. 2001. *Experimental Methods for Engineers*. 7th ed. New York: McGraw-Hill.

Holmquist, J.R., J.A. Rooks, and M.E. Richter. 2004. Practical approach for determining motor efficiency in the field using calculated and measured values. *IEEE Transactions on Industry Applications* 40(1): 242-8. doi:10.1109/TIA.2003.821654.

Hoshide, R.K. 1994. Electric motor do's and don'ts. *Energy Engineering: Journal of the Association of Energy Engineers* 91(1): 6-24.

Hsu, J.S., J.D. Kueck, M. Olszewski, D.A. Casada, P. Otaduy, and L.M. Tolbert. 1998. Comparison of induction motor field efficiency evaluation methods. *IEEE Transactions on Industry Applications* 34(1): 117-25. doi:10.1109/28.658732.

Huai, Y., R.V.N. Melnik, and P.B. Thogersen. 2003. Computational analysis of temperature rise phenomena in electric induction motors. *Applied Thermal Engineering* 23(7): 779-95.

Hunter, J. *Matplotlib, Version 0.98*. http://matplotlib.sourceforge.net. Accessed September 2009.

IEEE. 2004. *IEEE Std 112-2004 Standard Test Procedures for Polyphase Induction Motors and Generators*. IEEE Standards SH95211. New York: IEEE.

Johnson, J.H. 2004. Selection and application of test equipment. In *Handbook of Electric Motors*, 2nd ed., eds. H.A. Toliyat and G.B. Kliman, 400-404. Boca Raton, FL: CRC Press.

Jones, E., T. Oliphant, and P. Peterson. *SciPy: Open Source Scientific Tools for Python, Version 0.7.0*. http://www.scipy.org. Accessed July 2009.

Jowett, J., and W.D. Biesemeyer. 1994. Energy efficient motors for HVAC applications: An experimental approach. In *Competitive Energy Management & Environmental Technologies*, 1st ed., 245-254. Lilburn, GA: Fairmont Press.

Krarti, M. 2001. Electrical systems. In *Handbook of Heating, Ventilation, and Air Conditioning*, ed. J.F. Kreider. The Mechanical Engineering Handbook Series. New York: CRC Press.

Kueck, J.D. 1998. Development of a method for estimating motor efficiency and analyzing motor condition. In *Proceedings of the 1998 Annual Pulp and Paper Industry Technical Conference*, 67-72. IEEE. doi:10.1109/PAPCON.1998.685505.

Kueck, J.D., J.R. Gray, R.C. Driver, and J.S. Hsu. 1996. *Assessment of Available Methods for Evaluating In-service Motor Efficiency*. Prepared for the U.S. Dept. of Energy. Oak Ridge, TN: Oak Ridge National Laboratory.

Kueck, J.D., and P. Otaduy. 1997. Method for Assessing In-Service Motor Efficiency and In-Service Motor/Load Efficiency. U.S. Patent 5,661,386.

Liao, C.M., C.L. Chen, and T. Katcher. 1998. Thermal analysis for design of high performance motors. In *The Sixth Intersociety Conference on Thermal and Thermomechanical Phenomena in Electronic Systems*, 424-433. doi:10.1109/ITHERM.1998.689596.

Lindeborg, R. 1998. *Variable frequency drives*. Scientific Impeller. Sweden: ITT Flygt AB. http://www.flygtus.com/25975.pdf.

Little, A.D. 1999. *Opportunities for Energy Savings in the Residential and Commercial Sectors with High-efficiency Electric Motors*. Prepared for the U.S. Dept. of Energy. Washington, DC: Arthur D. Little, Inc., December. http://www.cee1.org/eval/db_pdf/268.pdf.

Liu, M., D.E. Claridge, and W.D. Turner. 2002. *Continuous Commissioning(SM) Guidebook: Maximizing Building Energy Efficiency and Comfort*. Washington, DC: U.S. Dept. of Energy Federal Energy Management Program, October. http://www1.eere.energy.gov/femp/operations_maintenance/om_ccguide.html.

Lobodovsky, K.K. 2007. Electric energy management. In *Energy Management Handbook*, 6th ed., eds. W.C. Turner and S. Doty, 273-299. Lilburn, GA: Fairmont Press.

Lu, Bin, T.G. Habetler, and R.G. Harley. 2006. A survey of efficiency-estimation methods for in-service induction motors. *IEEE Transactions on Industry Applications* 42, no. 4 (July): 924-33. doi:10.1109/TIA.2006.876065.

Markovic, M., L. Saunders, and Y. Perriard. 2006. Determination of the thermal convection coefficient for a small electric motor. In *Conference Record of the 41st IEEE Industry Applications Conference*, 1:58-61. Vol. 1. doi:10.1109/IAS.2006.256520.

Maru, B., and P.A. Zotos. 1989. Anti-friction bearing temperature rise for NEMA frame motors. *IEEE Transactions on Industry Applications* 25(5): 883-888. doi:10.1109/28.41253.

McCoy, G.A., and J.G. Douglass. 2000. *Energy Management for Motor Driven Systems*. 2nd ed. Washington, DC: U.S. Dept. of Energy Office of Industrial Technologies, March. http://www1.eere.energy.gov/industry/bestpractices/pdfs/NN0116.pdf.

McCoy, R.M., and E.L. Owen. 2004. Environmental considerations. In *Handbook of Electric Motors*, 2nd ed., eds. H.A. Toliyat and G.B. Kliman, 617-654. Boca Raton, FL: CRC Press.

Mecker, S. 1994. How loads affect efficiency of motors. *Electrical Construction and Maintenance* 93(8): 33-5.

Medinger, C. 1996. The hot topic of motor temperature. *Power Transmission Design* 38(9): 15-20.

Mello, H.G.G., and W.L. Pires. 2008. Extending motor life with optimal flux. *Heating/Piping/Air Conditioning Engineering* 80(7): 46-49.

Miles, J., and M. Shevlin. 2001. *Applying Regression & Correlation: A Guide for Students and Researchers*. London, U.K.: SAGE Publications.

Monarch Instrument. *TACH-4A/TACH-4AR Programmable Optical Tachometer*. Instruction Manual. Amherst, NH: Monarch Instrument.

http://www.monarchinstrument.com/pdfs/manuals/1071-4850-001%20T-4A%20Eng.pdf. Accessed April 2009.

Monarch Instrument. 2005. *ACT-2A, ACT-3A, ACT-3 Tachometers*. Instruction Manual. Amherst, NH: Monarch Instrument. http://www.monarchinstrument.com/pdfs/manuals/ACT-2-3%20Eng.pdf. Accessed April 2009.

Mukhopadhyay, S.C., S.P. Chowdhury, and S.K. Pal. 1994. A software package for the determination of steady state temperature of small cage rotor induction motor. *Journal of the Institution of Engineers (India) Electrical Engineering Division* 74 (February): 139-45.

Mukosiej, J. 1986. Measurement of average temperature of induction motor frame surface using thermocouples. *Proceedings of the International Conference on Electrical Machines,* 8-10 Sept. 1986, 360-3. Munchen, West Germany: Tech. Univ. Munchen.

Mukosiej, J. 2000. Problem of accuracy of thermal testing of electric machines. *Proceedings of International Conference on Electrical Machines,* 28-30 Aug. 2000, 1:166-70. Vol. 1. Espoo, Finland: Helsinki Univ. Technol.

Munoz, A., and P. Maldonado. 2003. On site efficiency measurements for electrical motors is possible and easier than thought. *Energy Efficiency in Motor Driven Systems*, 41-46. Berlin, Germany: Springer-Verlag.

Nadel, S., R.N. Elliot, M. Shepard, S. Greenberg, G. Katz, and A.T. de Almeida. 2002. *Energy-Efficient Motor Systems: A Handbook on Technology, Program, and Policy Opportunities*. 2nd ed. Energy Conservation and Energy Policy. Washington, DC: American Council for an Energy-Efficient Economy.

Nadel, S., M. Shepard, S. Greenberg, G. Katz, and A.T. de Almeida. 1992. *Energy-Efficient Motor Systems: A Handbook on Technology, Program, and Policy Opportunities*. revised edition. Energy Conservation and Energy Policy. Washington, DC: American Council for an Energy-Efficient Economy.

Nailen, R.L. 1989. "Can field tests prove motor efficiency?," *IEEE Transactions on Industry Applications* 25, no. 3: 391-396.

Nailen, R.L. 1994. Finding true power output isn't easy. *Electrical Apparatus* 47(2): 31-36.

Nailen, R.L. 1996. *Managing Motors*. 2nd ed. Chicago, IL: Barks Publications.

Nailen, R.L. 1998. Safe meter usage is no accident. *Electrical Apparatus* 51(1): 21-25.

Nailen, R.L. 2002. Just how important is drive motor efficiency? *Electrical Apparatus* 55(3): 32-33.

Nailen, R.L. 2003. When (and why) is motor surface temperature important? *Electrical Apparatus* 56(6): 33-38.

NEMA. 2001. *Application Guide for AC Adjustable Speed Drive Systems*. NEMA Standards Publication. Rosslyn, VA: National Electrical Manufacturers Association.

NEMA. 2002. *Information Guide for General Purpose Industrial AC Small and Medium*

Squirrel-Cage Induction Motor Standards. NEMA Standards Publication. Rosslyn, VA: National Electrical Manufacturers Association.

NEMA. 2006. *Motors and Generators*. NEMA Standards Publication MG 1-2006. Rosslyn, VA: National Electrical Manufacturers Association.

NEMA. 2007. *Energy Management Guide for Selection and Use of Fixed Frequency Medium AC Squirrel-Cage Polyphase Induction Motors*. NEMA Standards Publication MG 10-2001 (R2007). Rosslyn, VA: National Electrical Manufacturers Association.

Nicholas, J.V. 1999. Liquid-in-glass thermometers. *The Measurement, Instrumentation, and Sensors Handbook*, ed. J.G. Webster, 32-117 to 32-128. Boca Raton, FL: CRC Press.

O'Neal, D.L., J. Bryant, and K. Carlson. 1998. *Instrumenting Buildings to Determine Retrofit Savings: Murphy's Law Strikes Again*. 11th Annual Symposium on Improving Building Efficiency in Hot and Humid Climates. Energy Systems Laboratory, Texas Engineering Experiment Station. ESL-HH-98-06-34. http://handle.tamu.edu/1969.1/6747.

Ontario Hydro. 1997. *Adjustable Speed Drive Reference Guide*. 4th ed. Canada: Ontario Hydro. http://www.energyefficiency.org/eecentre/eecentre.nsf/128b945e3ee79d5b85256aec005a92fa/6d7fa84d5eb731d0852569f3006ff0ca/$FILE/ASD1997.pdf.

Pawlik, K-D.E., L.C. Capehart, and B.L. Capehart. 2001. Analyzing Facility Energy Use: A Balancing Act. *Strategic Planning for Energy and the Environment* 21(2): 8-33.

Penrose, H.W. 2004. Induction motor formulas. *Motorblog: An ongoing editorial about motor testing and diagnose featuring industry experts as authors*. http://www.maintenancetalk.com/motorblog/archives/000718.html.

Pickering, S.J., D. Lampard, N. Hay, and T.F. Roylance. 1998. Heat transfer in a through-ventilated induction motor. *IEE Proceedings--Electric Power Applications* 145(5): 429-33. doi:10.1049/ip-epa:19982169.

Polka, D. 2003. *Motors and Drives--A Practical Technology Guide*. Research Triangle Park, NC: Instrumentation, Systems, and Automation Society.

Preecha, P., J. Dejvises, S. Chusanapiputt, and S. Phoomvuthisarn. 2004. A temperature calculation and prediction of a three-phase induction motor with non sinusoidal voltage supply. *International Conference on Power System Technology*, 1:608-611. Vol. 1. IEEE. doi:10.1109/ICPST.2004.1460066.

Ramsay, D.C. 1996. *Principles of Engineering Instrumentation*. New York: Halstead Press.

Renier, B., K. Hameyer, and R. Belmans. 1999. Comparison of standards for determining efficiency of three phase induction motors. *IEEE Transactions on Energy Conversion* 14(3): 512-17. doi:10.1109/60.790906.

Revelt, J. 1997. On-site motor energy audits: Use with caution. *Electrical Construction and Maintenance* 96(1): 42, 44, 46.

Romo, J.L., and M.B. Adrian. 1998. Prediction of internal temperature in three-phase induction

motors with electronic speed control. *Electric Power Systems Research* 45(2): 91-99. doi:10.1016/S0378-7796(97)01189-9.

Saari, J. 1995. *Thermal Modelling of High-speed Induction Machines*. Acta Polytechnica Scandinavica, Electrical Engineering Series 82. Helsinki, Finland: Finnish Acad. of Technology.

Santos, A.H.M., and E. da Costa Bortoni. 1995. Analysis of three-phase induction motors under conditions of technical and economical uncertainty aiming energy conservation. *Conference Record of the Thirtieth IEEE Industry Applications Conference*, 2:1702-1706. Vol. 2. doi:10.1109/IAS.1995.530510.

Stanford, H.W. 2003. *HVAC Water Chillers and Cooling Towers: Fundamentals, Application, and Operation*. New York: Marcel Dekker.

Staton, D.A., and A. Cavagnino. 2008. Convection heat transfer and flow calculations suitable for electric machines thermal models. *IEEE Transactions on Industrial Electronics* 55(10): 3509-3516. doi:10.1109/TIE.2008.922604.

Stebbins, W.L. 1994. Are you certain you understand the economics for applying ASD systems to centrifugal loads? *Proceedings of the 1994 IEEE Annual Textile, Fiber & Film Industry Technical Conference*, 1-8. IEEE. doi:10.1109/TEXCON.1994.320725.

Stone, G.C., E.A. Boulter, I. Culbert, and H. Dhirani. 2004. *Electrical Insulation for Rotating Machines*. IEEE Press Series on Power Engineering. Hoboken, NJ: John Wiley & Sons.

Taber, G.E. 1998. Pumps and valves. *HVAC Maintenance and Operations Handbook*, ed. R.C. Rosaler, 319-390. New York: McGraw-Hill.

Takahashi, K., H. Kuwahara, K. Kajiwara, and T. Obata. 2002. Airflow and thermal conductance in a totally enclosed induction motor. *Heat Transfer-Asian Research* 31(1): 7-20. doi:10.1002/htj.10010.

Thumann, A., and H. Franz. 2009. *Efficient Electrical Systems Design Handbook*. Lilburn, GA: Fairmont Press.

Turner, D.R., K.J. Binns, B.N. Shamsadeen, and D.F. Warne. 1991. Accurate measurement of induction motor losses using balance calorimeter. *IEE Proceedings B--Electric Power Applications* 138(5): 233-42.

U.S. Dept. of Energy. Energy Information Administration. 2008a. *Annual Energy Review 2007*. Washington, DC: U.S. Government Printing Office, June. http://www.eia.doe.gov/aer.

U.S. Dept. of Energy. Energy Information Administration. 2008b. *2003 Overview of Commercial Buildings*. Commercial Buildings Energy Consumption Survey. http://www.eia.doe.gov/emeu/cbecs/cbecs2003/overview.pdf.

U.S. Dept. of Energy. Industrial Technologies Program. 2005. *Estimating motor efficiency in the field*. Energy Tips--Motor. September. http://www1.eere.energy.gov/industry/bestpractices/pdfs/estimate_motor_efficiency_motor_systemts2.pdf.

U.S. Dept. of Energy Motor Challenge Program. *Replacing an oversized and underloaded electric motor*. U.S. Dept. of Energy Motor Challenge Program. http://www.oit.doe.gov/bestpractices/motors/factsheets/mc-2463.pdf. Accessed June 2008.

Valenzuela, M.A., and J.A. Tapia. 2006. Heat transfer and thermal design of finned frames for TEFC variable speed motors. *32nd Annual Conference on IEEE Industrial Electronics, 6-10 Nov. 2006*, 4835-40. Paris, France: IEEE.

Valenzuela, M.A., J.A. Tapia, and J.A. Rooks. 2004. Thermal evaluation of TEFC induction motors operating on frequency-controlled variable-speed drives. *IEEE Transactions on Industry Applications* 40(2): 692-698. doi:10.1109/TIA.2004.824496.

Wallace, A., A. Von Jouanne, E. Wiedenburg, E. Matheson, and J.G. Douglass. 2001. A laboratory assessment of in-service and nonintrusive motor efficiency testing methods. *Electric Power Components and Systems* 29(6): 517-29. doi:10.1080/153250001300338754.

Washington State University Cooperative Extension Energy Program. 2003. *MotorMaster+4.0 User's Guide*. Developed for the U.S. Dept. of Energy.

Weisberg, S. 2005. *Applied Linear Regression*. 3rd ed. Wiley Series in Probability and Statistics. Hoboken, NJ: Wiley-Interscience.

Westphalen, D., and S. Koszalinski. 1999. *Volume II: Thermal Distribution, Auxiliary Equipment, and Ventilation*. Prepared for the U.S. Dept. of Energy Office of Building Equipment. Energy Consumption Characteristics of Commercial Building HVAC Systems. Cambridge, MA: Arthur D. Little, Inc.

Wilks, D.S. 2006. *Statistical Methods in the Atmospheric Sciences*. 2nd ed. International Geophysics Series. Burlington, MA: Elsevier Academic Press Publications.

Wilson, E.B. 1990. *An Introduction to Scientific Research*. New York: Dover Publications.

Yoon, M.K., and S.K. Kauh. 2005. Thermal analysis of a small, totally enclosed, fan-cooled induction motor. *Heat Transfer Engineering* 26(4): 77-86. doi:10.1080/01457630590916310.

APPENDIX A
GRAPHICALLY EXTENDING THE SLIP METHOD TO VFD-DRIVEN MOTORS

The following is a graphical approach for extending the Slip Method to VFD-driven motors. The results are the same as shown earlier in Section 3.1.

Development of Existing Slip Method for Motors Driven ATL

Before considering a VFD-driven motor, the development of the existing Slip Method on a grid-connected (no VFD) motor is first considered. Figure 61 shows a typical Torque-Speed curve for NEMA Design B motors (Polka 2003, 159). Notice that the majority of the curve represents the motor during startup; the motor speed during steady-state motor operation occurs between the base speed (rated full-load speed) and the synchronous speed.

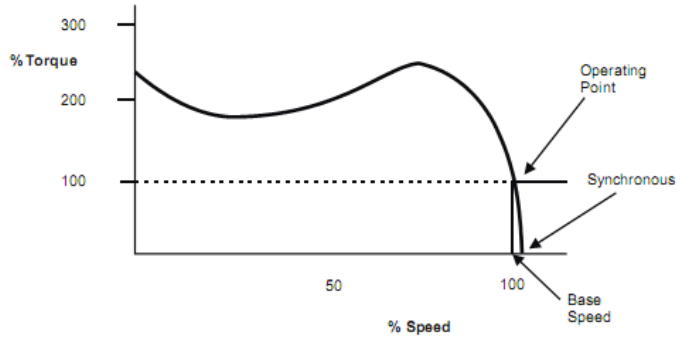

Figure 4-25. Motor speed/torque curve

Figure 61: Torque vs. Speed Curve for typical NEMA Design B induction motor (Polka 2003, 159). Copyright (c) 2003 ISA. Reprinted by permission. All rights reserved.

If this curve below 100% is approximated as a line[40] $(y = m \cdot x + b)$ then

[40] Santos investigates the effect of approximating the torque-speed curve as a line (1995, 1703-1704).

$$PT = m \cdot PS + b = m \cdot \left(\frac{N_{shaft}}{N_{sync}} \right) + b \tag{113}$$

where PT is percent torque, PS is percent speed, and m and b are constants. In order to find the constants m and b, two known points are used to fix the line: $(N_{shaft}, PT) = (N_{sync}, 0)$ and $(N_{shaft}, PT) = (N_{shaft,FL}, 1)$.

Solving for the constants and plugging them back in results in

$$PT = \frac{T}{T_{full\,load}} = \frac{N_{sync} - N_{shaft}}{N_{sync} - N_{shaft,\,full\,load}} \tag{114}$$

Equation 114 gives percent full load torque, not percent shaft or input power. Now shaft power can be given as

$$P_{shaft} = T \cdot N_{shaft} \cdot (2\pi/60) \tag{115}$$

Solving Equation 115 for torque gives

$$T = \frac{P_{shaft}}{N_{shaft} \cdot (2\pi/60)} \tag{116}$$

and it follows that at full-load:

$$T_{full\,load} = \frac{P_{shaft,\,full\,load}}{N_{shaft,\,full\,load} \cdot (2\pi/60)} \tag{117}$$

Plugging (116) and (117) into (114) gives

$$\frac{P_{shaft}}{P_{shaft,\,full\,load}} = \frac{N_{sync} - N_{shaft}}{N_{sync} - N_{shaft,\,full\,load}} \cdot \left(\frac{N_{shaft}}{N_{shaft,\,full\,load}} \right) \tag{118}$$

By using the standard definition for motor efficiency

$$\eta_{motor} = \frac{P_{shaft}}{P_{in}} \tag{119}$$

then Equation 118 can be extended to give the power consumption as a function of various nameplate values, a shaft speed measurement, and a motor efficiency:

$$P_{in} = \frac{N_{sync} - N_{shaft}}{N_{sync} - N_{shaft,\,full\,load}} \cdot \left(\frac{N_{shaft}}{N_{shaft,\,full\,load}} \right) \cdot \left(\frac{P_{shaft,\,full\,load}}{\eta_{motor}} \right) \tag{120}$$

It is interesting to note that the 2nd factor in Equation 120 is very close to 1 and is usually neglected in the literature (Hsu et al. 1998, 119). Astrom does include it (2004, 12).

VFD Extended Slip Method for Motors Driven by VFD

Next, a derivation for applying the Slip Method to a VFD-connected motor is shown. As mentioned earlier in Section 3.1., as the supply frequency from a VFD is reduced, the voltage is also reduced to avoid overfluxing the motor. In order to maintain the maximum torque developed, the voltage is adjusted so that the voltage-to-frequency ratio is kept constant (Guru and Hiziroğlu 2001, 551). This is known as Volts-per-Hertz (V/Hz or Volts/Hz) control and it is used extensively in fan and pump applications (Boldea and Nasar 2002, sec. 8.4).

Figure 62 that shows that a given motor has a unique torque-speed curve for each supply signal frequency (synchronous speed) that the VFD supplies if the Volts/Hz ratio is kept constant (Emadi 2005, 157).

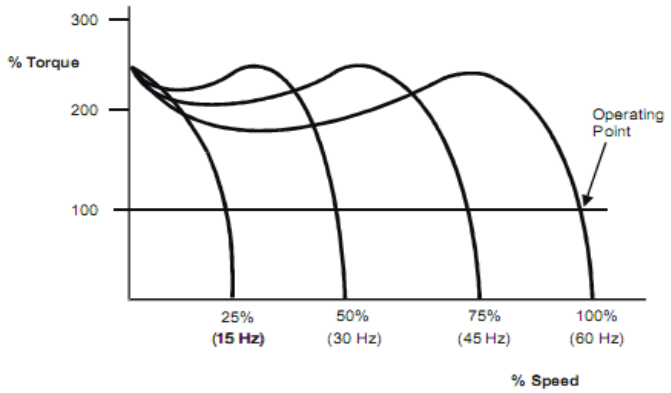

Figure 4-26. Drive frequency output vs. motor torque

Figure 62: Torque vs. Speed Curves for various supply frequencies (Polka 2003, 159). Copyright (c) 2003 ISA. Reprinted by permission. All rights reserved.

A derivation for the Slip Method for a grid-connected motor (supplied at 60 Hz) has just been shown. Now those assumptions will be revisited so that in order so that the Slip Method may apply to supply frequencies other than the nominal.

For the sake of argument, let us try to find the relation for the motor run at 30 Hz. If it is assumed that the curve to the right of each peak is linear, then for the 30 Hz case:

$$y = m_{30} \cdot x + b_{30} \tag{121}$$

or

$$PT = m_{30} \cdot PS + b_{30} \tag{122}$$

where the percent torque (*PT*) and percent speed (*PS*) are still relative to the rated (nameplate) full-load conditions.

If it is assumed that the slope of each approximation line (for every VFD speed) is equal to the slope at rated conditions, then

$$m_{30} = m_{60} = \frac{N_{sync,nameplate}}{N_{shaft,nameplate} - N_{sync,nameplate}} \tag{123}$$

Then the percent torque is

$$PT = \frac{N_{sync,nameplate}}{N_{shaft,nameplate} - N_{sync,nameplate}} \cdot \left(\frac{N_{shaft}}{N_{sync,nameplate}} \right) + b_{30} \tag{124}$$

In order to find b_{30}, we fix the equation by recognizing that $(N_{shaft}, PT) = (N_{sync,30}, 0)$. This gives

$$b_{30} = \frac{-N_{sync,30}}{N_{shaft,nameplate} - N_{sync,nameplate}} \tag{125}$$

By combining Equations 124 and 125 and allowing for all synchronous supply speeds (not just 30 Hz) results in:

$$PT = \frac{N_{sync,nameplate}}{N_{shaft,nameplate} - N_{sync,nameplate}} \cdot \left(\frac{N_{shaft}}{N_{sync,nameplate}} \right) - \frac{N_{sync,supply}}{N_{shaft,nameplate} - N_{sync,nameplate}} \tag{126}$$

which can be simplified to

$$PT = \frac{N_{sync,supply} - N_{shaft}}{N_{sync,nameplate} - N_{shaft,nameplate}} \tag{127}$$

Equation 127 looks remarkably similar to Equation 114 from the non-VFD connected discussion. Converting Equation 127 to give the input power (as done with Equations 116 to 120), gives

$$P_{in} = \frac{N_{sync,supply} - N_{shaft}}{N_{sync,nameplate} - N_{shaft,nameplate}} \cdot \left(\frac{N_{shaft}}{N_{shaft,nameplate}} \right) \cdot \left(\frac{P_{shaft,nameplate}}{\eta_{motor}} \right) \tag{128}$$

which is identical to Equation 39 in Section 3.1.

In summary, this extension of the Slip Method to VFD-driven motors has several underlying

assumptions:

1. Approximating the torque-speed curve at typical operation with a 1st order polynomial.
2. Assuming the slope of the other curves (e.g. 30 Hz) is the same as the 60 Hz slope.
3. Assuming the voltage-to-frequency ratio of the VFD supply signal is held constant.

APPENDIX B
UNCERTAINTY ANALYSIS OF TEMPERATURE APPROACH

The effect of efficiency uncertainty on the uncertainty of estimating motor input power using a temperature-based approach has already been examined in Section 3.3.1. The effect of other parameter uncertainties—such as from the motor thermal constant and temperature measurement—have not been considered yet. In order to simplify this uncertainty analysis, a simplified version of the temperature-based approach is used that only considers the convective heat transfer from the motor:

$$P_{in} = \frac{C_{conv} N_{shaft}^{C_{speed}} (T_s - T_\infty)}{1 - \eta_{motor}} \tag{129}$$

where the nomenclature was defined and elaborated earlier (see Equation 106).

By taking partial derivatives of each parameter in Equation 129 (except for $C_{speed} = 1$), a Kline-McClintock propagation-of-errors analysis can be constructed:

$$\Delta P_{input} = \left[\left(\frac{\partial P_{in}}{\partial C_{conv}} \cdot \Delta C_{conv} \right)^2 + \left(\frac{\partial P_{in}}{\partial N_{shaft}} \cdot \Delta N_{shaft} \right)^2 + \left(\frac{\partial P_{in}}{\partial T_s} \cdot \Delta T_s \right)^2 + \left(\frac{\partial P_{in}}{\partial T_\infty} \cdot \Delta T_\infty \right)^2 + \left(\frac{\partial P_{in}}{\partial \eta_{motor}} \cdot \Delta \eta_{motor} \right)^2 \right]^{1/2} \tag{130}$$

where each partial derivative can be determined from Equation 129. With the partial derivatives and Equation 130, a spreadsheet was created to determine input power uncertainty, as shown in Figure 63.

1	**Rough Uncertainty Analysis for Motor Input Power Uncertainty Considering Only External Convection**									
2	Inputs are in green cells									
3	**Important output cells are blue**									
4										
5			Nominal	Absolute	Relative					
6	**Parameter**	**Variable name**	**Value**	**uncertainty**	**uncertainty**	**Units**	**Typical values**			
7	Motor efficiency	efficiency	0.85	0.020	2%					
8	Regression Convection coeff	C	0.19	0.024	13%	W / (K*rad/s)	0.56 for Motor #1			
9	Surface temp. (convective)	T_sconv	338	1	0%	K	306 K is for 90 F, 320 K is 120 F			
10	Ambient temp.	T_inf	298	1	0%	K	298 K is 77 F			
11	Shaft speed	N_shaft	184	4.2	2%	rad/s	123 rad/s = 1175 RPM, 184 rad/s = 1760 RPM, 2.			
12	C_speed exponent		1							
13										
14										
15										
16	Input Power	Power_Input	9323	1757	19%	W	<===	***Uncertainty contribution from ea***		
17	Nominal Input Power		8773	1757	**20.0%**	W		**squared**		
18								efficiency term	1545104	
19								C term	1386742	
20								T_s,conv term	54320	
21								T_inf term	54320	
22								N_shaft	45284	

Figure 63: Estimating the uncertainty in motor input power using temperature-based approach (external convection only).

Recall that it is desired that motor input power be determined within ±20% of the nominal input power. Also note that running motor efficiency in the field is an unknown quantity. Even at full-load, a motor with a nameplate efficiency of 85.5% is allowed by NEMA to have a running full-load efficiency of 82.5% (NEMA 2006, sec. 12.58.2). Hsu et al. recommends a ±10% efficiency uncertainty with using the nameplate method for motors loaded between 50% and 100% (NEMA 2007, 2). Unfortunately, even if all other uncertainties in the spreadsheet are set to zero except for motor efficiency uncertainty, the maximum efficiency uncertainty that is allowed given the ±20% constraint in input power uncertainty is an efficiency uncertainty of 2.8%. In the field, that value for required motor efficiency uncertainty may be low compared to the efficiency uncertainty provided by Hsu et al. for approximating motor efficiency with the nameplate motor efficiency value.

For the sake of demonstrating a procedure for estimating the required level of measurement accuracy for the experiment with Motor #2, let's temporarily assume a motor efficiency uncertainty of ±2% in the field. Further assumptions are listed in Table 17.

Table 17: Parameter values and uncertainty for demonstrating a procedure for estimating measurement accuracy in the experiment. These values are for using the temperature approach in the field, not in the laboratory where one is trying to determine the motor coefficients.

Parameter	Value	Uncertainty	Units	Note
Motor Efficiency	0.85	± 0.02		85% is the nameplate efficiency for Motor #2. Assume 2% efficiency uncertainty for the sake of this demonstration.
Convection Coefficient	0.19	Solved to be ± 0.024	W/ (K·rad/s)	The value of 0.19 W/(K·rad/s) provided from Table 13.
Surface Temp.	338	± 1	K	148 ºF = 338 K, which is the max measured surface temperature on Path A for Motor #2. Assume ±1 K = 1.8 ºF uncertainty.
Ambient Temp.	298	± 1	K	79 ºF = 298 K. Assume ±1 K = 1.8 ºF uncertainty.
Shaft Speed	184	± 4.2	rad/s	1760 RPM = 184 rad/s, the average of the synchronous and full-load speed for Motor #2. The maximum uncertainty is therefore ±40 RPM = 4.2 rad/sec.
C_speed	1			The exponent C_{speed} is set to 1 until the literature or experimentation give another value for the exterior of ODP enclosures.

Figure 63 shows the uncertainty in input power due to the uncertainties in the parameter values. If the uncertainty in input power—relative to the nominal input power—is to be capped at ±20% and the data in Table 17 is assumed, then the uncertainty in the convective coefficient can be found by using the spreadsheet's solving facility. Using the specified values results in a uncertainty convective coefficient of ±0.024 W/(K·rad/s).

Once the desired uncertainty in convective coefficient is determined, the required level of accuracy in the laboratory—where the objective is to determine a motor's coefficients—can be considered. Solving Equation 129 for the convective coefficient gives

$$C_{conv} = \frac{P_{in}(1-\eta_{motor})}{N_{shaft}^{C_{speed}}(T_s - T_\infty)} \tag{131}$$

The uncertainty in the convective coefficient from the parameter uncertainties is determined by

$$\Delta C_{conv} = \left[\left(\frac{\partial C_{conv}}{\partial P_{in}} \cdot \Delta P_{in} \right)^2 + \left(\frac{\partial C_{conv}}{\partial \eta_{motor}} \cdot \Delta \eta_{motor} \right)^2 + \left(\frac{\partial C_{conv}}{\partial N_{shaft}} \cdot \Delta N_{shaft} \right)^2 + \left(\frac{\partial C_{conv}}{\partial T_s} \cdot \Delta T_s \right)^2 + \left(\frac{\partial C_{conv}}{\partial T_\infty} \cdot \Delta T_\infty \right)^2 \right]^{1/2} \quad (132)$$

where the partial derivatives are determined from Equation 131.

In the laboratory—where the objective is to determine the motor coefficients—multiple experiments can be done. As more experiments on the same motor are completed, the random error in the uncertainty is reduced by $1/\sqrt{n}$, where n is the number of experiments (Wilson 1990, 252). Figure 64 shows the uncertainty in the convective coefficient resulting from implementing Equations 131 and 132.

	A	B	C	D	E	F	G	H	I
1	**Rough Uncertainty Analysis for determining Coefficient Uncertainty using only External Convection**								
2	Inputs are in green cells								
3	**Important output cells are blue**								
4									
5			**Nominal**	**Absolute**	**Relative**				
6	**Parameter**	**Variable name**	**Value**	**uncertainty**	**uncertainty**	**Units**	**Typical values**		
7	Motor efficiency	efficiency	0.85	0.03	4%				
8	Surface temp.	T_sconv	338	3	1%	K	306 K is for 90 F, 320 K is 120 F		
9	Ambient temp.	T_inf	298	3	1%	K	298 K is 77 F		
10	Shaft speed	N_shaft	184	4.2	2%	rad/s	123 rad/s = 1175 RPM, 2.6 rad/s = 25 RPM		
11	C_speed exponent		1						
12	Input Power		8773	175	2%	W			
13									
14									
15									
16	Number of Experiments		10						
17	Convection Coefficient (dete	Cconv	0.18	0.041	23%	W / (K*rad/s)	<===	***Uncertainty contribution from ea***	
18	Convection Coefficient (dete	Cconv, averaged		0.013		W / (K*rad/s)		**squared**	
19								efficiency term	0.001279
20								T_s,conv term	0.000180
21								T_inf term	0.000180
22								N_shaft	0.000017
23								P_input	0.000013

Figure 64: Estimating the uncertainty in determining a motor's convection constant from experiments.

Notice that Equation 131 does not have $1-\eta_{motor}$ in the denominator and so does not suffer from the effect from motor efficiency uncertainty as much as Equation 129 does. Therefore in the laboratory—where the objective is to determine a motor's thermal coefficients—motor efficiency uncertainty requirements can be relaxed.[41] For example, a motor efficiency uncertainty of ±3%,

[41] It is unfortunate that motor efficiency estimation in the field (where the objective is to predict motor input power) requires tighter uncertainty than motor efficiency estimation in the laboratory (where the objective is to determine motor thermal coefficients).

temperature measurement uncertainty of ±5.4 ºF (3 K), and 10 experiments gives an uncertainty in convective coefficient of 0.013 W/(K·rad/s), which is below the target uncertainty of 0.024 W/(K·rad/s) established earlier.

These uncertainty analyses do not consider error in estimating a motor's thermal coefficient(s) in the field. Furthermore, they do not account for errors in the model. These uncertainty analyses merely show how the parameter uncertainties affect the uncertainty in the predicted value. It should be noted that the method shown above was not used for experiment planning, due to the high uncertainty in motor efficiency which makes other laboratory measurement uncertainties to be marginalized. It is recommended that future experiments include a method that measures or estimates motor efficiency.

VITA

Kevin David Christman received his Bachelor of Science in engineering degree with a concentration in mechanical engineering from Walla Walla University in August of 2006. He entered the mechanical engineering graduate program at Texas A&M University in September of 2006, and became a graduate research assistant for Dr. David Claridge in September of 2007. In May of 2010, he received the Master of Science in mechanical engineering degree. His research interests include building energy assessments and HVAC.

Mr. Christman may be reached by postal mail at Energy Systems Laboratory, 3581 TAMU, College Station, TX 77843-3581. His email address is KevinChristman@tees.tamus.edu.